2004-09

Sensitivity of satellite altimetry data assimilation on a Naval Anti-Submarine Warfare Weapon System

Mancini, Steven

Monterey, California. Naval Postgraduate School

NAVAL POSTGRADUATE SCHOOL

MONTEREY, CALIFORNIA

THESIS

SENSITIVITY OF SATELLITE ALTIMETRY DATA ASSIMILATION ON A NAVAL ANTI-SUBMARINE WARFARE WEAPON SYSTEM

by

Steven Mancini

September 2004

Thesis Advisor:	Peter C. Chu
Second Reader:	Charlie N. Barron

Approved for public release; distribution is unlimited

THIS PAGE INTENTIONALLY LEFT BLANK

REPORT DOCUMENTATION PAGE			Form Approved OMB No. 0704-0188
Public reporting burden for this collection of information is estimated to average 1 hour per response, including the time for reviewing instruction, searching existing data sources, gathering and maintaining the data needed, and completing and reviewing the collection of information. Send comments regarding this burden estimate or any other aspect of this collection of information, including suggestions for reducing this burden, to Washington headquarters Services, Directorate for Information Operations and Reports, 1215 Jefferson Davis Highway, Suite 1204, Arlington, VA 22202-4302, and to the Office of Management and Budget, Paperwork Reduction Project (0704-0188) Washington DC 20503.			
1. AGENCY USE ONLY *(Leave blank)*	**2. REPORT DATE** September 2004	**3. REPORT TYPE AND DATES COVERED** Master's Thesis	
4. TITLE AND SUBTITLE: Sensitivity of Satellite Altimetry Data Assimilation on a Naval Anti-Submarine Warfare Weapon System			**5. FUNDING NUMBERS**
6. AUTHOR: Mancini, Steven			
7. PERFORMING ORGANIZATION NAME(S) AND ADDRESS(ES) Naval Postgraduate School Monterey, CA 93943-5000			**8. PERFORMING ORGANIZATION REPORT NUMBER**
9. SPONSORING /MONITORING AGENCY NAME(S) AND ADDRESS(ES) N/A			**10. SPONSORING/MONITORING AGENCY REPORT NUMBER**
11. SUPPLEMENTARY NOTES The views expressed in this thesis are those of the author and do not reflect the official policy or position of the Department of Defense or the U.S. Government.			
12a. DISTRIBUTION / AVAILABILITY STATEMENT **Approved for public release; distribution is unlimited**			**12b. DISTRIBUTION CODE**

13. ABSTRACT (maximum 200 words)

The purpose of this thesis is to assess the benefit of assimilating satellite altimeter data into the Modular Ocean Data Assimilation System (MODAS). To accomplish this, two different MODAS fields were used by the Weapon Acoustic Preset Program (WAPP) to determine suggested presets for a Mk 48 variant torpedo. The MODAS fields differ in that one uses altimeter data assimilated from three satellites while the other uses no altimeter data. The metric used to compare the two sets of outputs is the relative difference in acoustic coverage area generated by WAPP. Output presets are created for five different scenarios, two Anti-Surface Warfare scenarios and three Anti-Submarine Warfare scenarios, in each of three regions: the East China Sea, the Sea of Japan, and an area south of Japan that includes the Kuroshio current. Analysis of the output reveals that, in some situations, WAPP output is very sensitive to the inclusion of the altimeter data because of the resulting differences in the subsurface predictions. The change in weapon presets could be so much that the effectiveness of the weapon might be affected.

14. SUBJECT TERMS Satellite Altimetry, MODAS, Anti-Submarine Warfare, ASW, MK-48 Torpedo, WAPP			**15. NUMBER OF PAGES** 93
			16. PRICE CODE
17. SECURITY CLASSIFICATION OF REPORT Unclassified	**18. SECURITY CLASSIFICATION OF THIS PAGE** Unclassified	**19. SECURITY CLASSIFICATION OF ABSTRACT** Unclassified	**20. LIMITATION OF ABSTRACT** UL

NSN 7540-01-280-5500 Standard Form 298 (Rev. 2-89)
Prescribed by ANSI Std. 239-18

THIS PAGE INTENTIONALLY LEFT BLANK

Approved for public release; distribution is unlimited

SENSITIVITY OF SATELLITE ALTIMETRY DATA ASSIMILATION ON A NAVAL ANTI-SUBMARINE WARFARE WEAPON SYSTEM

Steven Mancini
Lieutenant Commander, United States Navy
B.S., Xavier University, 1992

Submitted in partial fulfillment of the
requirements for the degree of

MASTER OF SCIENCE IN METEOROLOGY AND PHYSICAL OCEANOGRAPHY

from the

NAVAL POSTGRADUATE SCHOOL
September 2004

Author: Steven Mancini

Approved by: Peter C. Chu
Thesis Advisor

Charlie N. Barron
Second Reader

Mary Batteen
Chairman, Department of Oceanography

THIS PAGE INTENTIONALLY LEFT BLANK

ABSTRACT

The purpose of this thesis is to assess the benefit of assimilating satellite altimeter data into the Modular Ocean Data Assimilation System (MODAS). To accomplish this, two different MODAS fields were used by the Weapon Acoustic Preset Program (WAPP) to determine suggested presets for a Mk 48 variant torpedo. The MODAS fields differ in that one uses altimeter data assimilated from three satellites while the other uses no altimeter data. The metric used to compare the two sets of outputs is the relative difference in acoustic coverage area generated by WAPP. Output presets are created for five different scenarios, two Anti-Surface Warfare scenarios and three Anti-Submarine Warfare scenarios, in each of three regions: the East China Sea, the Sea of Japan, and an area south of Japan that includes the Kuroshio current. Analysis of the output reveals that, in some situations, WAPP output is very sensitive to the inclusion of the altimeter data because of the resulting differences in the subsurface predictions. The change in weapon presets could be so much that the effectiveness of the weapon might be affected.

THIS PAGE INTENTIONALLY LEFT BLANK

TABLE OF CONTENTS

THIS PAGE INTENTIONALLY LEFT BLANK

LIST OF FIGURES

LIST OF TABLES

THIS PAGE INTENTIONALLY LEFT BLANK

ACKNOWLEDGMENTS

Several people deserve many thanks for their roles in helping with the creation of this thesis. Professor Peter Chu provided the framework, guidance, and encouragement, as well as hours of counsel. David Cwalina and his team at NUWC made the WAPP runs possible and provided much needed expertise. CDR Eric Gottshall and Dr. Charlie Barron provided insight and expertise. Chenwu Fan was extremely helpful with preparing the MODAS data for the NUWC folks and with producing the Matlab graphics. CDR Ben Reeder provided advice and suggestions. Thank you all for your contributions.

THIS PAGE INTENTIONALLY LEFT BLANK

I. INTRODUCTION

A. BACKGROUND

The outcome of a battlefield engagement is often determined by the advantages and disadvantages held by each adversary. On the modern battlefield, the possessor of the best technology often has the upper hand, but only if that advanced technology is used properly and efficiently. In order to exploit this advantage and optimize the effectiveness of high technology sensor and weapon systems, it is essential to understand the impact on them by the environment. In the arena of Anti-Submarine Warfare (ASW), the ocean environment determines the performance of the acoustic sensors employed and the success of any associated weapon systems. Since acoustic sensors detect underwater sound waves, understanding how those waves propagate is crucial to knowing how the sensors will perform and being able to optimize their performance in a given situation. To gain this understanding, an accurate depiction of the ocean environment is necessary.

How acoustic waves propagate from one location to another under water is determined by many factors, some of which are described by the sound speed profile (SSP). If the environmental properties of temperature and salinity are known over the entire depth range, the SSP can be compiled by using them in an empirical formula to calculate the expected sound speed in a vertical column of water. One way to determine these environmental properties is to measure them in situ, such as by conductivity-temperature-depth or expendable bathythermograph (XBT) casts. This method is not always tactically feasible and only gives the vertical profile at one location producing a very limited picture of the regional ocean structure. Another method is to estimate the ocean conditions using a computer analysis tool, such as the Modular Ocean Data Assimilation System (MODAS) developed by the Naval Research Laboratory (NRL) at the Stennis Space Center in Mississippi. MODAS is often used by the U.S. Navy to represent the water column hydrographic properties where in situ measurements are sparse or not available.

MODAS does a better job of representing the actual ocean structure than static climatology databases (Fox et. al., 2002; Chu et. al., 2004). It is expected that this

representation becomes even better when an increased number of in situ measurements and remotely sensed data from satellites are assimilated into MODAS. The satellites use radiometers to measure the thermal radiation emitted by the sea surface (from which sea surface temperature is derived) and radar altimeters to measure sea surface height. MODAS uses this information to create a "dynamic climatology" that more accurately reflects the mesoscale variability present in the ocean. Just how valuable a resource is this altimetry information? This thesis constitutes a first step in trying to answer this question by using MODAS as the end user of the altimetry data and the Weapon Acoustic Preset Program (WAPP) for the Mk 48 torpedo as the yardstick.

B. PURPOSE

If the assumption is that MODAS provides an improved representation of actual ocean conditions when satellite altimetry data is assimilated, a MODAS field that has this information would differ from one that does not, especially in regions of high mesoscale activity. If these differences are large enough, a tactical decision aid may give very different sound propagation characteristics depending on which MODAS field is used to represent the ocean environment. This, in turn, would cast doubt on predicted sensor performance and could render the technology ineffective, possibly changing the outcome of an engagement.

The purpose of this thesis is to quantify the sensitivity of a naval ASW system, specifically the Mk 48 torpedo WAPP, to the assimilation of satellite altimetry data when MODAS is used as WAPP's source of SSP information. This was done by examining the relative difference (RD) in the output of WAPP when two different MODAS fields were used as separate SSP inputs, as depicted in Figure 1. The MODAS fields were identical in each case except that one had satellite altimetry data assimilated while the other did not.

If a significant degree of sensitivity is discovered, then the next logical step would be to determine if the addition of satellite altimetry caused WAPP to respond more like it would have if in situ measurements were used as SSP input. This could be achieved in an experiment designed to compare WAPP output when MODAS fields and in situ measurements are used as separate SSP inputs. The question of how valuable this

altimetry data is can then be more fully explored. On the other hand, if this study shows little sensitivity to the different MODAS fields, then the value of satellite altimetry information, at least as an input to MODAS, can be assessed as low.

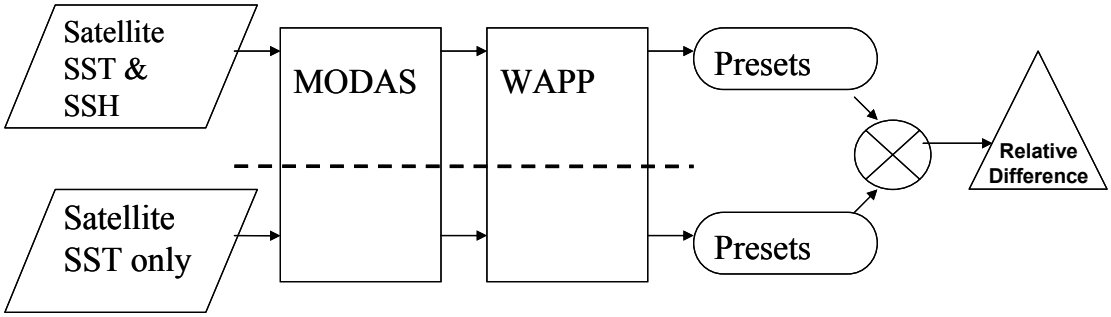

Figure 1. Thesis process flowchart.

C. THESIS SCOPE

The daily MODAS fields chosen for analysis were produced on two days picked in two different seasons to introduce some seasonal variability. For each day there were two fields: one with altimetry data assimilated into it and one without altimetry data. The fields that included altimetry received the data from the three satellite systems having operational altimeters at the time: NASA's TOPEX, the U.S. Navy's GEOSAT Follow-On, and the European Space Agency's ERS-2 (Fox et. al., 2002). In order to keep the data analysis manageable, but at the same time to gather a large enough number of data comparison points, three geographic regions, each five by five degrees in latitude and longitude, were cut out of the MODAS fields for each day. The boxes, shown in Figure 2, were located in the East China Sea region (ECS), the Sea of Japan region (SOJ), and the Kuroshio Current area south of Japan (KCA), and were chosen for their varying amounts of mesoscale variability as well as their tactical significance. Segregating these regions by the two dates created six MODAS cases to analyze.

WAPP was used to run five different tactical scenarios for each case: two Anti-Surface Warfare (ASUW) scenarios and three ASW scenarios. One of the ASUW scenarios involved a low Doppler, or slow moving, target while the other had a high Doppler target. One of the ASW scenarios involved a low Doppler target in a shallow depth band, representative of a diesel submarine. The other two ASW scenarios

consisted of a high and a low Doppler target in a deep depth band, representative of nuclear submarine capabilities. The output of WAPP used for comparison was area coverage, or the fraction of the search region having signal excess greater than 0 dB. A statistical software package was then used to determine the number of search depth/search angle combinations with relative differences in area coverage within a specified range. Histograms were generated to graphically display these statistics for each scenario in each case.

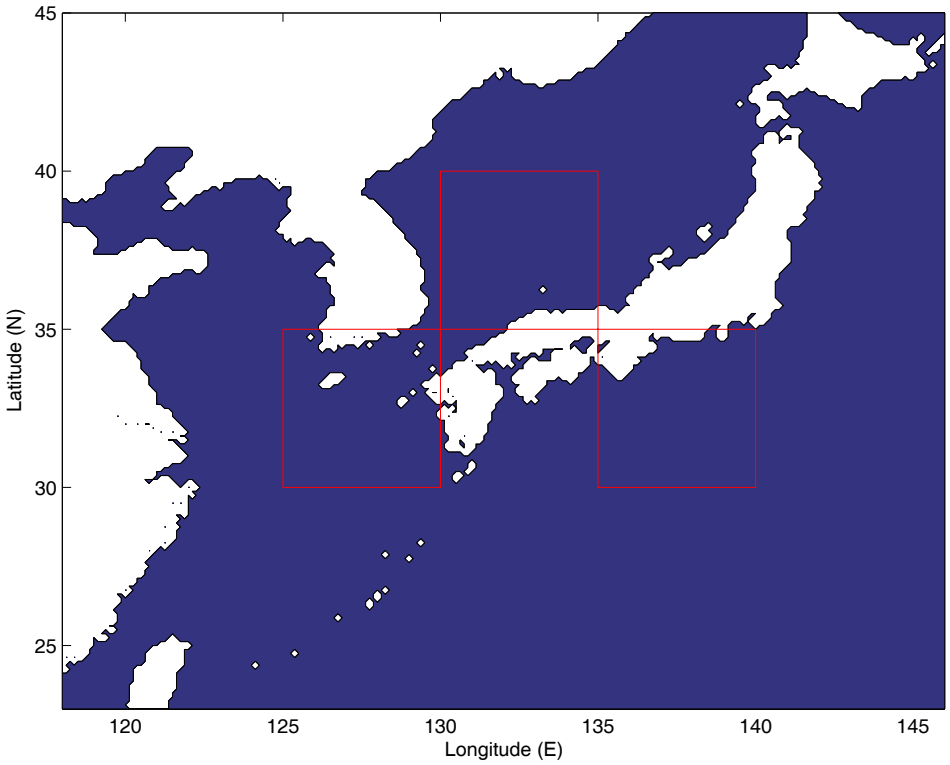

Figure 2. Geographic regions.

II. MODAS

A. BACKGROUND

MODAS, developed in the mid 1990s, is a global ocean analysis tool presently running at various navy facilities. It produces three-dimensional grids of temperature and salinity with horizontal resolutions ranging from one half to one eighth of a degree and uses these fields to derive other oceanographic fields of interest, such as density, sound speed, mixed layer depth, and geostrophic velocity. Unlike traditional "static climatologies," such as Levitus Climatology and the Generalized Digital Environmental Model that simply represent historical averages of ocean conditions, MODAS can assimilate real-time observations and produce an "adjusted" climatology that more closely represents the actual ocean conditions (Fox et. al., 2002).

To produce its "dynamic climatology," MODAS starts with a static, bi-monthly, gridded climatology of temperature and salinity that is derived from an archive of millions of profile measurements. The sea surface temperature (SST) and sea surface height (SSH) observations from satellites are used to generate two-dimensional, gridded fields of SST and SSH. This is accomplished by using optimum interpolation (OI) to calculate the SST and SSH values at the regularly spaced grid points within the fields. OI is a technique used for combining a background, or first guess, field and measured data by using a model of how nearby data are correlated (Fox et. al., 2002a). In the case of SST for example, the interpolated temperature is calculated by adding an interpolated temperature anomaly to the first guess grid value, as shown in the following equation:

$$T_k^a = T_k^f + \sum_{j=1}^{N} \alpha_{kj} (T_j^o - T_j^f), \qquad (1)$$

where T_k^a is the analyzed SST at the k-th grid point, T_k^f is the first guess temperature at the k-th grid point valid at the analysis time, T_j^o is the observed SST at location j, T_j^f is the first guess temperature at location j valid at the observation time, α_{kj} is a weighting factor applied to the observation, and N is the number of observations assimilated at the k-th

grid point. The anomaly is, therefore, determined as the linear combination of observed anomalies after each one is weighted to account for spatial and temporal sampling.

The weighting factors are estimated by minimizing the least square difference between the interpolated and actual grid point values and solving the following set of equations for the space-time autocorrelation between location j and grid point k, η_{kj}:

$$\sum_{j=1}^{N}(\eta_{ij}+\delta_{ij}\lambda_i^o)\alpha_{kj}=\eta_{kj}\,, \tag{2}$$

for i = 1, 2, …N, where λ_i^o is the signal to noise ratio for the i-th observation. To simplify this, the autocorrelation function for i-th observation at location j, η_{ij}, is given the simple form of

$$\eta_{ij}=\exp(-A_k^2\Delta x_{ij}^2-B_k^2\Delta y_{ij}^2-C_k^2\Delta t_{ij}^2)\,, \tag{3}$$

where Δx_{ij}, Δy_{ij}, and Δt_{ij} are the east-west, north-south, and time separation of location j from the grid point, respectively. The values A_k^{-1}, B_k^{-1}, and C_k^{-1} are east-west, north-south, and temporal decorrelation scales.

The first guess fields used by MODAS for the OI calculations are yesterday's MODAS field for SST and a large-scale weighted average of 35 days of altimetry for SSH. For the first OI iteration, the static climatology is used for the SST first guess. Synthetic temperature profiles can then be created by projecting these fields downward in the water column to a depth of 1500 m using relationships determined from a least-squares regression analysis of historical temperature profiles that relate both SST and SSH to the subsurface temperature (Fox et. al., 2002).

The result is a "dynamic climatology" that more accurately reflects the mesoscale temperature variability, as seen in Figure 3. The figure shows a vertical cross-section along a line where XBTs were dropped. The center panel shows the measurements made by the XBTs and reveals a subsurface cold-core eddy just to the right of center. The climatology panel on the left, as expected, indicates no mesoscale eddy. The MODAS synthetic analysis on the right was produced by assimilating satellite sensed SST and

SSH only (no in situ data). The MODAS cross-section indicates the eddy is present, although it does not quite resolve the smaller variations within the eddy itself.

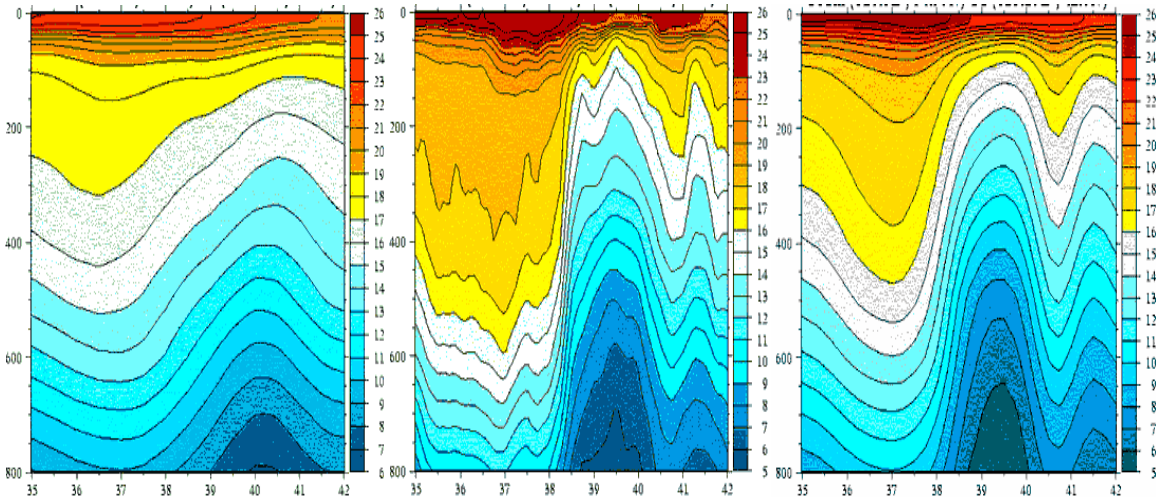

Figure 3. Comparison of climatology, XBTs, and MODAS (After Ref. Fox, 2004).

OI is also used to merge in situ temperature measurements into the dynamic climatology to produce a final temperature analysis. From this, a salinity analysis is produced using temperature-salinity regression relationships to estimate salinity at each depth. Similar to the temperature analysis, in situ salinity measurements can then be combined using OI to produce the final salinity analysis (Fox et. al., 2002a). An outline of the MODAS process is presented in Figure 4. The final temperature and salinity analyses are what MODAS uses to produce the other derived fields, such as sound speed.

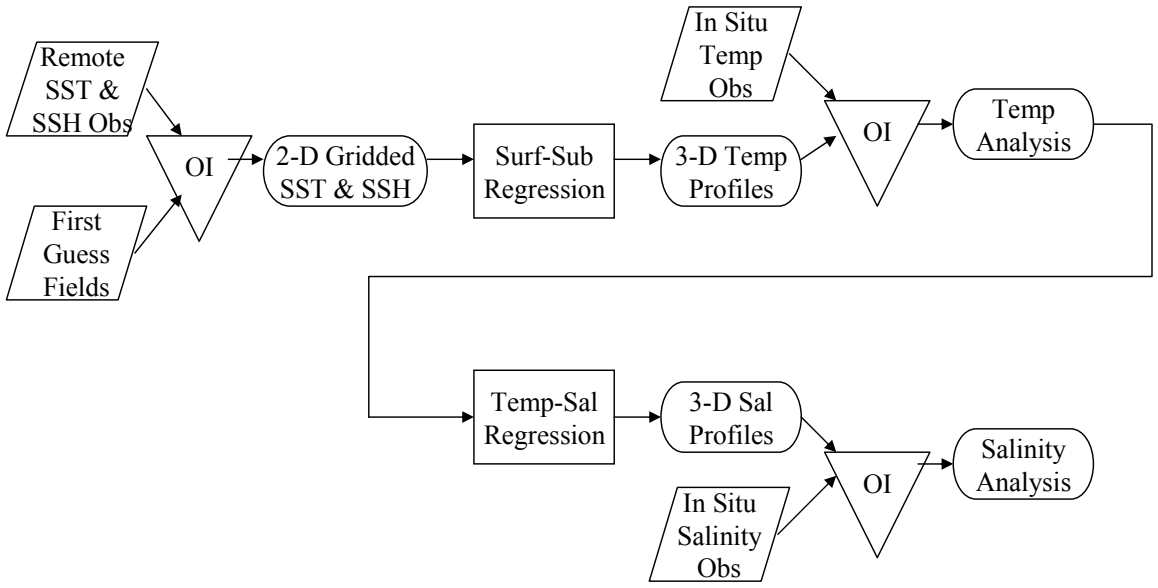

Figure 4. MODAS process flowchart.

B. APPLICATION

Global MODAS fields are produced at the Naval Oceanographic Office on a daily basis. The daily MODAS fields chosen for analysis were produced on June 30, 2001 and October 10, 2001. Two versions of each daily field were used to provide the environmental properties needed by WAPP to run its ray tracing model. The MODAS field versions were identical for the given day, with the exception of one had satellite altimetry data assimilated while the other did not. It was out of these global fields that the three five by five degree geographic regions mentioned earlier were selected. They are described by boxes located at 30-35N and 125-130E in ECS, 35-40N and 130-135E in SOJ, and 30-35N and 135-140E in KCA. The resolution of MODAS in these regions is one eighth of a degree, which yielded three grids of 41 by 41 points each. After eliminating grid points over areas of land, the number of vertical profiles made available to WAPP for each case was: 1,495 pairs for SOJ; 1,448 pairs for ECS; and 1,436 pairs for KCA, for a total of 4,379 pairs of profiles. Each vertical profile pair was for the same location and day, but one each was taken from the two different versions of MODAS fields. The output of WAPP could therefore be compared using each pair of vertical profiles to determine the sensitivity of the output to the altimetry data.

C. COMPARISON OF MODAS FIELDS

1. Statistical Methods

The two versions of MODAS fields for each case were compared by computing the difference in temperature, salinity, and sound speed (all denoted as ΔX_i, where X can be any of the aforementioned parameters) at each horizontal grid point and depth. The mean of these differences, or bias,

$$\Delta\bar{X} = \frac{1}{n}\sum_{i=1}^{n}\Delta X_i \,, \tag{4}$$

standard deviation of these differences,

$$\sigma_{\Delta X} = \sqrt{\frac{1}{n-1}\sum_{i=1}^{n}(\Delta X_i - \Delta\bar{X})^2} \,, \tag{5}$$

and root mean square difference,

$$RMSD = \sqrt{\frac{1}{n}\sum_{i=1}^{n}\Delta X_i^2}\ , \qquad (6)$$

over the entire volume for each case were calculated. Also, histograms were generated using these differences, scatter plots were produced, and vertical profiles of horizontally averaged bias and RMSD were produced for each parameter and case.

2. Volume RMSD

The volume RMSD values, plotted in Figure 5, give a general indication of how much difference there was in the MODAS analyses for each case. The largest differences in the temperature fields occurred in KCA on both days and in SOJ on Oct 10, where the volume RMSD values ranged from 1.58 to 1.80 °C. The other cases had RMSD values of 1.18 °C or less. Salinity differences were also largest in KCA on both days, but ECS on Jun 30 had a large volume salinity RMSD as well. These three cases had values ranging from 0.0759 to 0.0822 psu, whereas the other cases had values of 0.056 psu or less. The derived sound speed analyses closely followed the temperature fields, which is to be expected as temperature changes typically have the largest affect on sound speed. The largest sound speed volume RMSD values ranged from 1.62 to 1.84 m/s and occurred in the same cases as they did for the temperature analyses. The remaining cases had values of 1.15 m/s and smaller.

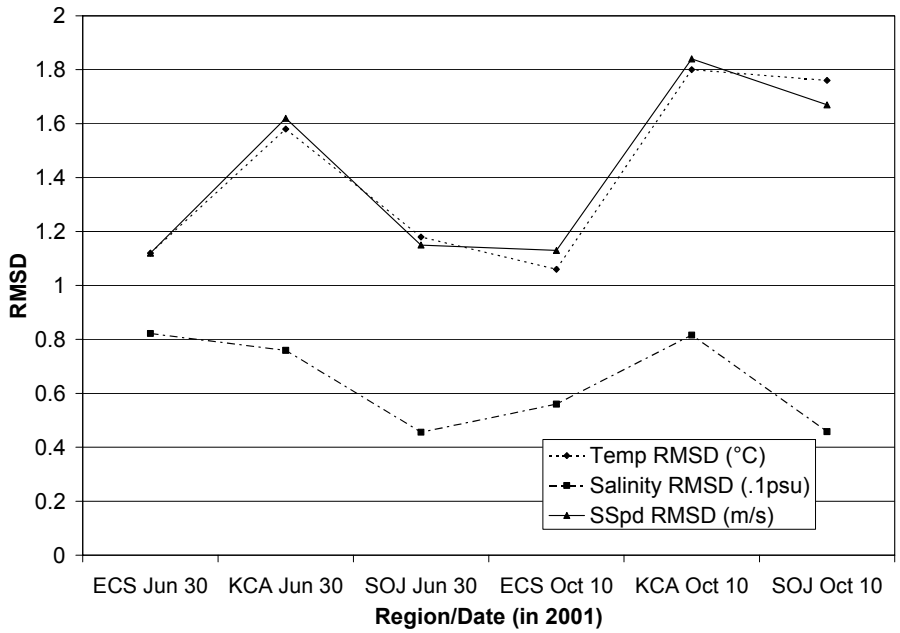

Figure 5. MODAS field RMSDs.

3. Horizontally Averaged RMSD

The vertical profiles of horizontally averaged RMSD allow for a more detailed comparison by showing at what depths the largest average differences occurred for each case. The largest differences in the temperature analyses occurred in the Oct 10 profiles for KCA and SOJ. Both had horizontally averaged RMSD values of well over 3 °C at different depths, as shown in Figure 6. The maximum values in the KCA profile occurred between 300 and 500 m, whereas in the SOJ profile they were in the 50 to 200 m range.

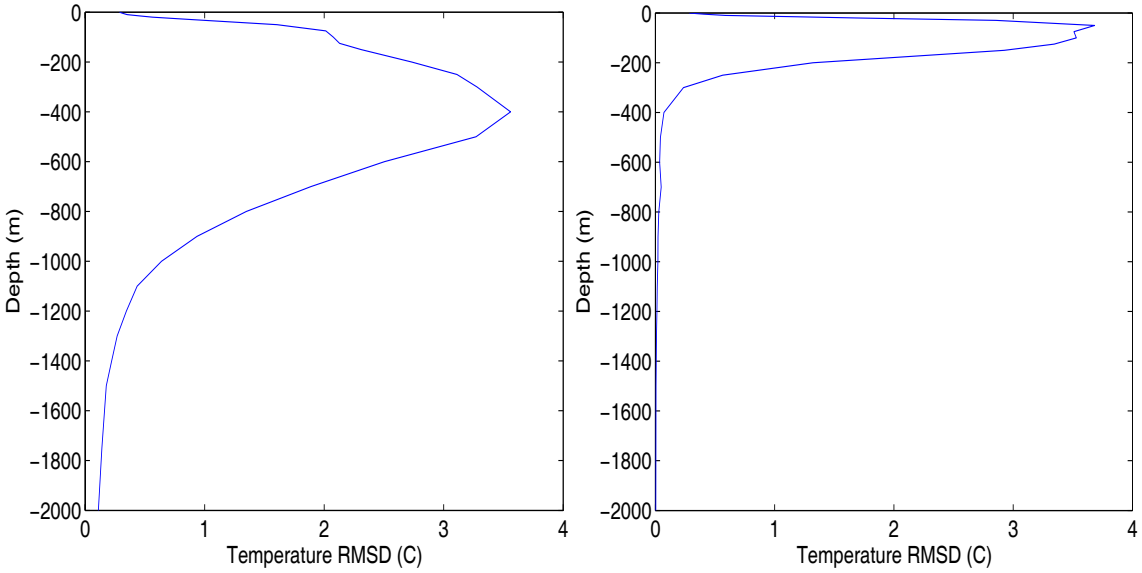

Figure 6. Vertical RMSD profiles for KCA (left) and SOJ (right) October.

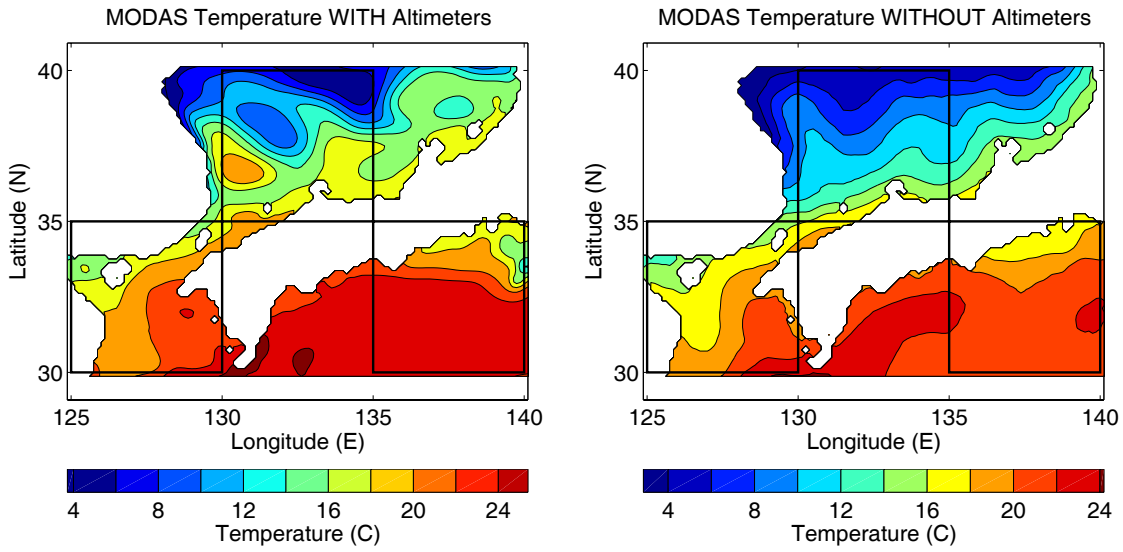

Figure 7. MODAS temperature at 100 m on Oct 10, 2001.

A comparison of the horizontal temperature fields on Oct 10 at 100 m (Figure 7) and 500 m (Figure 8) lend some explanation for the high RMSD values in these cases. The panel with altimeter data in Figure 7 reveals a subsurface eddy system, comprised of both a warm-core and a cold-core eddy, and a stronger Polar Front in SOJ; the eddies are noticeably absent from the panel without altimeter data. The panel with altimeter data in Figure 8 shows a much stronger subsurface front in KCA, including cooler water to the north and warmer water to the south of the front, than the panel without altimeter data.

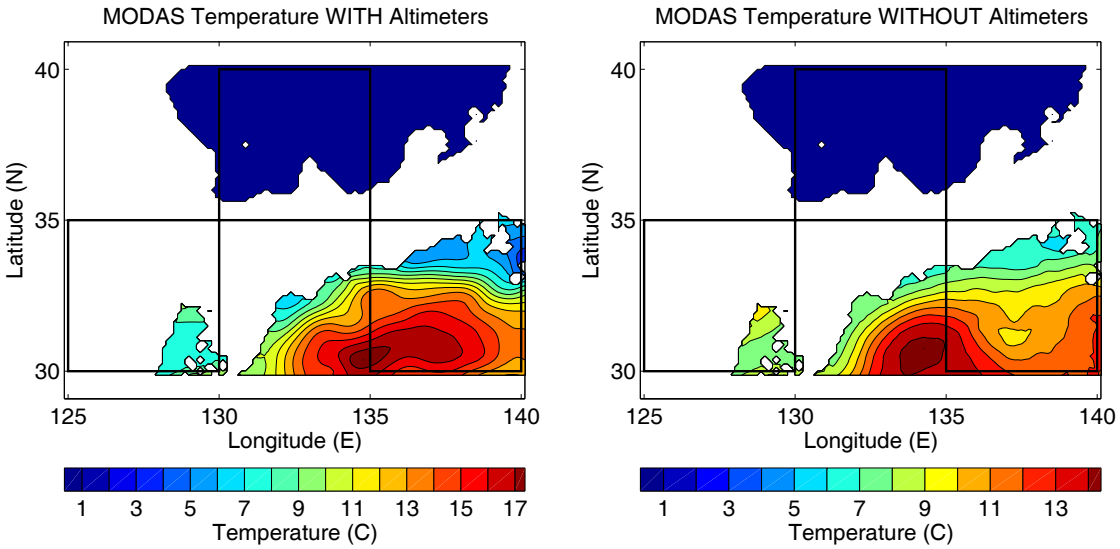

Figure 8. MODAS temperature at 500 m on Oct 10, 2001.

The largest differences in the salinity analyses occurred in the KCA profiles on both days. They had horizontally averaged RMSD values of about 0.15 psu or more, with maximum values in the 200 to 400 m range, as shown in Figure 9. The horizontal salinity fields at 300 m are shown in Figures 10 and 11. Similar to the temperature field shown above, a much stronger front is depicted in the panel with altimetry data, with a larger contrast in salinity on either side of the front. This is true for both days.

As is to be expected, the horizontally averaged RMSD plots for the sound speed fields look very similar to the temperature plots. It follows, then, that the largest values of well over 3 m/s occurred in the Oct 10 profiles for KCA and SOJ at the same depth ranges as the temperature profiles: 300 to 500 m in the KCA profile and 50 to 200 m in the SOJ profile. The other cases with smaller differences in their analyses show similar, although less obvious, patterns between the horizontally averaged RMSD vertical profiles

and the horizontal parameter fields. (All of the MODAS field temperature, salinity, and sound speed statistical plots for each case can be found in Appendix A.)

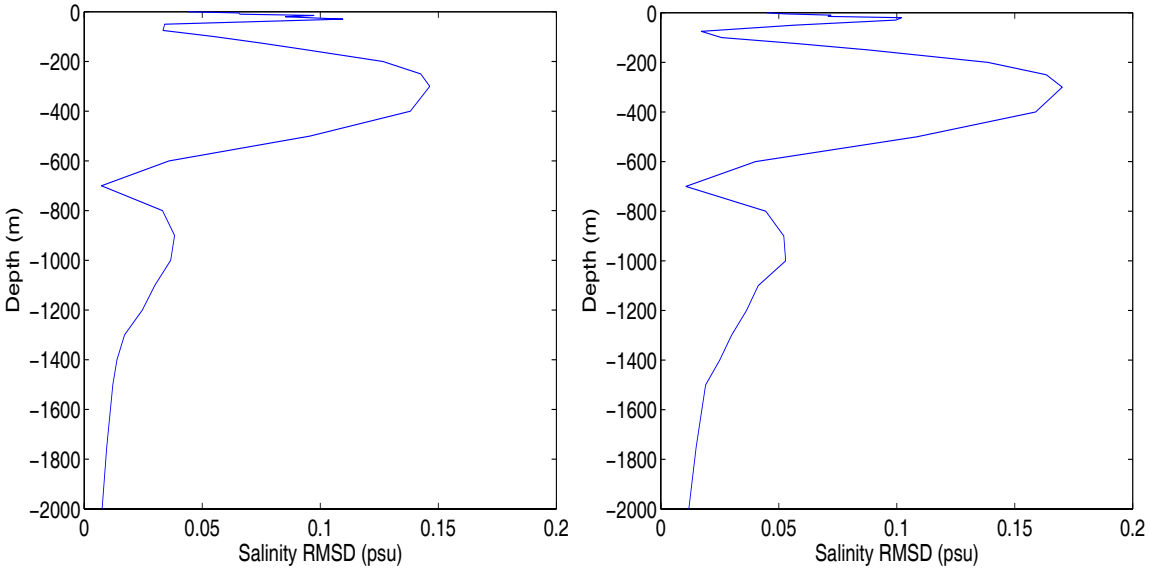

Figure 9. Vertical RMSD profiles for KCA June (left) and October (right).

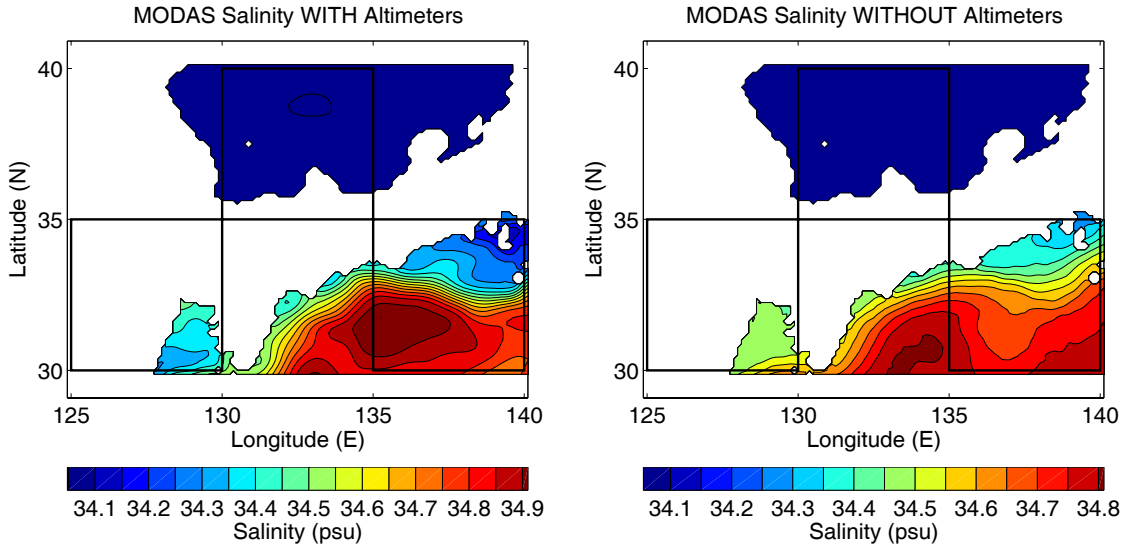

Figure 10. MODAS salinity at 300 m on Jun 30, 2001.

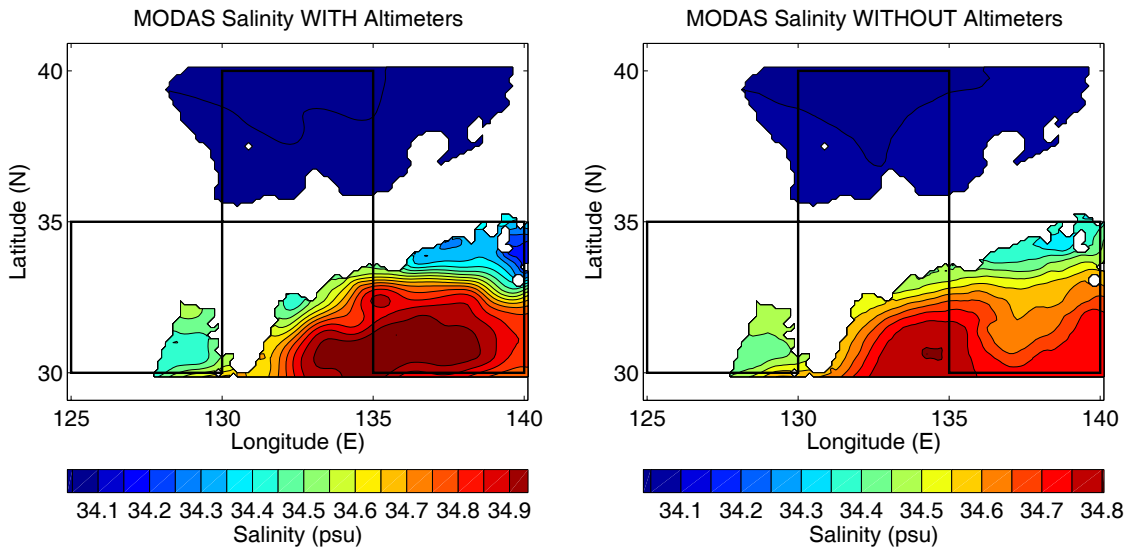

Figure 11. MODAS salinity at 300 m on Oct 10, 2001.

4. Sound Speed Profiles

The horizontally averaged RMSD plots previously discussed help to explain the SSP pattern observed for each case. Figures 12 and 13 illustrate this well for the two cases with the largest differences in the sound speed (and temperature) MODAS analyses, the Oct 10 fields for KCA and SOJ. The nine SSP pairs in each figure are displayed so that their positions correspond to their locations within the area. For example, the top left panel shows the SSP pair for a location in the northwest portion of the box; the center panel is for a location near the center of the box, and so on. (Note: the horizontal scale may change from panel to panel, so care must be taken to understand the relative changes between panels.) This type of display provides the additional information of horizontal positioning of the largest differences as well as their depths. (Appendix B contains all of the MODAS SSP diagrams.)

The largest deviations seen in the SSP pairs in Figure 12 correspond to the depth band already identified as having the largest RMSD values for KCA on Oct 10, that being 300 to 500 m. The top-right, center, and two bottom-left panels show the most deviation and correspond to the locations of the largest temperature differences in Figure 8. The top three panels are profiles from within the front, showing the stronger gradient discovered earlier for the field with altimetry than for the one without. These stronger gradients produce the stronger sound channels evident in the right two panels. The

middle and bottom panels show the result of the field with altimetry having much warmer water to the south of the front: the sound speeds are much faster there. They also show more of a gradient in the non-altimetry field; a result of that field depicting a more spread out front than the tightly packed, stronger front of the altimetry field. Another obvious difference in the center and two bottom-left panels is the second, shallow sound channel in the altimetry field profiles, where one does not exist (or is very weak) in the non-altimetry field.

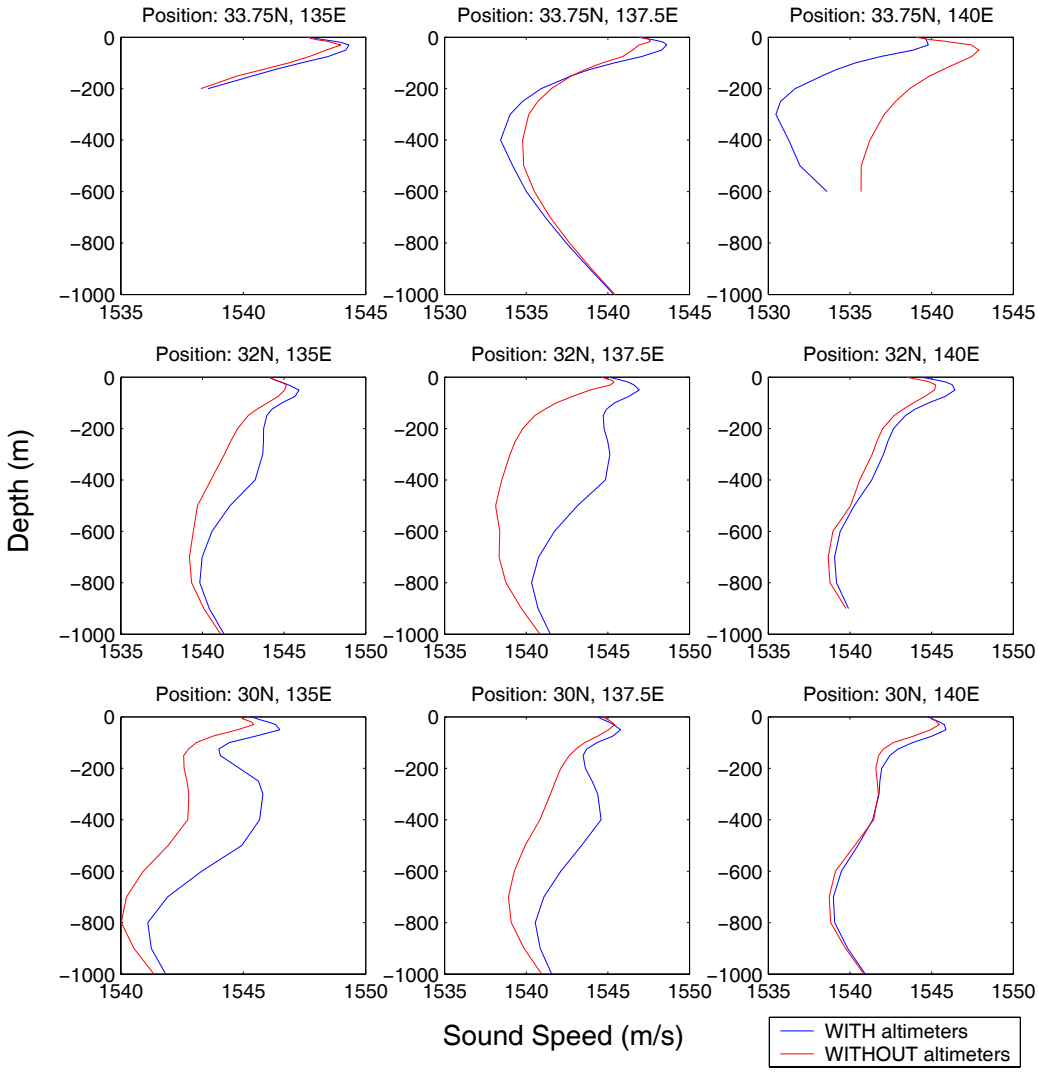

Figure 12. MODAS SSPs for KCA October.

Looking now at SOJ on Oct 10, shown in Figure 13, the largest deviations in the SSP pairs are seen in the left most panels in the upper 200 m, corresponding to where the eddy system was located in Figure 7. In all the panels, for the most part, the altimetry

profiles show higher sound speeds in the upper 300 m or so, this mostly being due to the prevalent warmer temperatures in the altimetry field there. Very noticeable in the middle and bottom panels is a more pronounced sonic layer at the surface in the altimetry fields, corresponding to the existence of, or a deeper, mixed layer.

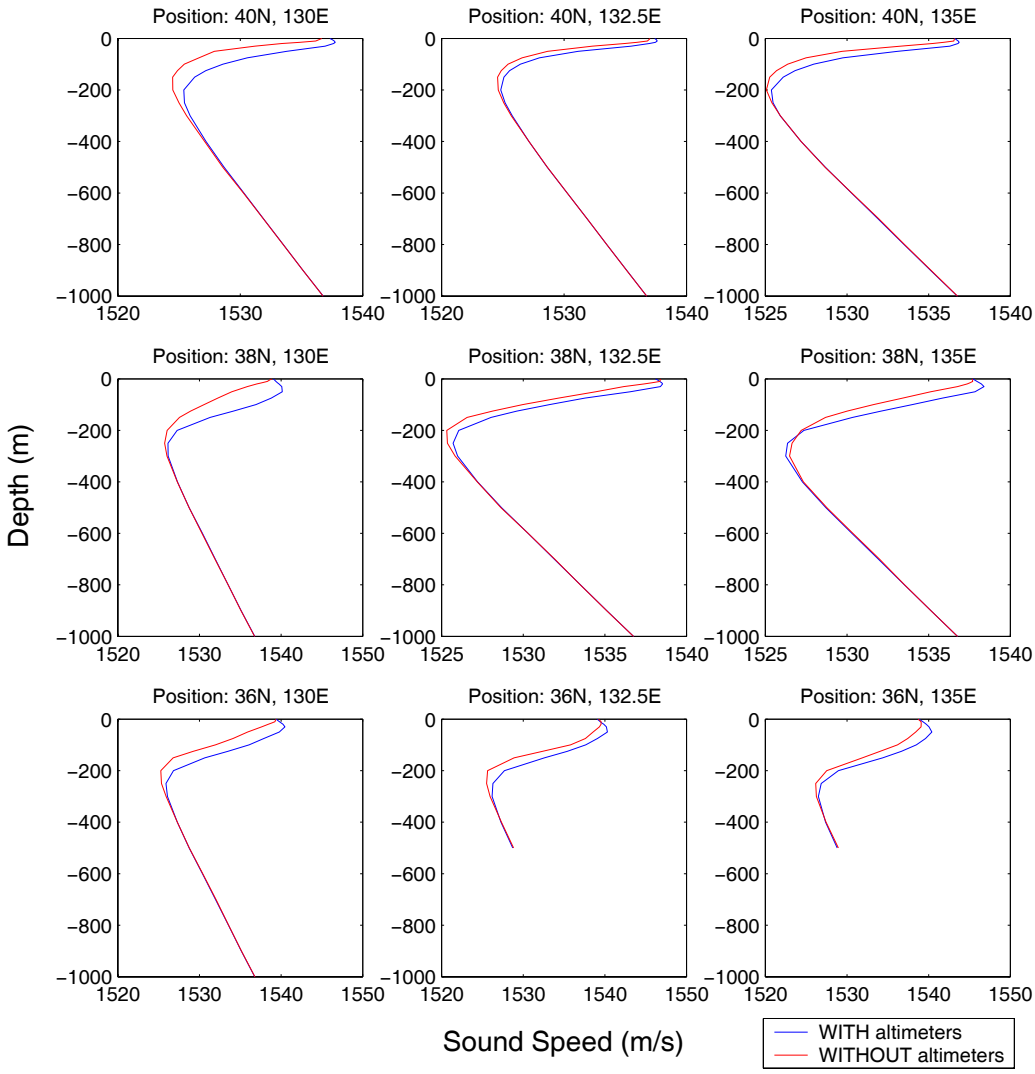

Figure 13. MODAS SSPs for SOJ October.

The differences in the MODAS fields may have an effect on the output of WAPP, depending on the sensitivity of WAPP to changes in input. The cases highlighted here have fairly significant differences in the temperature, salinity, and sound speed fields. WAPP would have to be extremely insensitive to changes in input for these differences to have little impact on its output.

THIS PAGE INTENTIONALLY LEFT BLANK

III. WAPP

A. BACKGROUND

WAPP is an automated, interactive program designed to provide the fleet with an onboard means of generating acoustic presets for multiple variants of Mk 48 torpedoes and visualizing their performance. Developed by Naval Undersea Warfare Center (NUWC), Division Newport, RI, it consists of several elements including a graphical user interface (GUI) for entering various data, a computational engine for generating acoustic performance predictions, and various forms of output (NUWC, 2004).

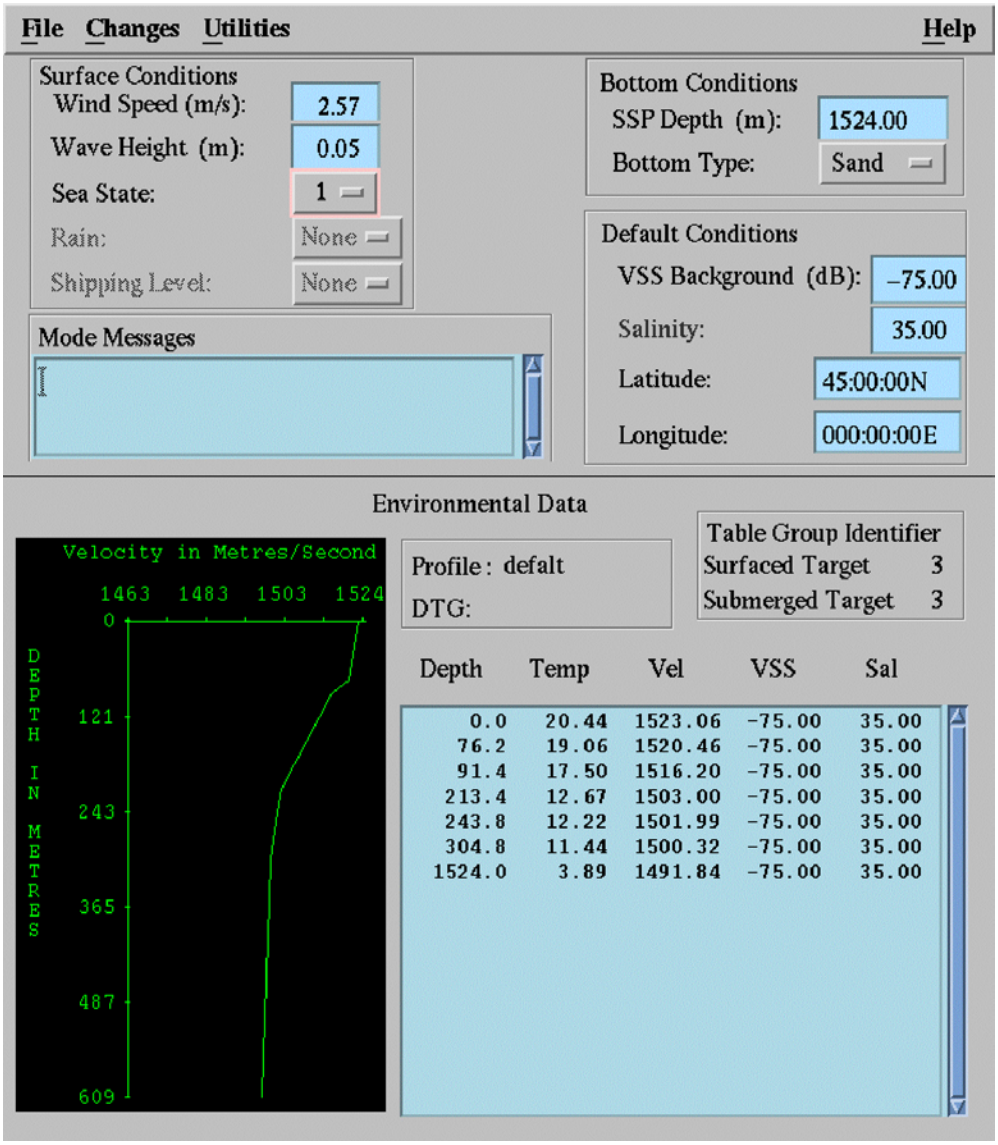

Figure 14. EDE window (From Ref. NUWC, 2004).

The GUI has several pull-down menus that allow the user to select between various data input, processing, and output display screens. The types of input data necessary include tactical (such as tactic type and depth zone of interest), target (such as acoustic and Doppler characteristics), weapon (such as type, mod, and active or passive acoustic mode), and environmental information. To input the environmental information, the user selects the "environment" pull-down menu of the GUI to bring up the Environmental Data Entry (EDE) window. This window, shown in Figure 14, allows the entry of water column parameter profiles (such as temperature, salinity, sound speed, and volume scattering strength) for a specified latitude and longitude. Other environmental input entered via the EDE consists of sea surface conditions (wind speed, wave height, and sea state) and bottom conditions (depth and type). Operationally the environmental data is received from the Sonar Tactical Decision Aid.

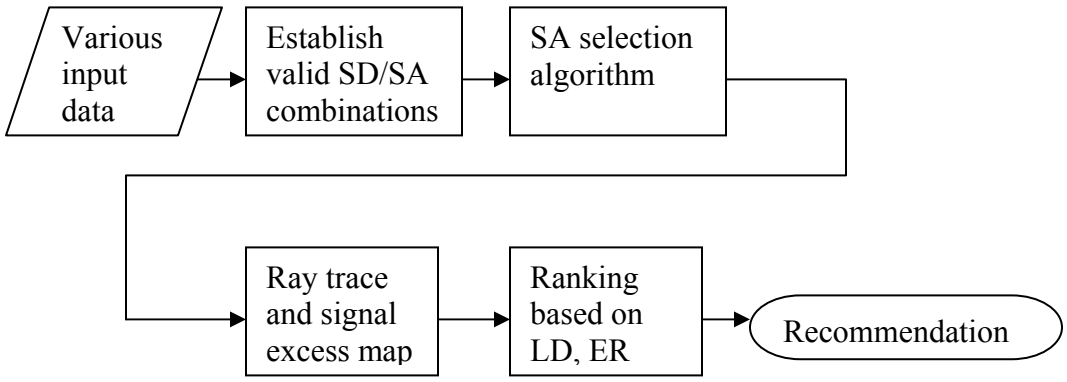

Figure 15. WAPP presetting process flowchart.

Once the necessary information is input (or default values are selected), WAPP is ready to undergo the presetting process. This process is begun by using the "compute" pull-down menu of the GUI and is outlined in Figure 15. The first step is to establish a valid set of search depth / search angle (SD/SA) combinations. The program then invokes a search angle selection algorithm to identify the optimal pitch angle for each search depth. Next, the computational engine traces, in a series of time steps, a fan of rays that bound the torpedo beam pattern for each resulting SD/SA combination (NUWC, 2004). A signal excess computation is performed and mapped to a gridded search region at each time step using the monostatic, active sonar equation for the reverberation limited case,

$$SL - 2TL + TS - RL - DT = SE, \tag{7}$$

where SL is the active sonar source level, 2TL is the two-way transmission loss between the sonar and the target, TS is the target strength, RL is the reverberation level, and DT is the detection threshold (Etter, 1991). The signal excess map is used to determine the effectiveness ratio (the fraction of the prosecutable search region with signal excess greater than 0 dB, also called area coverage) and laminar distance (the location of signal excess center of mass). WAPP then ranks the SD/SA combinations based on these computations (along with some other mitigating factors) and makes a recommendation as to the best preset for the given scenario (NUWC, 2004).

In solving equation (7), the SL, DT, and TS terms are based on properties of the sonar system and target involved, so they are selected by the program or entered by the user, as is the case for TS. The TL and RL terms are computed using a range-independent, ray theory propagation model that accounts for geometric spreading, refractive effects, volumetric effects, and boundary interactions with the ocean surface and bottom. The vertical sound speed profiles used by the ray tracing model can be input via the EDE window or calculated by WAPP from the temperature and salinity profiles using the Chen-Millero-Li equation (APL-UW, 1994). Geometric spreading and refractive losses are determined using the transmission loss equation derived using ray theory

$$TL = 10\log\left(\frac{R_k\left|\frac{\partial R_k}{\partial \theta_o}\sin\theta_k\right|}{\cos\theta_o}\right), \tag{8}$$

where R_k is the horizontal range at some position downrange, θ_o is the initial angle of the ray, and θ_k is the angle of the ray at range R_k. Volume absorption is introduced into the transmission loss term using absorption coefficients calculated from the chemical relaxation equation of Francois-Garrison (APL-UW, 1994).

The reverberation field and losses created by scattering and absorption at the surface and bottom are handled by a group of algorithms included in the Oceanographic

and Atmospheric Master Library's (OAML) High Frequency Environmental Acoustic (HFEVA) Component Models. The HFEVA algorithms are based on environmental acoustic models used in simulation studies at the Applied Physics Laboratory, University of Washington, and include the Surface Absorption Loss Algorithm, the Surface Backscattering Strength Algorithm, the Surface Reflection Loss Algorithm, the Bottom Reflection Loss Algorithm, and the Bottom Backscattering Strength Algorithm (NAVO, 2004). The water column profile values and surface and bottom conditions input via the EDE window are used by these FORTRAN routines.

To offer a means of user interaction, the output of WAPP is in the form of a ranked listset of search depths, pitch angles, laminar distances, and effectiveness values. This allows the user to view all SD/SA combinations, not just the recommended one, and select the most appropriate one for the situation. The listset is, therefore, a list of possible presetting choices from which the operator can choose. In addition, the ray traces and signal excess maps are viewable using the GUI's "acoustic coverage" pull-down menu. These forms of output provide a visual interpretation of the acoustic performance of the torpedo, including boundary interactions and refraction effects.

B. RAY THEORY MODEL

Ray theory models, such as the one used by WAPP, use a technique called ray tracing to calculate transmission loss (Etter, 1991). Beginning with the linear, second-order, time-dependent form of the wave equation,

$$\nabla^2 \Phi = \frac{1}{c^2} \frac{\partial^2 \Phi}{\partial t^2}, \tag{9}$$

where ∇^2 is the Laplacian operator, Φ is the potential function for the sound pressure field, c is the sound speed, and t is the time; if a harmonic type disturbance of the form $\Phi = \phi e^{-i\omega t}$, which describes a fixed source that vibrates at a single sinusoidal frequency, ω, is assumed to be the solution, then equation (9) reduces to the Helmholtz equation,

$$\nabla^2 \phi + k^2 \phi = 0. \tag{10}$$

In equation (10), ϕ is the time-independent potential function, or the sound pressure field's spatial structure, and k is the wave number (ω/c). The objective of ray theory is to solve the Helmholtz equation by trying a local plane wave solution of the form $\phi = Ae^{iP}$, where $A = A(r,z)$ is the pressure amplitude function and $P = P(r,z)$ is the phase function, or eikonal. Doing this and collecting real and imaginary terms yields an equation that defines the ray geometry,

$$\frac{1}{A}\nabla^2 A - \left[\nabla P\right]^2 + k^2 = 0, \tag{11}$$

and one that determines the wave amplitudes,

$$2\left[\nabla A \bullet \nabla P\right] + A\nabla^2 P = 0, \tag{12}$$

respectively.

The basic assumption behind ray theory is the geometrical acoustics approximation, $\frac{1}{A}\nabla^2 A \ll k^2$, which simply requires that the change in sound speed be small over one wavelength. Using this approximation, the first term in equation (11) can be neglected, reducing it to the eikonal equation,

$$\left[\nabla P\right]^2 = k^2, \tag{13}$$

from which differential equations for rays can be derived (Etter, 1991). The rays are the normals to surfaces of constant phase (P=constant), or the wavefronts, along which the wavefronts propagate. For the range-independent case, where c=c(z), solving the ray equations produces Snell's Law:

$$\frac{\sin\theta}{c} = \frac{\sin\theta_0}{c_0} = a, \tag{14}$$

where θ is the angle of incidence of the ray, the subscripted terms denote initial values, and a is the ray parameter. For the more complicated range-dependent case, c=c(r,z), the solution requires a modification to Snell's Law. In either case, ray tracing is accomplished by determining the path along which the ray parameter is conserved.

Since the propagation model uses ray theory, it has all the shortcomings associated with it, such as being limited to higher frequencies. In this case, this is an acceptable condition because the Mk 48 torpedo has a suitably high operating frequency. Another deficiency of ray theory is the poor handling of shadow zones due to the assumption that no acoustic energy leaks out of the ray tube. This is also acceptable because, from a weapon presetting standpoint, it is unrealistic to direct a torpedo to home in on a target in a shadow zone, so an accurate description of the sound field there is not necessary. Finally, ray theory has the issue of causing energy to approach infinity at caustics and turning points. This last concern is mitigated through the use of a caustic correction that modifies the propagation equations, thereby avoiding the case where the denominator becomes zero, and approximates the signal level near the caustic.

Because the propagation model is range-independent, it assumes cylindrical symmetry, meaning it does not have range-varying properties. For example, sound speed is a function of depth only and, since bathymetry is absent, a flat, homogeneous bottom is used. Therefore, the resulting ray traces are assumed to be valid for any direction from the source location, as the model environment looks the same down any bearing (Etter, 1991). This is not ideal for determining accurate sound propagation characteristics, especially in regions where the oceanography changes rapidly with horizontal distance, and could affect the weapon presets. Under less variable conditions, this shortcoming would probably have little or no affect on the weapon presets, as the typical Mk 48 torpedo engagement would only involve a few kilometers of ocean. Regardless, there is an effort currently underway to utilize the Comprehensive Acoustic Sonar Simulation (CASS) for range-dependent performance predictions for torpedo presetting. The assumption of range independence is consistent with the large number of areas where there is little to no bathymetric variation over torpedo detection ranges and also with cross-slope predictions in more variable environments, and so provides a reasonable assessment of the importance of satellite altimetry data using the current weapon system.

C. APPLICATION

As stated earlier, WAPP was used in this study as the yardstick for measuring sensitivity to satellite altimetry data assimilation by MODAS. To accomplish this, a

routine was developed by NUWC, Division Newport, that broke down each MODAS field into its constituent grid points and fed them into WAPP one by one (bypassing the EDE manual data entry window). WAPP then performed its presetting process for each MODAS grid point using the vertical profile data for each location. (Grid points over land had no vertical profiles, of course, and were discarded.) The vertical sound speed profile was calculated by WAPP from the temperature and salinity profiles, as opposed to using the sound speed profile available from the MODAS field. The same default values for volume scattering strength and surface and bottom conditions were used for each run. This procedure was repeated for the two MODAS field versions, for both days, for each geographic region, and for all five tactical scenarios. The tactical scenarios were prescribed using the GUI to change the tactic ("surface craft" for the ASUW scenarios, "unknown sub" for the ASW scenarios), the target maximum depth (50 ft for the ASUW scenarios, 700 ft for the shallow ASW scenarios, and 1300 ft for the deep ASW scenarios), and the target Doppler ("low" for the low Doppler scenarios, "high" for the high Doppler scenarios).

Recalling from the MODAS section, the number of vertical profiles available for each case (region and day) was: 1,495 pairs for SOJ; 1,448 pairs for ECS; and 1,436 pairs for KCA, for a total of 4,379 pairs. Since one listset was produced for each profile and five different tactical scenarios were run for each case, five times as many listsets were produced as there were MODAS profiles. These listsets can be considered as pairs, just as the vertical profiles were; one pair for each location, day, and tactical scenario, each being comprised of one listset for each of the two MODAS field versions.

To compare each pair of listsets, a configuration management program and its included statistical software package was employed. This program was actually designed to check WAPP output for differences during verification testing upon completion of software upgrades. In that application, the input is held constant between the two WAPP software versions, so any differences in output are due to software changes (the aim is to have no differences). For the current application, the input was varied and the WAPP version was held constant. Therefore, any differences in the output can be attributed to differences in the input.

The statistical package produced multiple tables of various differences in the listsets. The tables that listed relative differences in area coverage for different SD/SA combinations were selected for in depth analysis based on the following reasoning. The presetting process had generated pairs of listsets in which some SD/SA combinations were the same and some were different. The listset can be thought of as a list of presetting choices; the choices on one list sometimes matched those on the other list and sometimes they did not. The instances in which WAPP produced different SD/SA combinations for a profile pair are the cases in which an actual engagement would have greater potential for a different outcome because, given these different choices, the torpedo would not be searching at the same depth, looking at the same search angle, or both. Determining the sensitivity of WAPP to input differences in these cases was important because of the potential for weapon effectiveness to be affected. The thing to remain aware of here is that the actual environment is whatever it is, regardless of differences in the MODAS fields. In the cases where the same SD/SA combinations (same choices) were generated for the two MODAS versions, the outcome of the engagement would be very similar, subject to other targeting considerations, because the same presets and environment were involved.

Utilizing MATLAB coding and graphing tools, the table for each scenario was converted into a histogram by reading in digital versions of the tables and plotting the values. Each histogram displays the number of different SD/SA combinations with area coverage relative differences in specified ranges, or bins. The probabilities of the relative difference being greater than 0.1, 0.2, and 0.5 were determined, as was the mean of the relative differences for each histogram. These histograms were the basis for the technical analysis that follows.

IV. RESULTS

A. GENERAL STATISTICS

For the most part, in each of the 30 scenario histograms (found in Appendix C), the number of different SD/SA combinations dropped off with increasing relative difference. In other words, the peak in relative difference was usually in the lowest bin (less than 0.05) and decreased with each successive bin in a decaying fashion, as illustrated by the left panel in Figure 16. The most notable exceptions are the two ASUW tactics for the SOJ October case, which have peaks in the bin for 0.3 to 0.4, one of which is shown in the right panel of Figure 16. (Relative difference as used here is the fractional change in area coverage obtained by dividing the absolute difference in the two area coverages by the original one: $RD = |AC_1-AC_2|/AC_1$.)

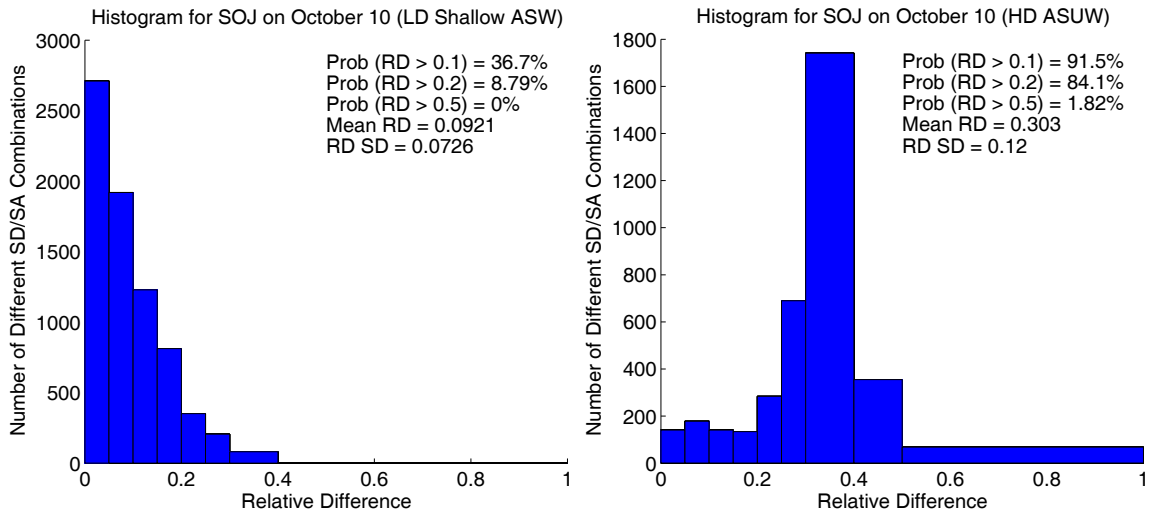

Figure 16. Example histograms.

The next two figures display collectively some of the values determined for each histogram, including the probabilities of the relative differences being greater than 0.1 and 0.2, hereafter referred to as Prob(RD>0.1) and Prob(RD>0.2), respectively; and the mean of the relative differences, hereafter referred to as mean RD. The results are grouped by case and broken down into each tactic.

Figure 17 shows the two probability curves, which tend to parallel each other with varying amounts of separation between them. The general trend for each case (except for SOJ June) was for the probability values to decrease with increasing tactic depth band. In

other words, one or both ASUW tactics tended to have the highest probability values followed by the shallow ASW tactic, with the deep ASW tactics having the lowest probability values. Interestingly, this trend was reversed for the SOJ June case. The other obvious tendency was for the values of Prob(RD>0.1) to be several times greater than the values of Prob(RD>0.2), reiterating the decaying pattern.

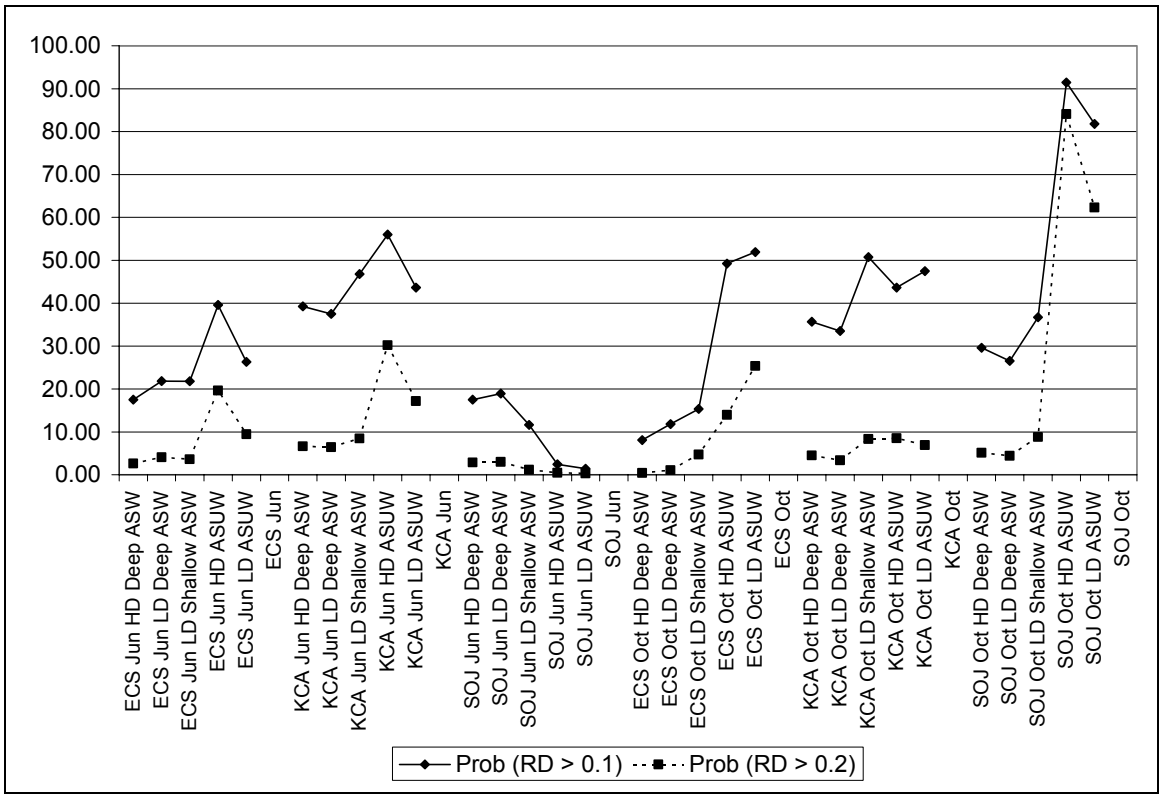

Figure 17. WAPP RD probabilities by scenario.

The highest Prob(RD>0.1) was 91.5%, attained by the high Doppler ASUW tactic in the SOJ October case. The low Doppler ASUW tactic in the same case also had a high value at 81.8%. The next highest were in the fifty percent range. The same two scenarios also achieved the highest Prob(RD>0.2), with 84.1% and 62.3%, respectively. The next highest values were about 30 percent or lower. Only nine of the histograms had non-zero Prob(RD>0.5) values (not shown in the figure), all of them being for ASUW tactics, the largest of which was a mere 1.8%. These scenarios with high probability values are the ones in which the outcome of an engagement would most probably be different because they had a higher chance of having large differences in predicted performance.

The lowest Prob(RD>0.1) was 1.4%, attained by the low Doppler ASUW tactic in the SOJ June case. The high Doppler ASUW tactic in that case also had a very low value of 2.4%. The next lowest was over three times the probability at 8.1%. The same two scenarios also achieved two of the lowest Prob(RD>0.2), with 0.3% and 0.5%, respectively. The high Doppler deep ASW tactic for ECS October had the other lowest value of 0.4%. The next lowest values were greater than one percent. These scenarios with low probability values are the ones least likely to have had an impact on engagement outcome because they have a very low chance of having large differences in predicted performance.

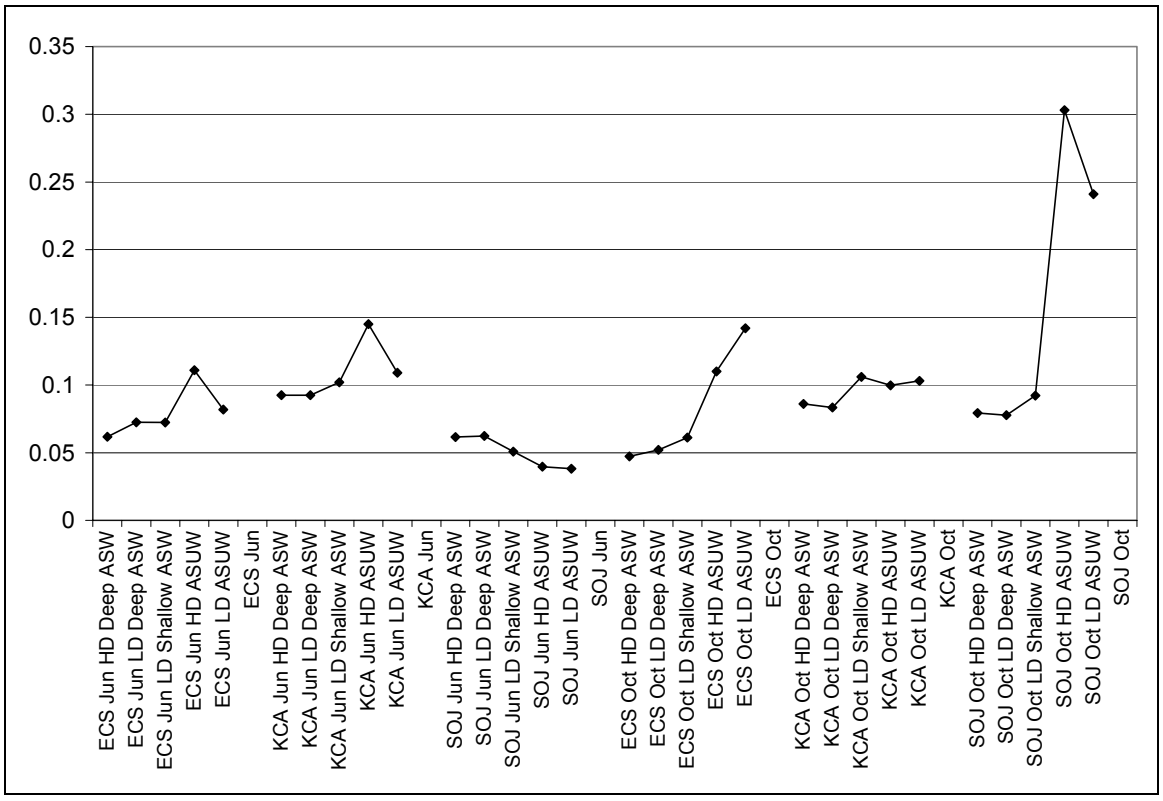

Figure 18. WAPP mean RDs by scenario.

Figure 18 shows the mean RDs, which followed the probability curves fairly closely. Once again, the values decreased with tactic depth band, except for the same maverick as before: the SOJ June case. This pattern makes sense since scenarios with a higher mean RD would be expected to have a higher probability of having larger relative differences. The highest mean RDs were 0.303 and 0.241, attained again by the high and low Doppler ASUW tactics in the SOJ October case, respectively. The next highest were

less than 0.15. The lowest mean RDs were 0.0382 and 0.0396, attained again by the low and high Doppler ASUW tactics in the SOJ June case. The next lowest was 0.0472.

The following tables, each for a different case, display in tabular format the same information as the two previous figures, but with the addition of Prob(RD>0.5) values.

	ECS Jun HD Deep ASW	ECS Jun LD Deep ASW	ECS Jun LD Shallow ASW	ECS Jun HD ASUW	ECS Jun LD ASUW
Prob (RD > 0.1)	17.51	21.82	21.77	39.59	26.29
Prob (RD > 0.2)	2.64	4.10	3.65	19.63	9.45
Prob (RD > 0.5)	0.00	0.00	0.00	0.28	0.06
Mean RD	0.0618	0.0725	0.0723	0.111	0.0818

Table 1. ECS June WAPP output.

	KCA Jun HD Deep ASW	KCA Jun LD Deep ASW	KCA Jun LD Shallow ASW	KCA Jun HD ASUW	KCA Jun LD ASUW
Prob (RD > 0.1)	39.26	37.52	46.76	55.98	43.62
Prob (RD > 0.2)	6.63	6.44	8.46	30.19	17.20
Prob (RD > 0.5)	0.00	0.00	0.00	0.05	0.04
Mean RD	0.0924	0.0925	0.102	0.145	0.109

Table 2. KCA June WAPP output.

	SOJ Jun HD Deep ASW	SOJ Jun LD Deep ASW	SOJ Jun LD Shallow ASW	SOJ Jun HD ASUW	SOJ Jun LD ASUW
Prob (RD > 0.1)	17.50	18.91	11.63	2.43	1.43
Prob (RD > 0.2)	2.86	3.03	1.20	0.47	0.34
Prob (RD > 0.5)	0.00	0.00	0.00	0.00	0.00
Mean RD	0.0616	0.0623	0.0509	0.0396	0.0382

Table 3. SOJ June WAPP output.

	ECS Oct HD Deep ASW	ECS Oct LD Deep ASW	ECS Oct LD Shallow ASW	ECS Oct HD ASUW	ECS Oct LD ASUW
Prob (RD > 0.1)	8.11	11.83	15.36	49.23	51.90
Prob (RD > 0.2)	0.42	1.09	4.71	13.99	25.39
Prob (RD > 0.5)	0.00	0.00	0.00	0.00	0.99
Mean RD	0.0472	0.052	0.0611	0.11	0.142

Table 4. ECS October WAPP output.

	KCA Oct HD Deep ASW	KCA Oct LD Deep ASW	KCA Oct LD Shallow ASW	KCA Oct HD ASUW	KCA Oct LD ASUW
Prob (RD > 0.1)	35.68	33.48	50.74	43.63	47.49
Prob (RD > 0.2)	4.53	3.38	8.34	8.51	6.93
Prob (RD > 0.5)	0.00	0.00	0.00	0.02	0.07
Mean RD	0.0861	0.0834	0.106	0.0997	0.103

Table 5. KCA October WAPP output.

	SOJ Oct HD Deep ASW	SOJ Oct LD Deep ASW	SOJ Oct LD Shallow ASW	SOJ Oct HD ASUW	SOJ Oct LD ASUW
Prob (RD > 0.1)	29.61	26.55	36.71	91.45	81.77
Prob (RD > 0.2)	5.11	4.41	8.79	84.11	62.30
Prob (RD > 0.5)	0.00	0.00	0.00	1.82	1.01
Mean RD	0.0793	0.0777	0.0921	0.303	0.241

Table 6. SOJ October WAPP output.

For the deeper-based tactics, at least three factors seemed to influence the amount of relative difference in the WAPP output. The first was the horizontally averaged sound speed RMSD peak value for the MODAS fields (refer to Appendix A for MODAS sound speed RMSD and other statistical plots). When this was high, so were the mean RD and probability values. The second factor was the depth of this peak. A deep RMSD peak axis tended to lead to high WAPP output values. Finally, the shape of the peak played a part, as the higher values can also be associated with broader peaks vice narrower ones. The cases with the obviously larger values in Figure 19, which shows WAPP output values for both of the deep ASW tactics, are the SOJ October case and both of the KCA cases (the same is true for the shallow ASW tactic). All three of these had one or more of the aforementioned factors in their favor.

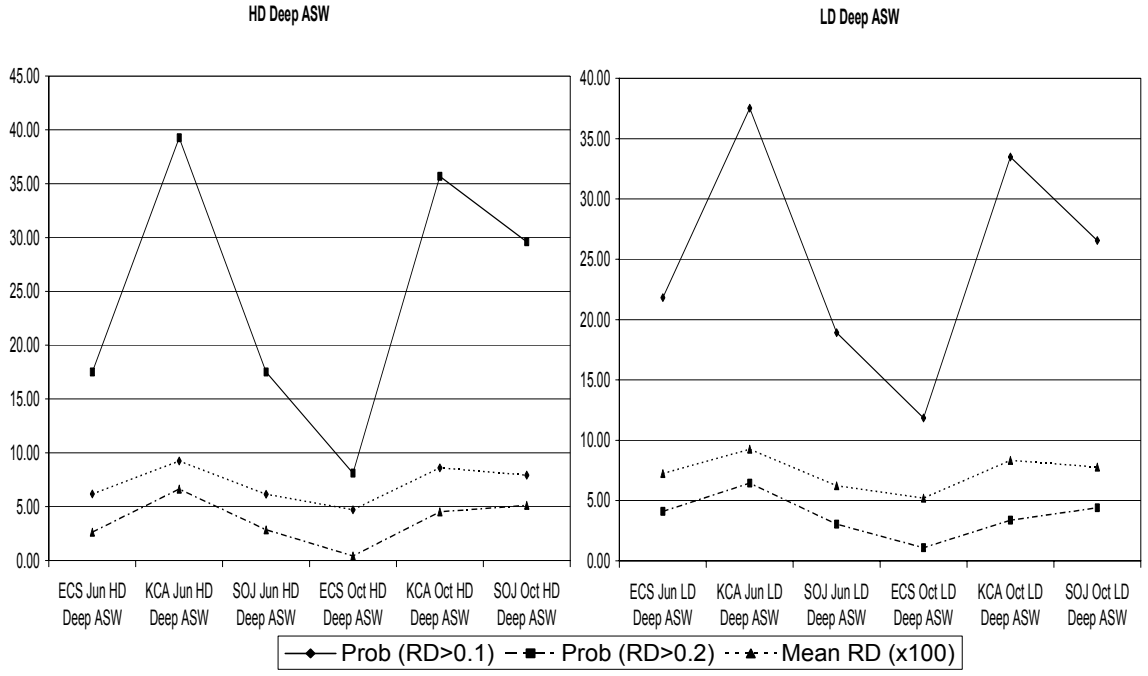

Figure 19. Deep ASW WAPP output values.

These results can be understood with help from Figure 6, the RMSD plot for KCA October, which shows that RMSDs of 2 m/s or more occurred in a band from about 100

m to 700 m. This band encompasses much of the depth zones of interest for both the deep and shallow ASW tactics (down to about 400 m and 200 m, respectively). The MODAS SSPs in Figure 12 further illustrate the large differences in the sound speed fields at these depths. The larger these differences (higher the RMSD peak value) and the more they extend into the depth zone of interest (owing to the depth and shape of the peak), the larger the difference in the predicted sound propagation for the two MODAS fields in that depth zone, thus leading to the large probability and mean RD values in WAPP's output for the ASW tactics.

B. PHYSICAL MECHANISMS

1. Sonic Layer

A quick look at the SSPs, shown in Appendix B, helps to physically explain the reason why the ASUW tactics often had large mean RDs. In every case, except SOJ June, one of the two MODAS fields showed a more pronounced sonic layer at the surface in at least one location, as seen earlier in Figures 12 and 13. A sonic layer occurs when the sound speed increases with depth from the surface to a maximum then decreases below, as seen in Figure 20.

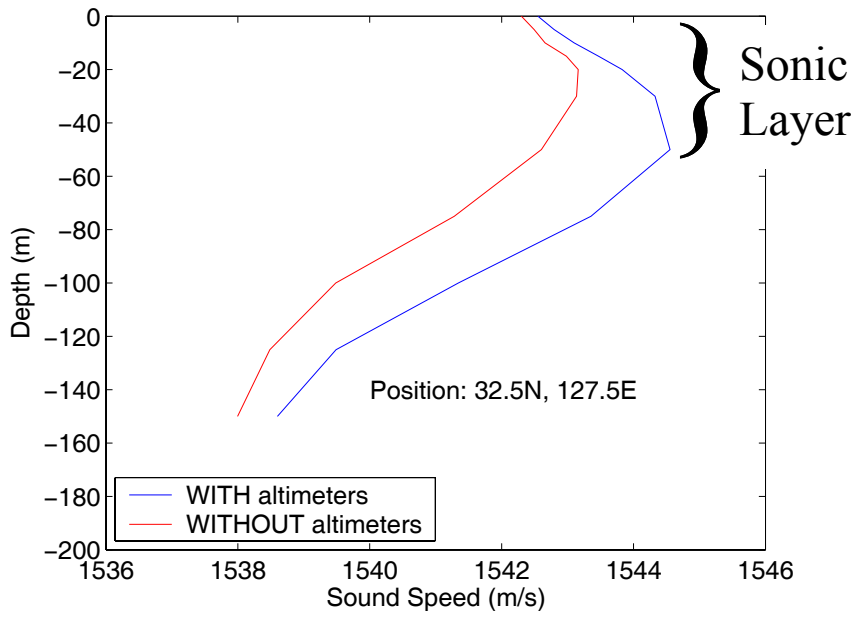

Figure 20. Existence of a sonic layer (October 10, 2001).

A stronger sonic layer would have two effects on near surface sound propagation characteristics. If the sound source were in the layer, it would more effectively trap the sound energy by refracting it back to the surface, where it would be reflected back into the water, allowing it to travel greater distances before being diminished. For a source below the layer it would more effectively prevent sound energy from penetrating into it by refracting it down away from the layer, creating a relatively sound-free layer near the surface. Because only one of the MODAS fields produced these effects in each case, the sound propagation characteristics near the surface would differ substantially resulting in equally dissimilar predictions of sound propagation. This is what led to more significant differences in the presets that WAPP produced for the shallower-based tactics.

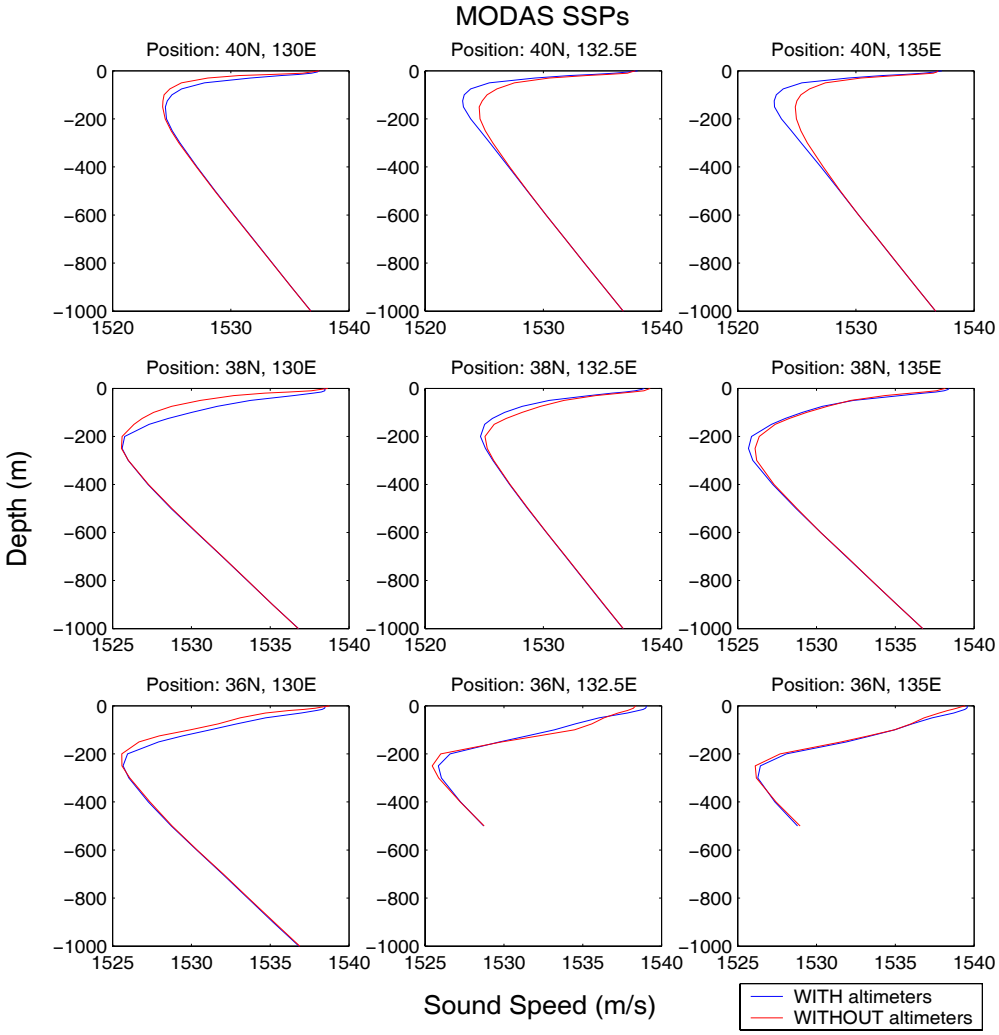

Figure 21. No sonic layer for SOJ June case.

On the other hand, as shown in Figure 21, none of the SSPs in the SOJ June case had a sonic layer or any other near surface variations between the two MODAS sound speed fields, leading to very similar sound propagation characteristics near the surface. The sound propagation predictions would, therefore, be alike and resulted in the minimal differences in output for these ASUW scenarios.

2. Sound Channel

One reason for the differences in the ASW scenarios is the existence of sound channels. Sound channels exist when sound speed first decreases with depth then increases again (see Figure 22). This produces a refractive environment that focuses the sound energy in a depth band about the channel axis, due to bending above and below the axis. This focusing allows the sound to be detectable at longer distances than it otherwise would because it is less spread out and, thus, more intense. When a sound channel exists or is stronger in one MODAS field, the channeling effect produces significant differences in sound propagation between the two fields.

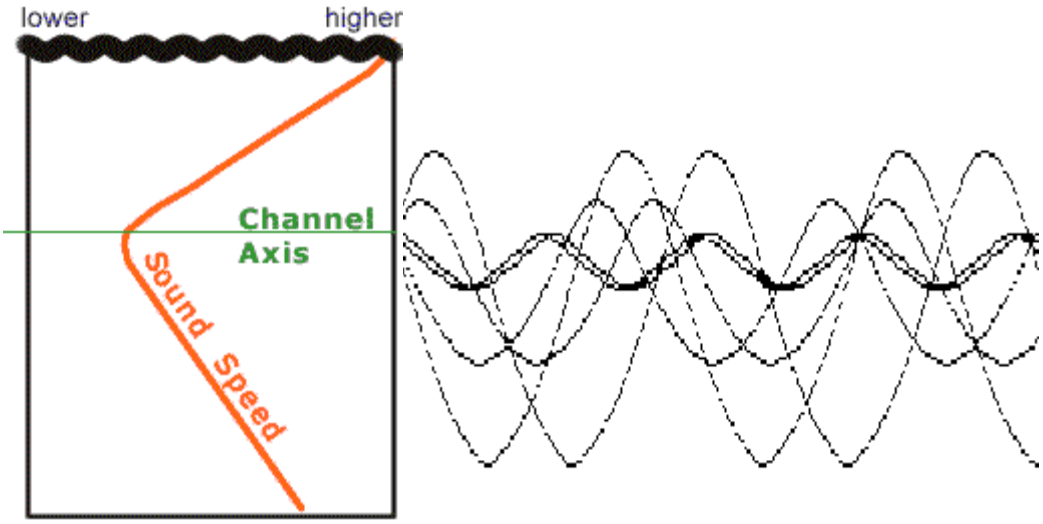

Figure 22. Sound channel depiction.

C. EXTREME CASES

The two cases with the largest relative differences in WAPP area coverage for ASUW and ASW tactics deserve a closer look: the SOJ October case for ASUW tactics, and the KCA Jun case for ASW tactics. The former case was examined in detail during the MODAS discussion. Recall that RMSDs greater than 3 °C existed in a band from 50

to 200 m due to both a subsurface eddy system and a stronger SOJ Polar Front. These produced large differences in the SSPs in this depth band, shown again in Figure 23 for ease of reference, and now shown statistically in Figure 24 by the horizontally averaged RMSD and bias plots. The result was a very pronounced sonic layer over much of the SOJ region in the altimetry MODAS field, but almost no layer in the non-altimetry field.

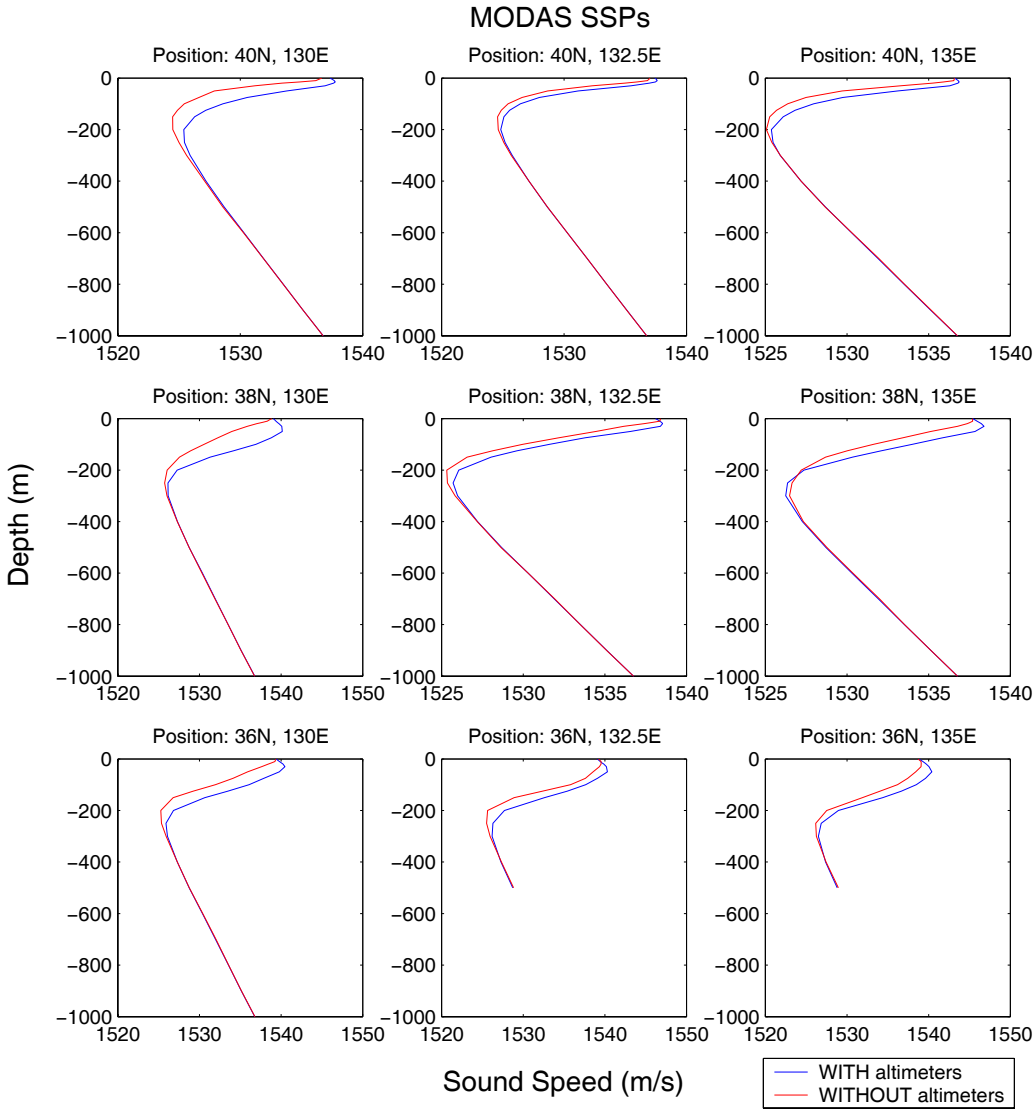

Figure 23. MODAS SSPs for SOJ October.

As discussed earlier, the effect of the sonic layer would be to cause WAPP to generate very different near surface sound propagation predictions for the two MODAS fields, leading to the large relative differences in area coverage. In the histograms for the two ASUW tactics, shown in Figure 25, the radically displaced relative difference peaks

(in the bin for 0.3 to 0.4) as compared to the rest of the histograms are apparent. Once again, these two scenarios had the highest probability values and mean RDs of all the scenarios, not just the ASUW ones, and so were very likely to have had a different outcome in an actual engagement.

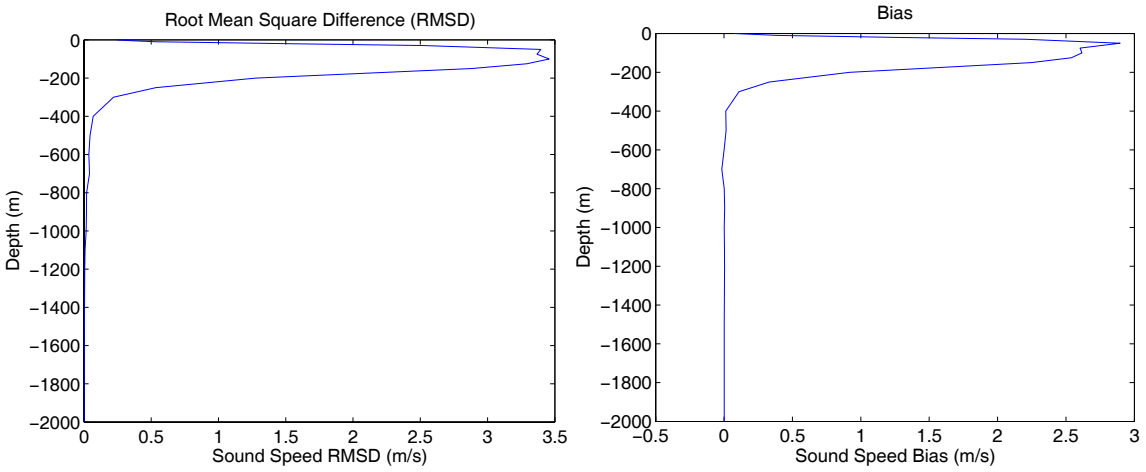

Figure 24. MODAS sound speed statistics for SOJ October.

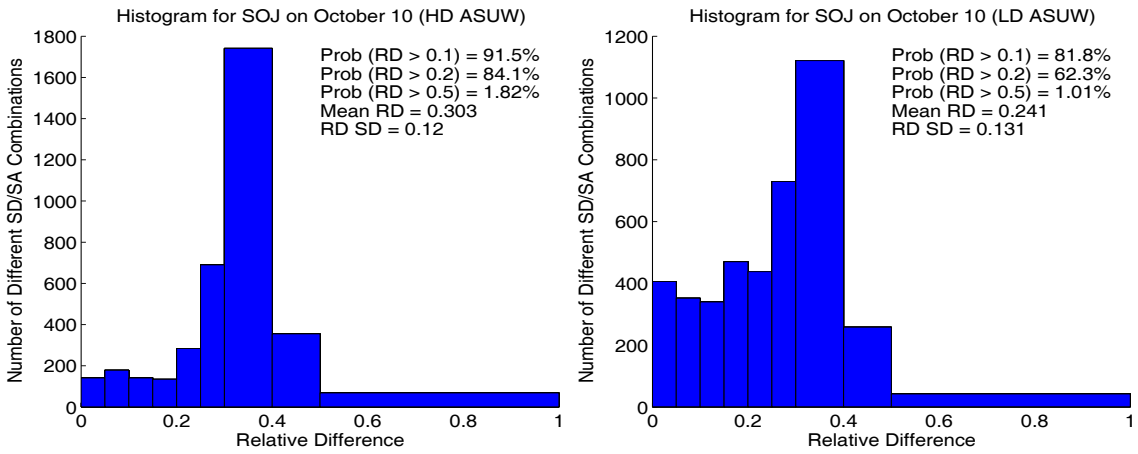

Figure 25. ASUW histograms for SOJ October.

The much larger differences seem to be due to the extra large differences in the MODAS fields. Looking at Figure 23, the sonic layer in the altimetry field was very strong, with sound speed increasing by several meters per second over the depth of the layer in several locations. Some of the other scenarios had equally strong sonic layers, but only in one or two locations. The other big difference that sets these two scenarios apart from the rest is that the other MODAS field (non-altimetry, in this case) had no appreciable sonic layer anywhere in the region. The other scenarios with strong sonic

layers in one field also had a weaker sonic layer in the other field, which helped to offset the difference and apparently limited the affect on WAPP's output.

Shifting now to the largest WAPP output differences for ASW tactics, the KCA June case just edged out the October case in the same region. These two cases had very similar MODAS fields, as discussed in the MODAS chapter, and they were both mentioned earlier as having all three influencing factors in their favor: a high sound speed RMSD peak value, a peak axis well into the depth zone of interest, and a broad peak increasing the extent of the high RMSD values throughout more of the zone of interest.

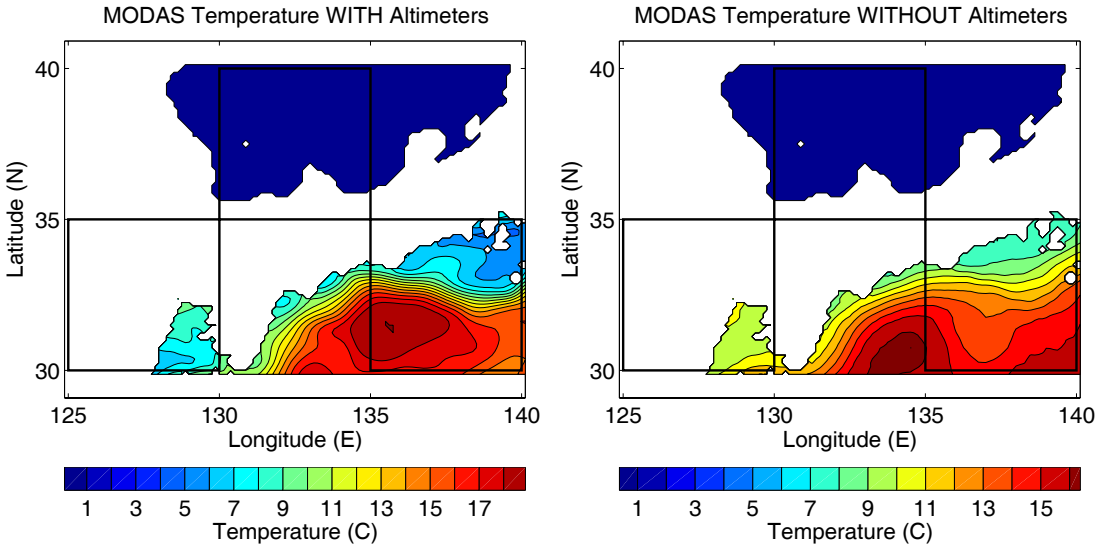

Figure 26. MODAS temperature at 400 m on Jun 30, 2001.

Just like the October 10 temperature fields in Figure 8, the June 30 temperature fields in Figure 26 show a much stronger subsurface front in the panel with altimetry, as well as cooler water to the north and warmer water to the south of the front as compared to the panel without altimetry. The salinity field with altimetry (Figure 10) also indicates the existence of a stronger front.

The combination of these temperature and salinity fields produced the MODAS sound speed field, some of the statistics for which are displayed in Figure 27. Similar to the October timeframe, the largest RMSD and bias values exist in a band from about 100 to 600 m. As discussed for the general case, this depth zone includes much of the ASW zone of interest. Therefore, the predicted sound propagation for the two MODAS fields

in the ASW zone was more dissimilar, thus leading to the large differences in WAPP's output for the ASW tactics.

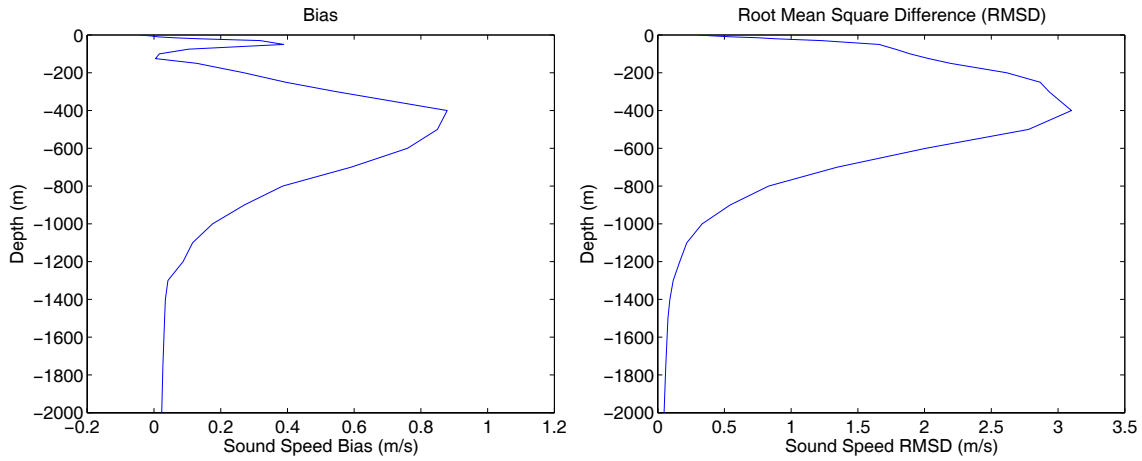

Figure 27. MODAS sound speed statistics for KCA June.

The MODAS SSPs in Figure 28 illustrate characteristics similar to the SSPs for KCA October in Figure 12. The large differences in the sound speed fields in the ASW depth zone of interest are partially due to the MODAS field with altimetry having a stronger sound channel, evident in the top-right two panels, which are produced by the stronger frontal gradients in that MODAS field. Another contribution to the sound speed differences in the ASW band can be seen in the four bottom-left panels, which show a second sound channel with an axis near 100 m in the altimetry field profiles, where one does not exist (or is very weak) in the non-altimetry field. As discussed earlier, these sound channels would refract sound in a way that would significantly affect sound propagation and, therefore, the output of WAPP when using this MODAS field. The outcome of an engagement would probably have been significantly different, depending on which MODAS field was used. For completeness, the histograms for the three ASW tactics are shown in Figure 29.

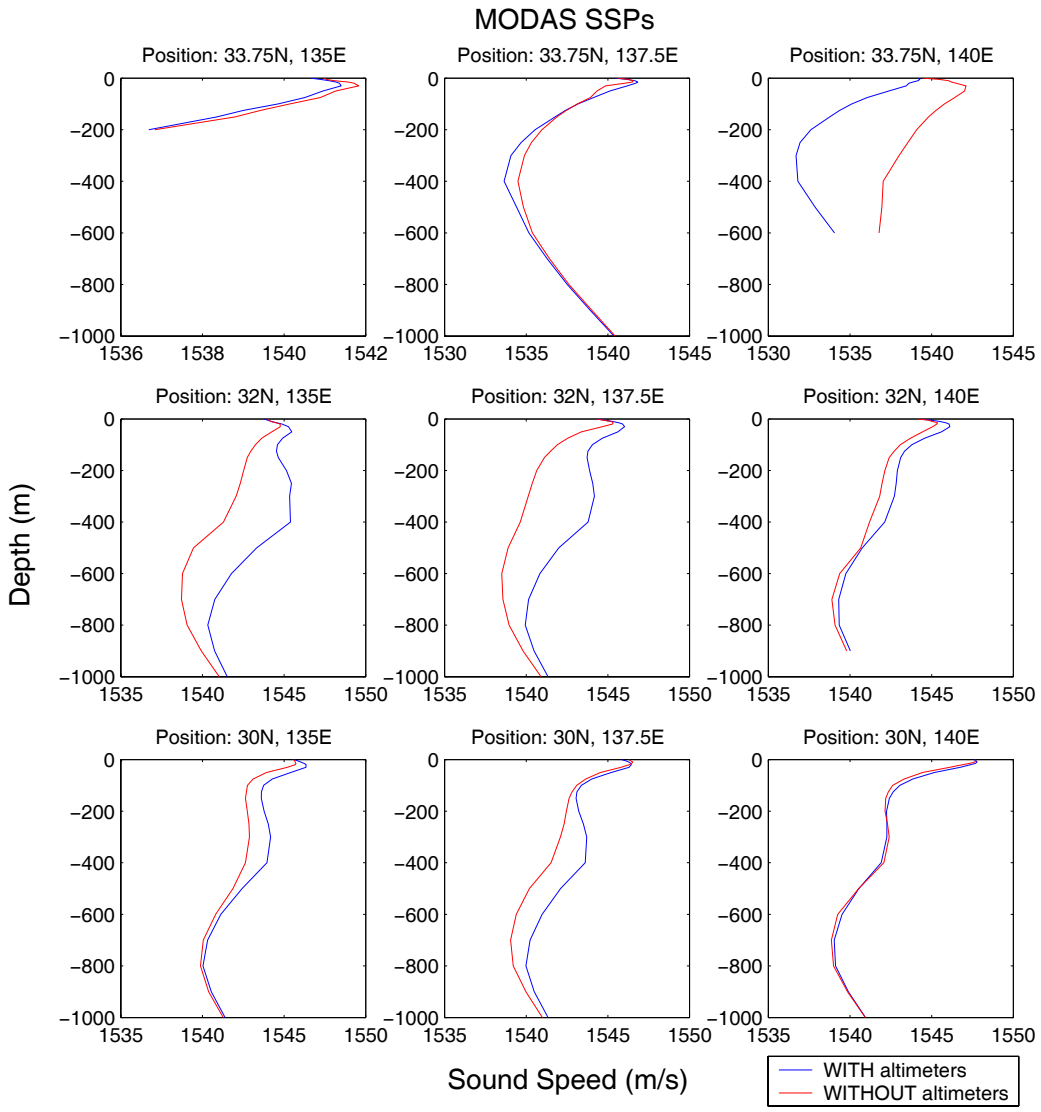

Figure 28. MODAS SSPs for KCA June.

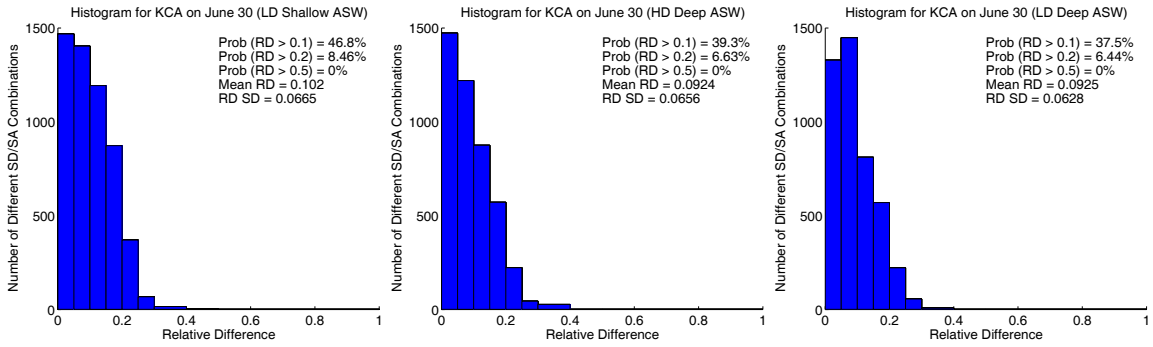

Figure 29. ASW histograms for KCA June.

THIS PAGE INTENTIONALLY LEFT BLANK

V. CONCLUSIONS AND RECOMMENDATIONS

A. CONCLUSIONS

From the preceding discussion it is apparent that, in some of the scenarios, WAPP output was quite sensitive to changes in input environmental fields, such as MODAS with satellite altimetry data assimilated versus MODAS without altimetry data. Table 7 is a compilation of the probability values for each scenario, grouped by case, in an effort to more easily compare the sensitivities of each scenario. The Prob(RD>0.1) and Prob(RD>0.2) columns represent the chance of having a different engagement outcome if one assumes 0.1 and 0.2 are large enough relative differences in area coverage to change the outcome, respectively.

With this in mind, the Prob(RD>0.1) values ranged from 1.4 to 91.5 and the Prob(RD>0.2) values ranged from 0.3 to 84.1, which suggests that the sensitivity of WAPP was extremely variable and, therefore, so was the chance of affecting the outcome of an engagement. Although the ranges were large, most of the 30 scenarios were in the lower halves of them; only one sixth had Prob(RD>0.1) values greater than 50%, one third had values greater than 40%, just over half had values greater than 30%, and only one tenth of the scenarios had Prob(RD>0.2) values greater than 30%. Based on this sensitivity analysis, the satellite altimetry data contributed as much as an 80-90% chance of having a different engagement outcome (once again, assuming 0.1-0.2 is enough of a relative difference in area coverage to change the outcome), but in most of the scenarios the contribution was less than 50%.

The scenarios in which WAPP was the most sensitive were the ones where the input MODAS fields differed significantly, especially in the depth zone of interest for the given tactic. The MODAS fields usually differed in their depiction of mesoscale features, such as eddy systems (as in the case of SOJ October) and subsurface fronts (as in the KCA October and June cases), due to only one field having the benefit of satellite altimetry data to help MODAS resolve them. This resulted in differences in the SSP characteristics for the two fields, such as the sonic layer being more pronounced, sound channels being stronger and, in some cases, one of the fields having no sonic layer or

having secondary sound channels. Quite expectedly, this led to large differences in the sound propagation predictions made by WAPP for the two fields, and thus to large relative differences in area coverage.

Scenario	Prob(RD>0.1)	Prob(RD>0.2)
ECS Jun HD Deep ASW	17.5	2.6
ECS Jun LD Deep ASW	21.8	4.1
ECS Jun LD Shallow ASW	21.8	3.6
ECS Jun HD ASUW	39.6	19.6
ECS Jun LD ASUW	26.3	9.4
KCA Jun HD Deep ASW	39.3	6.6
KCA Jun LD Deep ASW	37.5	6.4
KCA Jun LD Shallow ASW	46.8	8.5
KCA Jun HD ASUW	56.0	30.2
KCA Jun LD ASUW	43.6	17.2
SOJ Jun HD Deep ASW	17.5	2.9
SOJ Jun LD Deep ASW	18.9	3.0
SOJ Jun LD Shallow ASW	11.6	1.2
SOJ Jun HD ASUW	2.4	0.5
SOJ Jun LD ASUW	1.4	0.3
ECS Oct HD Deep ASW	8.1	0.4
ECS Oct LD Deep ASW	11.8	1.1
ECS Oct LD Shallow ASW	15.4	4.7
ECS Oct HD ASUW	49.2	14.0
ECS Oct LD ASUW	51.9	25.4
KCA Oct HD Deep ASW	35.7	4.5
KCA Oct LD Deep ASW	33.5	3.4
KCA Oct LD Shallow ASW	50.7	8.3
KCA Oct HD ASUW	43.6	8.5
KCA Oct LD ASUW	47.5	6.9
SOJ Oct HD Deep ASW	29.6	5.1
SOJ Oct LD Deep ASW	26.6	4.4
SOJ Oct LD Shallow ASW	36.7	8.8
SOJ Oct HD ASUW	**91.5**	**84.1**
SOJ Oct LD ASUW	**81.8**	**62.3**

Table 7. Sensitivity table.

B. RECOMMENDATIONS FOR FUTURE WORK

The most accurate way to assess the satellite altimetry data's overall value is to relate it to how it would affect the outcome of actual engagement, or weapon effectiveness. The value could then be based on whether or not the outcomes were affected positively, which in an ASW engagement typically means the torpedo hit the

target versus missed it. In this study, torpedo performance in the real world was not readily quantifiable because, although the MODAS field with satellite altimetry is certainly closer to the actual environmental conditions, neither field could be considered as being the actual environment like an in situ measurement could (within the accuracy of the device used). Therefore, there was no way to relate the performance predictions to the expected real world performance. (The only real world performance assertion was made to single out the different SD/SA combinations for the sensitivity analysis, namely that the engagement would have been very similar if the weapon was assigned the same presets, regardless of which MODAS field was used). Also, a relative difference in area coverage of 0.1 to 0.2 was arbitrarily chosen for analysis, although higher or lower levels of difference may actually be necessary to affect engagement outcome.

To quantify the effect on weapon effectiveness, a two-part study needs to be conducted. Part 1 would compare the output of WAPP using MODAS fields (one with altimetry data and one without, as done here) and in situ measurements of the local environment. The in situ measurements could be performed by any number of assets, such as a U. S. Navy ship during an exercise or a research vessel, although the area sounded should be one with large variability, such as in the Gulf Stream or Kuroshio Current, to obtain the most benefit from the altimetry data. Of course, as with any experiment involving in situ measurements, the data set will be much smaller than the one used in this study.

With this type of comparison, any differences in WAPP output could be correlated to the torpedo's predicted real world performance and, therefore, so could the benefit of the satellite altimetry data. For example, if the predicted performance was similar for the MODAS field with altimetry and the in situ data, but the performance differed appreciably for the MODAS field without altimetry, the altimetry data would be quite valuable. If the predicted performance differed appreciably between all three inputs or between the in situ input and both MODAS fields, the altimetry data would be deemed as being less beneficial. Of course, the predicted performance is still not real world performance, however.

To even better assess the effect of the satellite altimetry data on weapon effectiveness, Part 2 would need to include simulations of torpedo engagements. The Weapons Analysis Facility (WAF) at NUWC, Division Newport has the capability to simulate engagements using torpedo hardware-in-the-loop and a high fidelity virtual environment. Using the WAF and presets generated by the MODAS fields and in situ data in Part 1, many virtual torpedo engagements could be conducted to examine the effects of the different MODAS fields on virtual performance. This could be done for any number of scenarios, by alternately using presets generated by each of the environmental inputs to WAPP: the MODAS field without altimetry, the MODAS field with altimetry, and the in situ data; and then comparing the ratios of hits to misses for the virtual engagements.

This experiment introduces an operational element by enabling the presets to be chosen by an operator for each engagement. It would also eliminate the need to use the relative difference in area coverage and the associated uncertainty in the threshold that produces changes in engagement outcome. This is because the proposed metric, the hit-miss ratio, is not a prediction of performance (like area coverage) but, rather, a direct assessment of it (once again, in a virtual environment). Aside from the cost and logistics prohibitive alternative of putting many torpedoes in the water, an experiment such as this would provide the next best analysis of the value of assimilating satellite altimetry data into MODAS with regard to torpedo effectiveness.

Finally, to arrive at answers to some of the broader questions in this line of research, other comparisons need to be included. These are the questions of how many satellite altimeters are required to ensure maximum weapon effectiveness and at what point does additional altimeter input no longer increase weapon effectiveness. To answer these questions, MODAS fields with varying numbers of altimeters assimilated would need to be used as environmental inputs to WAPP and could be incorporated into Part 1 or added at a later date.

APPENDIX A MODAS FIELD STATISTICAL PLOTS

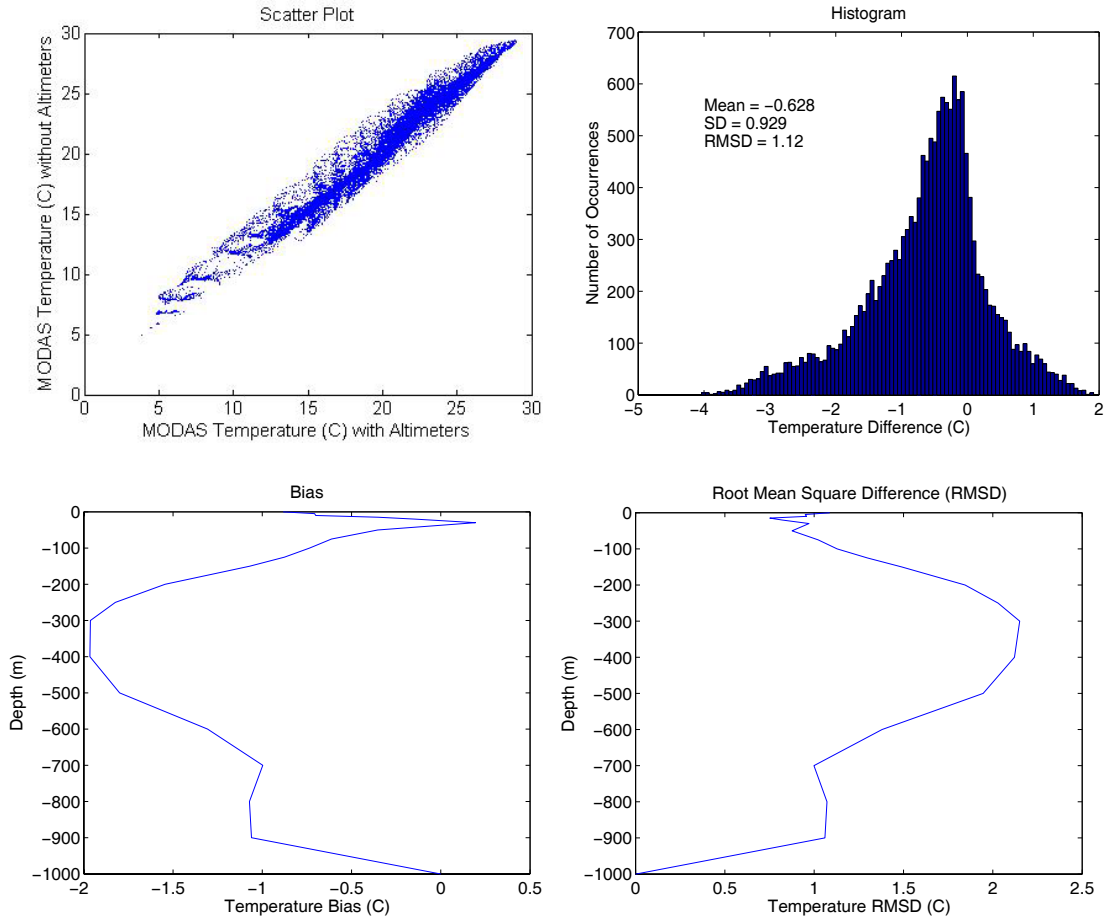

Figure 30. ECS MODAS temperature statistics for June 30.

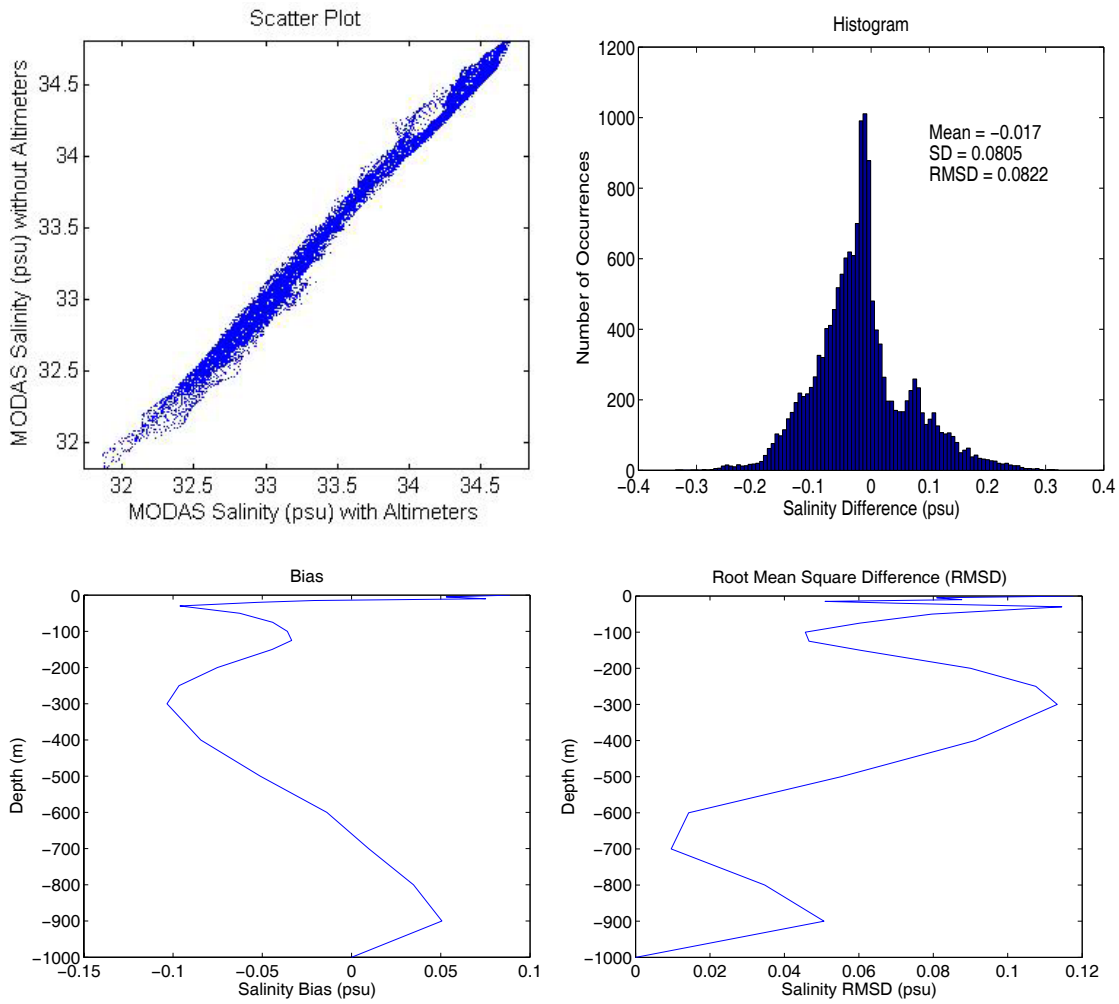

Figure 31. ECS MODAS salinity statistics for June 30.

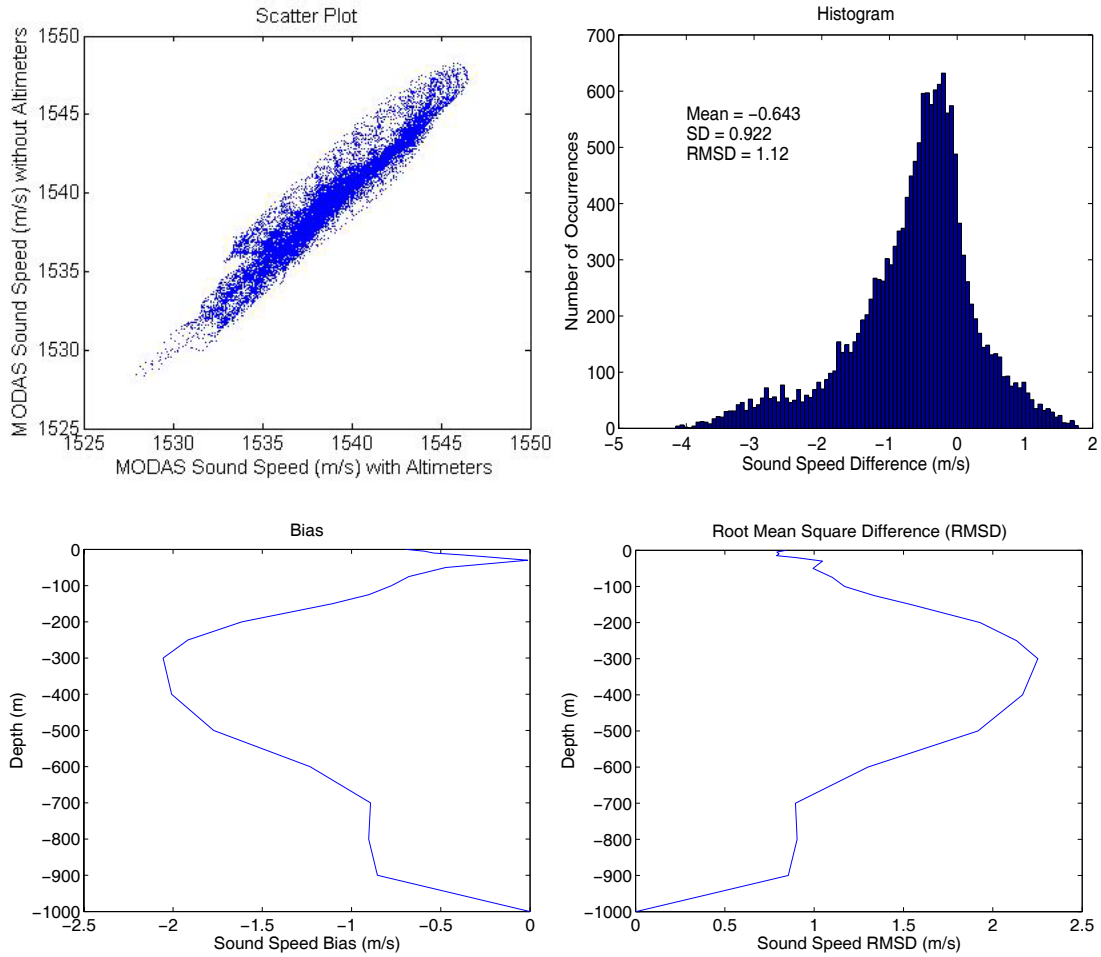

Figure 32. ECS MODAS sound speed statistics for June 30.

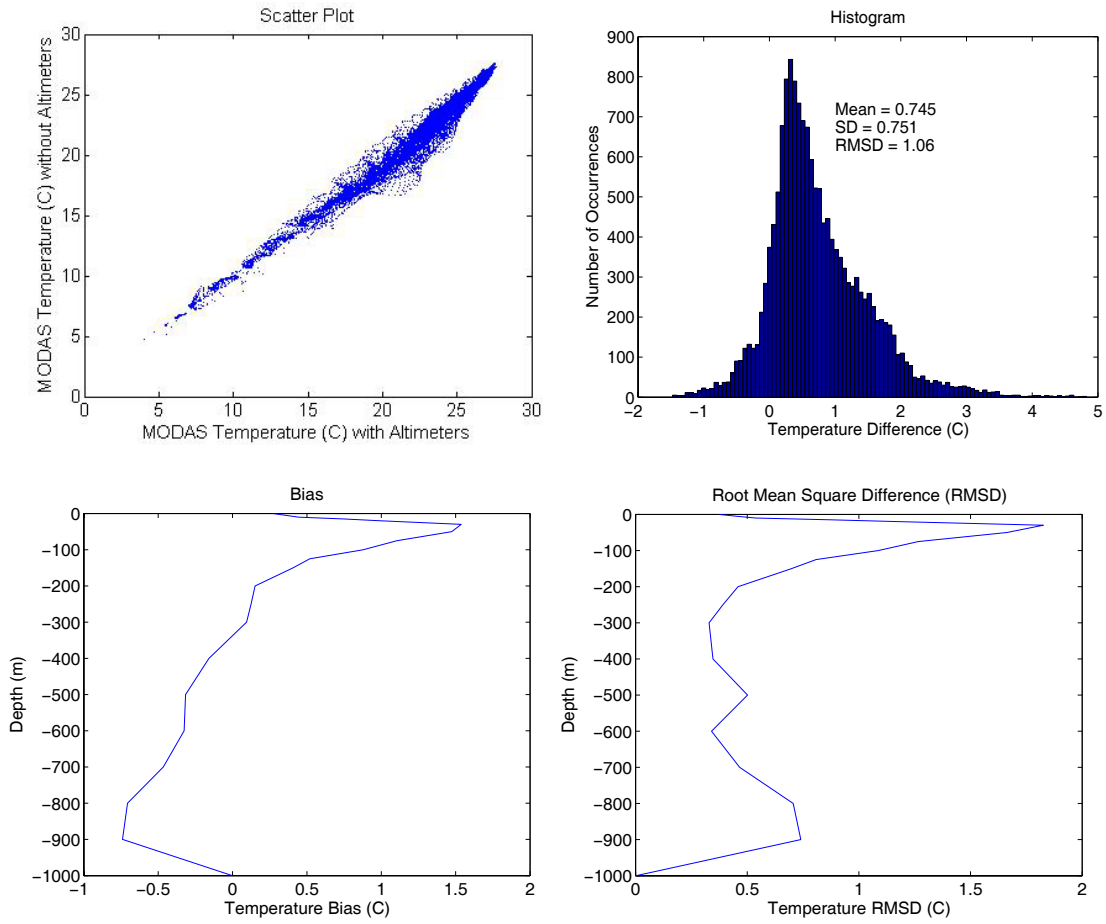

Figure 33. ECS MODAS temperature statistics for October 10.

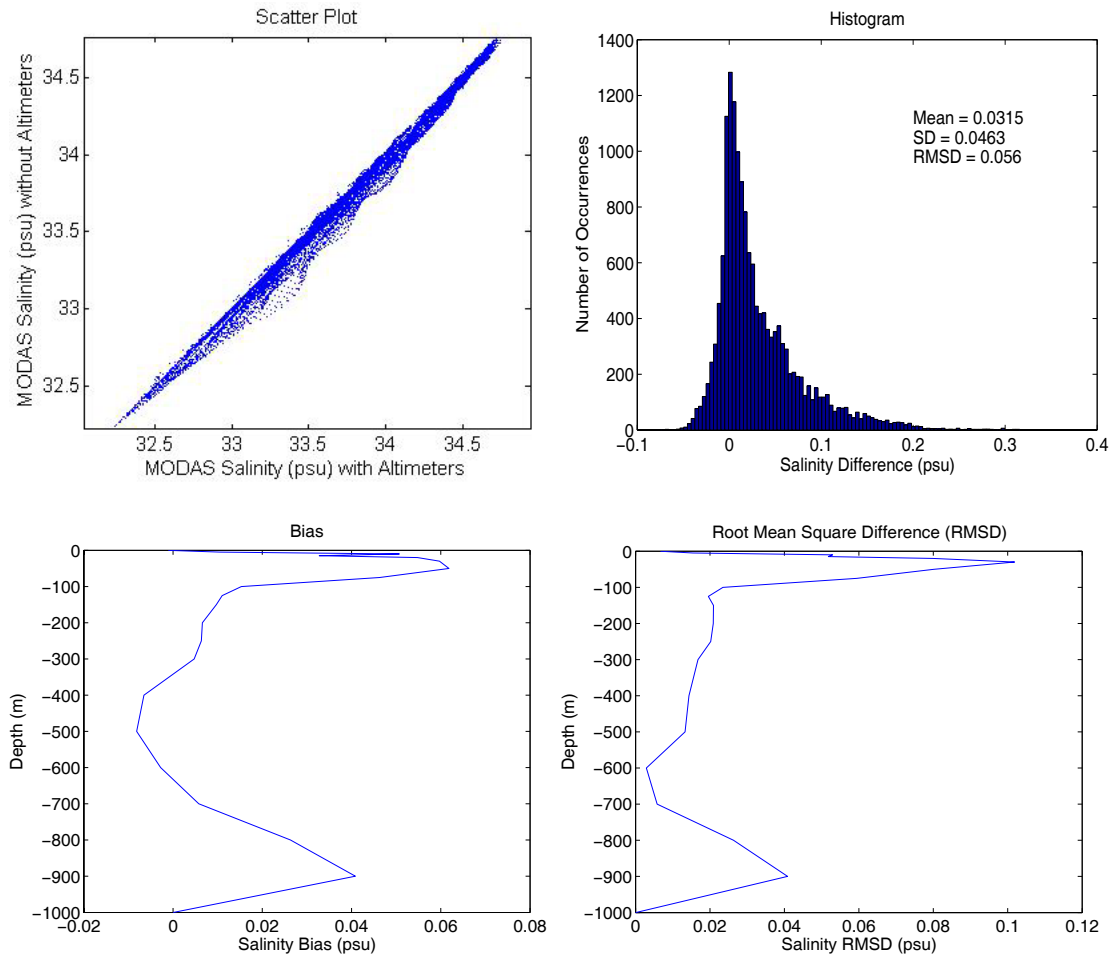

Figure 34. ECS MODAS salinity statistics for October 10.

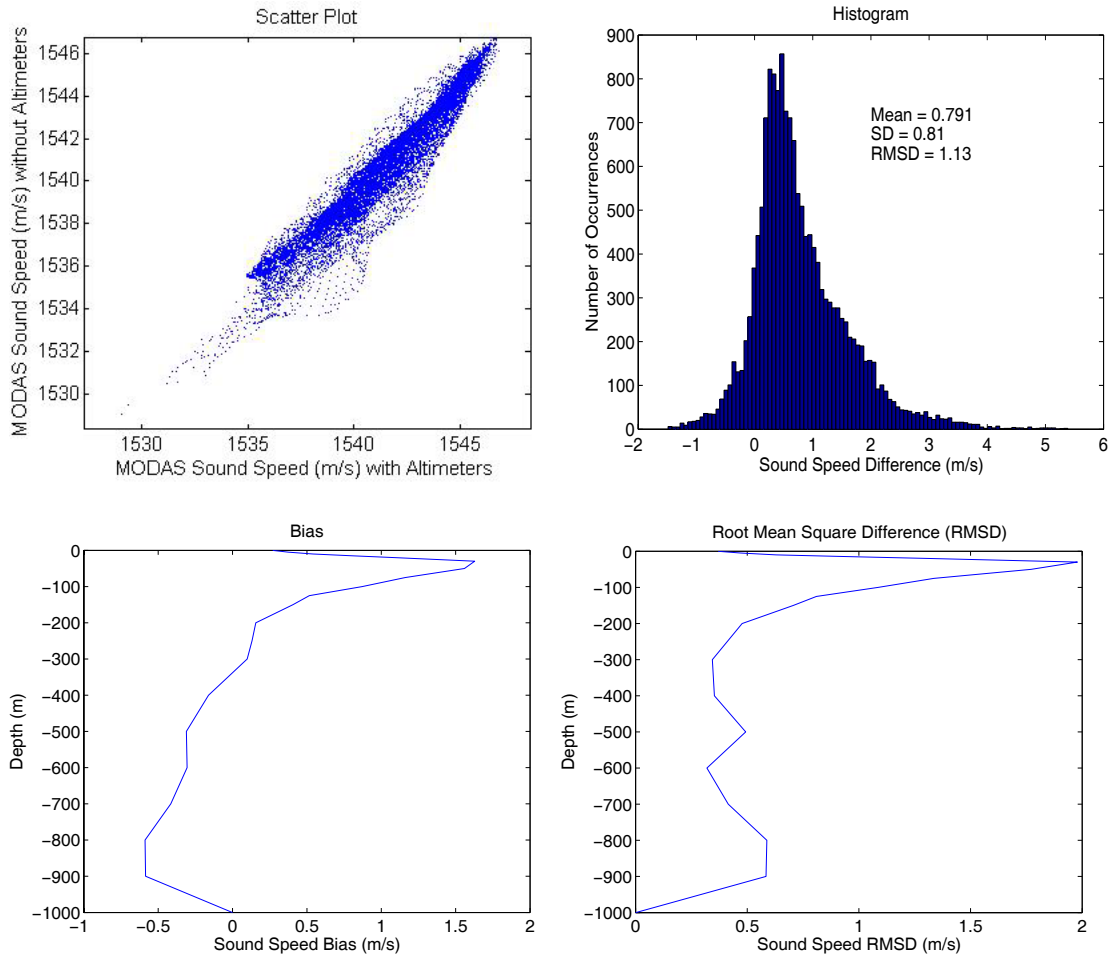

Figure 35. ECS MODAS sound speed statistics for October 10.

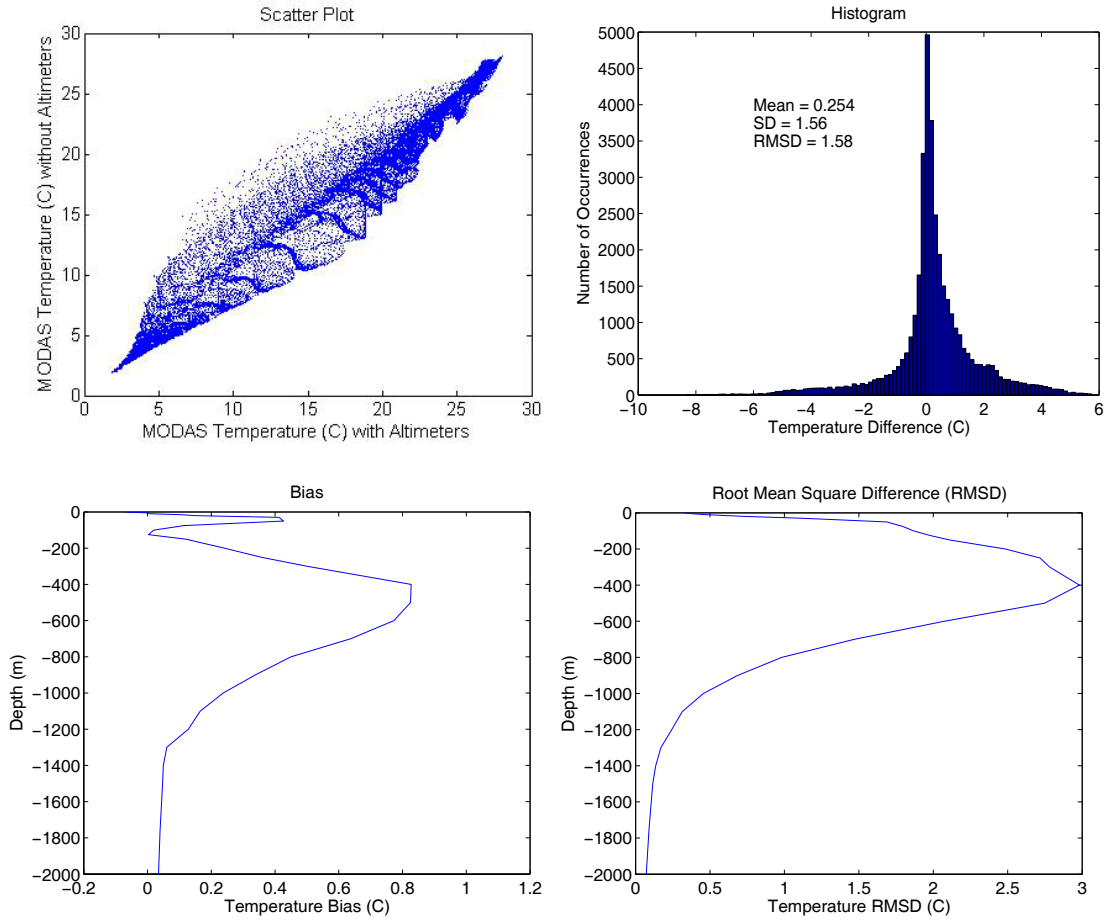

Figure 36. KCA MODAS temperature statistics for June 30.

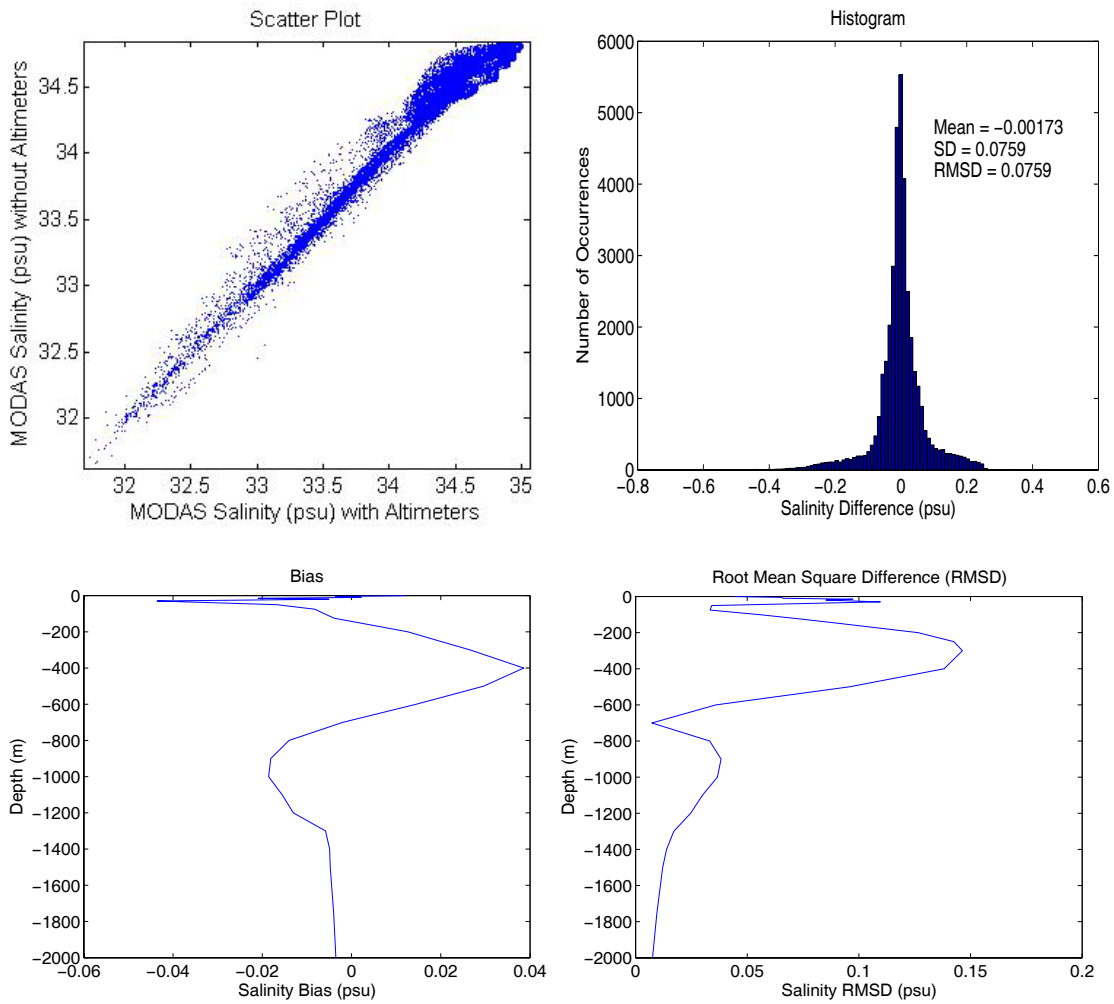

Figure 37. KCA MODAS salinity statistics for June 30.

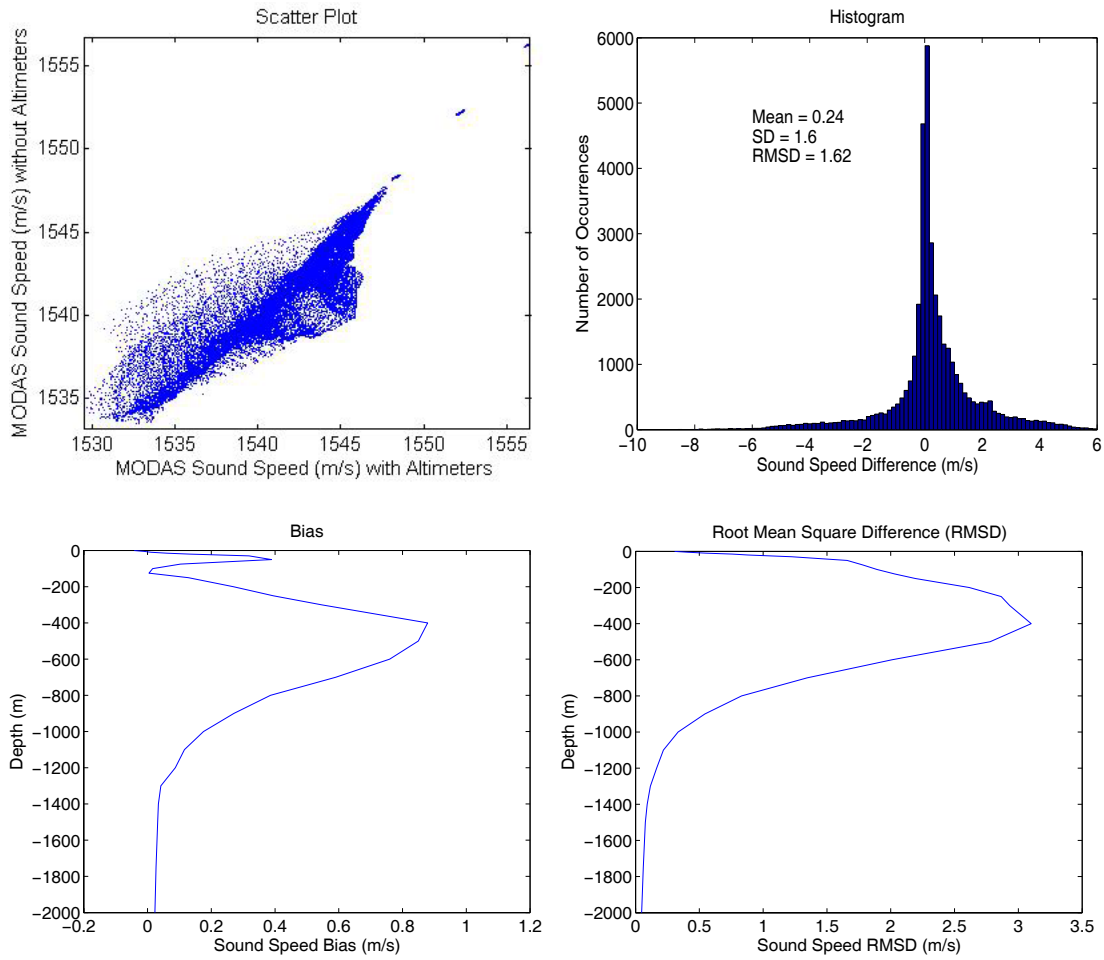

Figure 38. KCA MODAS sound speed statistics for June 30.

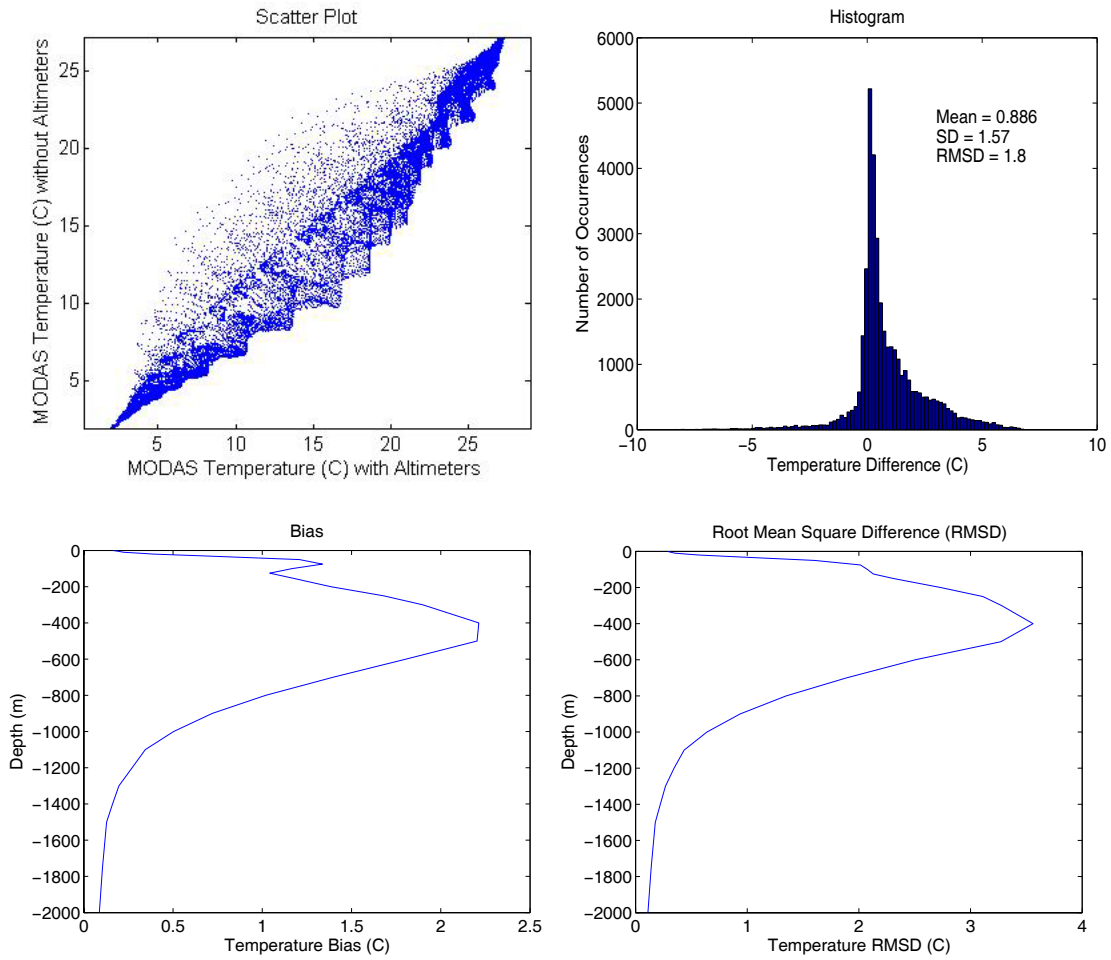

Figure 39. KCA MODAS temperature statistics for October 10.

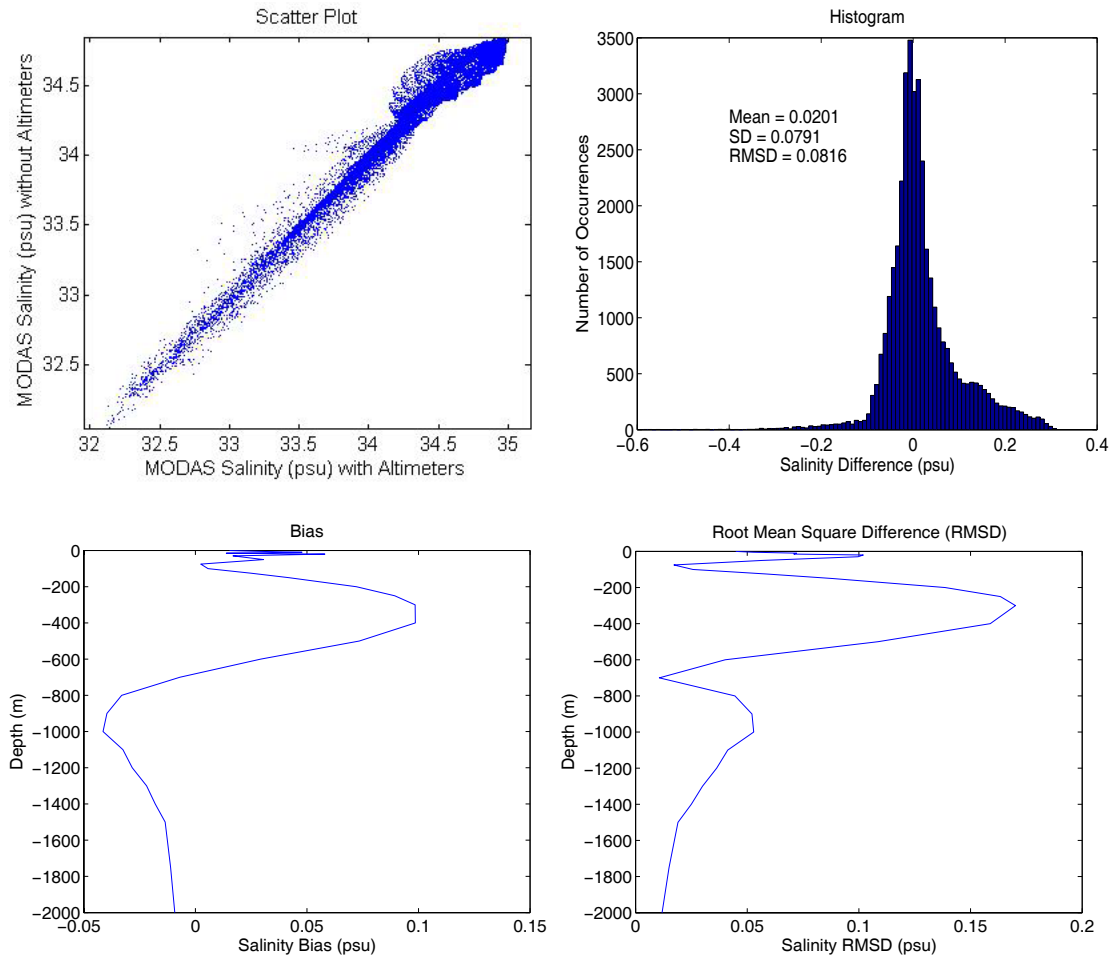

Figure 40. KCA MODAS salinity statistics for October 10.

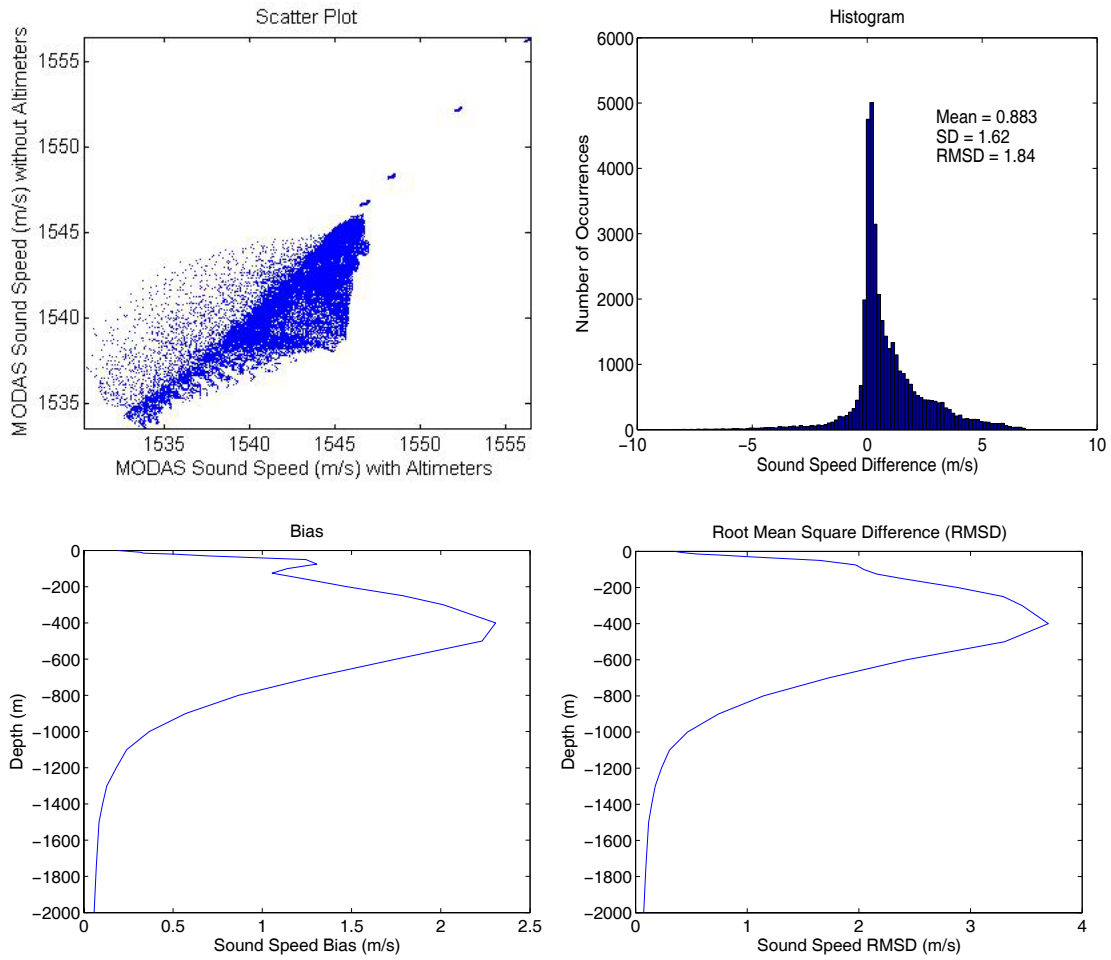

Figure 41. KCA MODAS sound speed statistics for October 10.

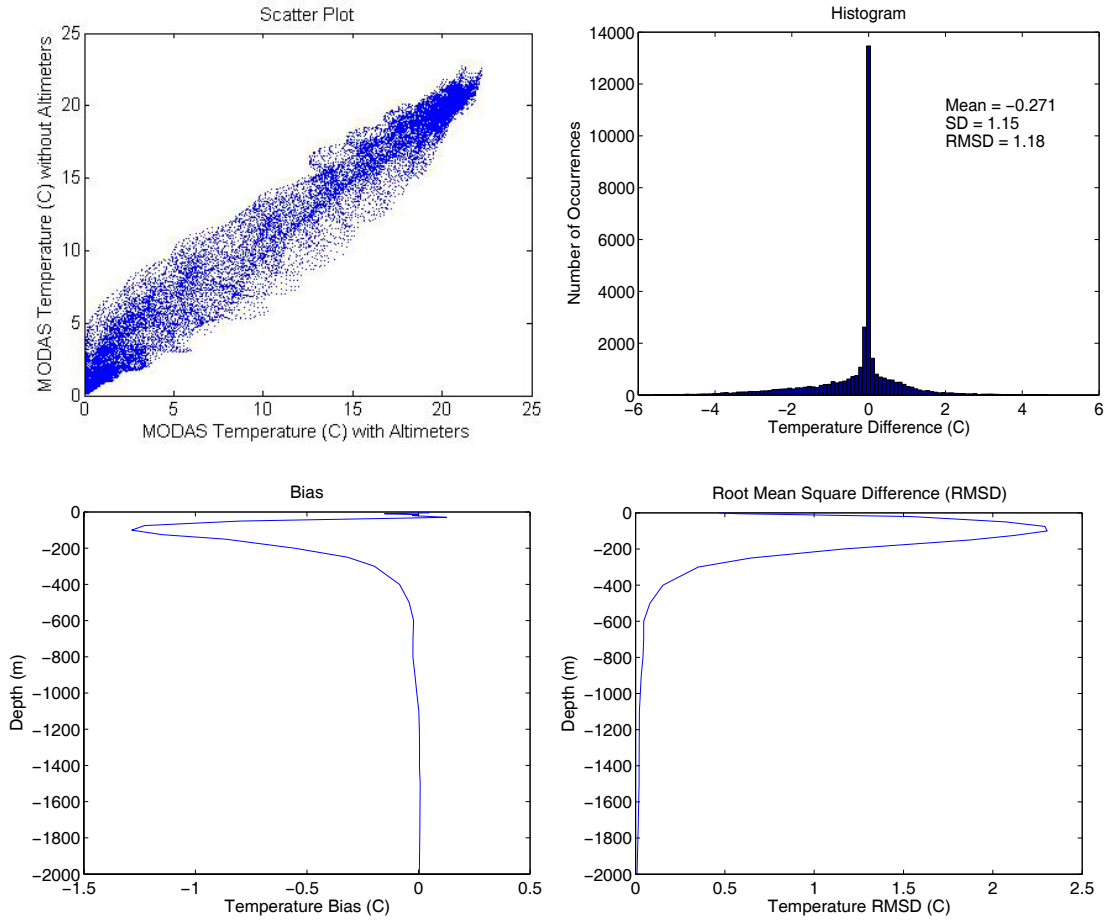

Figure 42. SOJ MODAS temperature statistics for June 30.

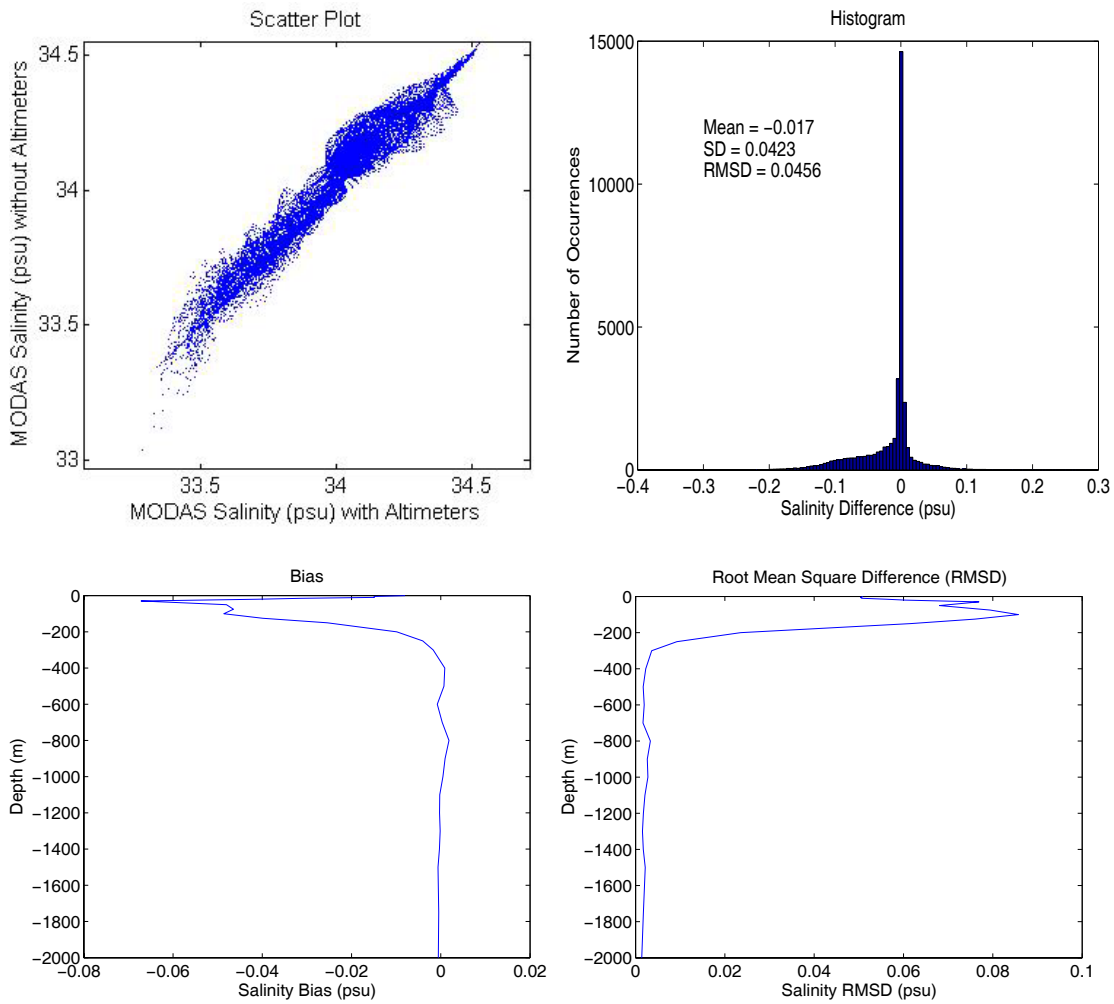

Figure 43. SOJ MODAS salinity statistics for June 30.

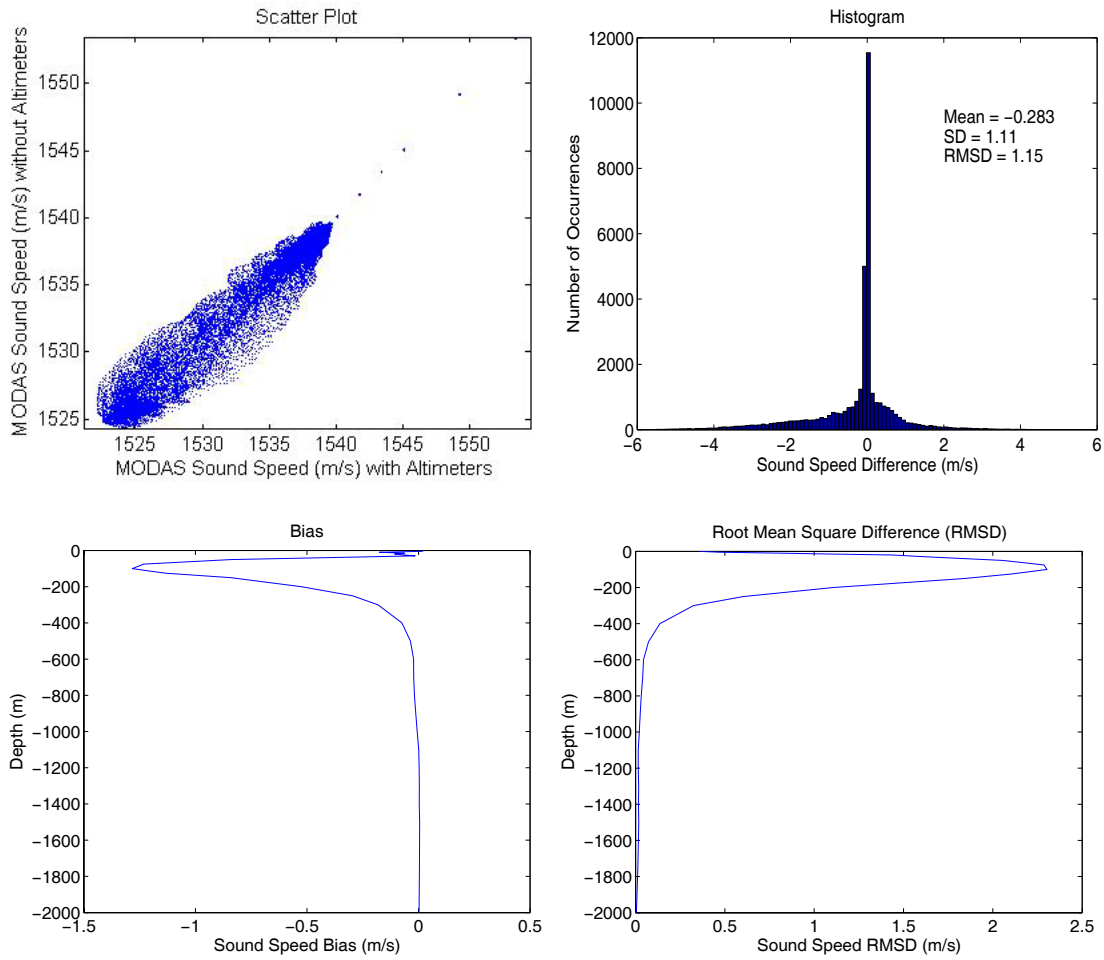

Figure 44. SOJ MODAS sound speed statistics for June 30.

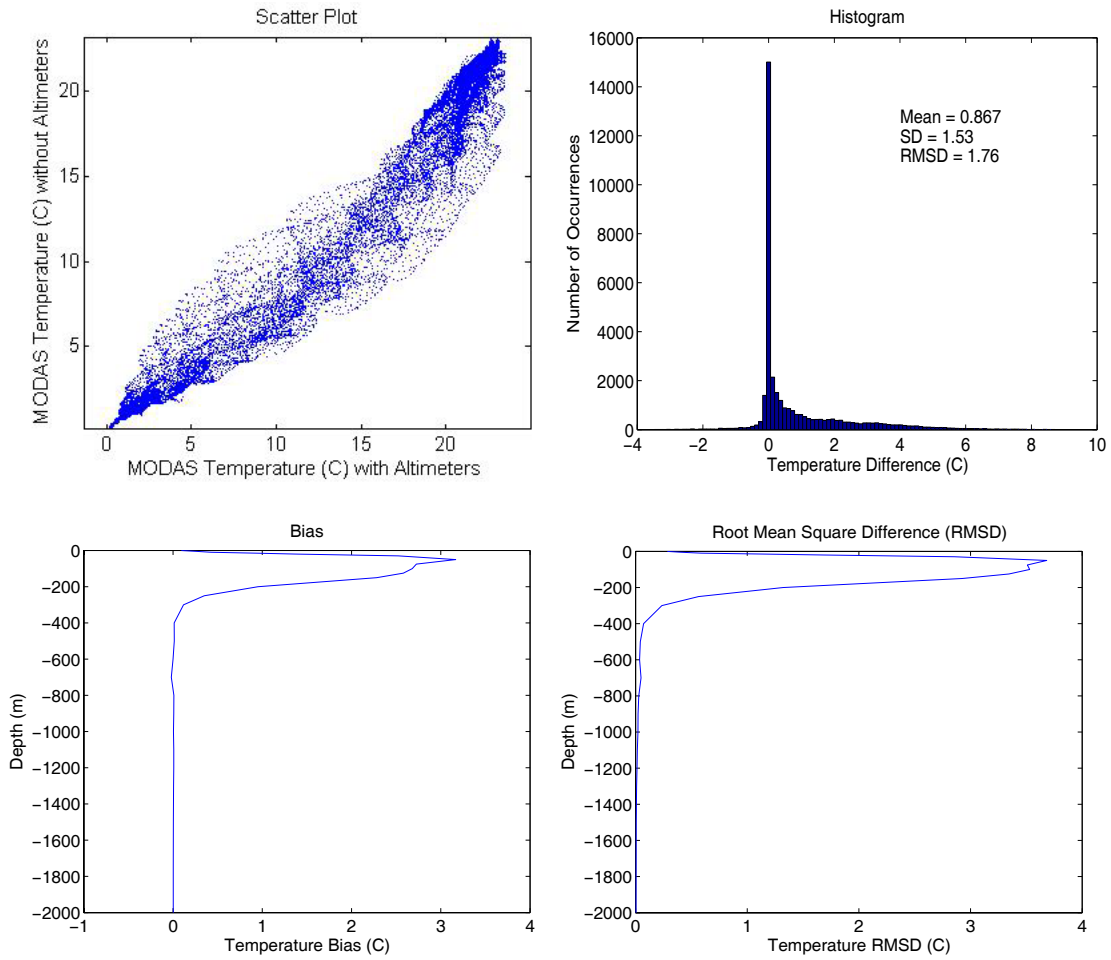

Figure 45. SOJ MODAS temperature statistics for October 10.

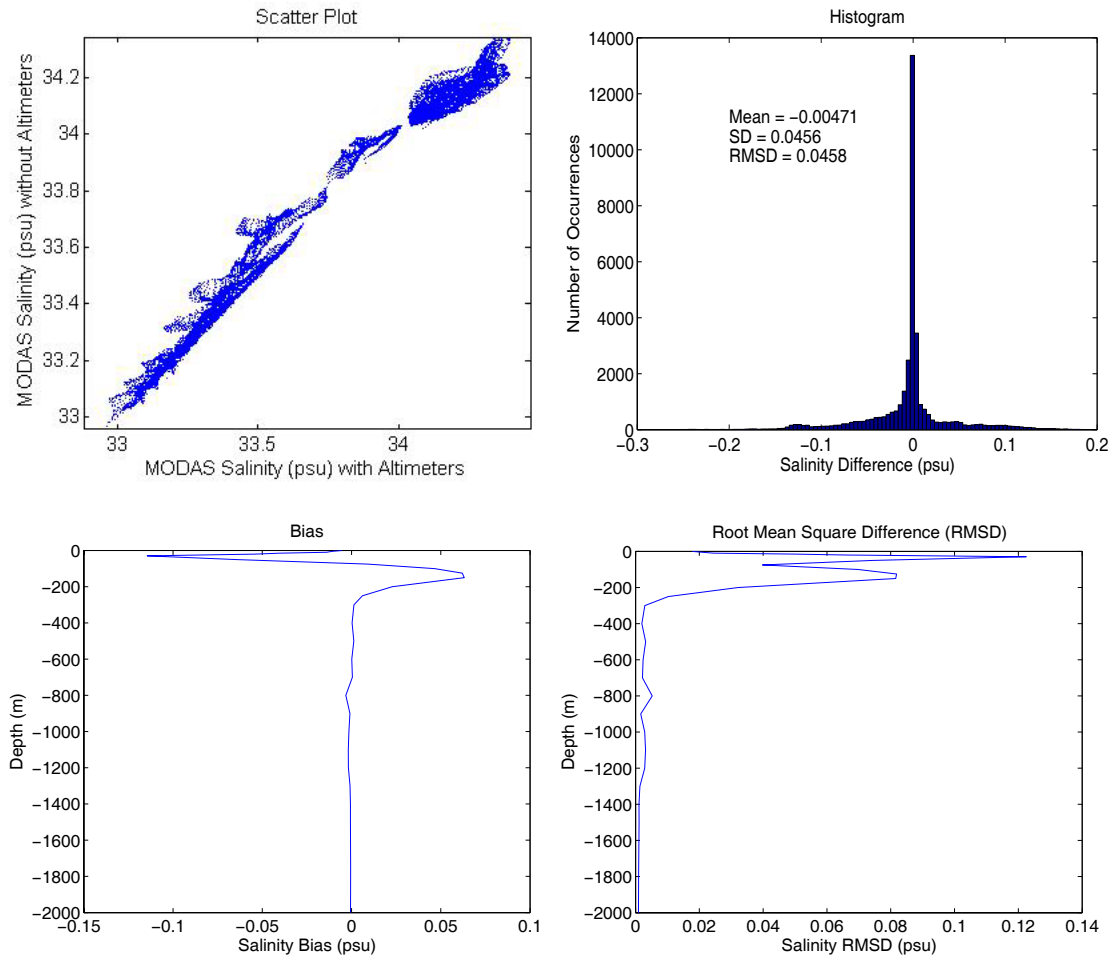

Figure 46. SOJ MODAS salinity statistics for October 10.

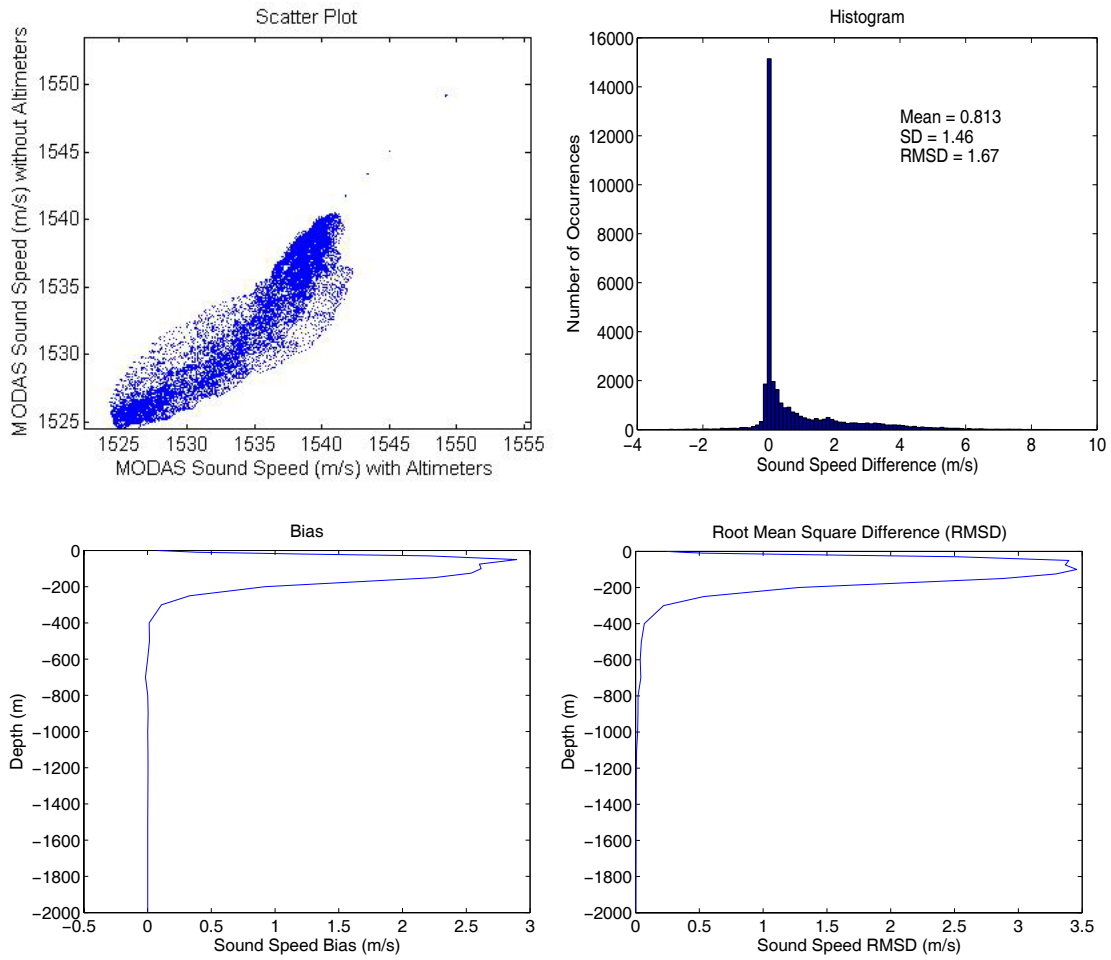

Figure 47. SOJ MODAS sound speed statistics for October 10.

APPENDIX B MODAS SOUND SPEED PROFILES

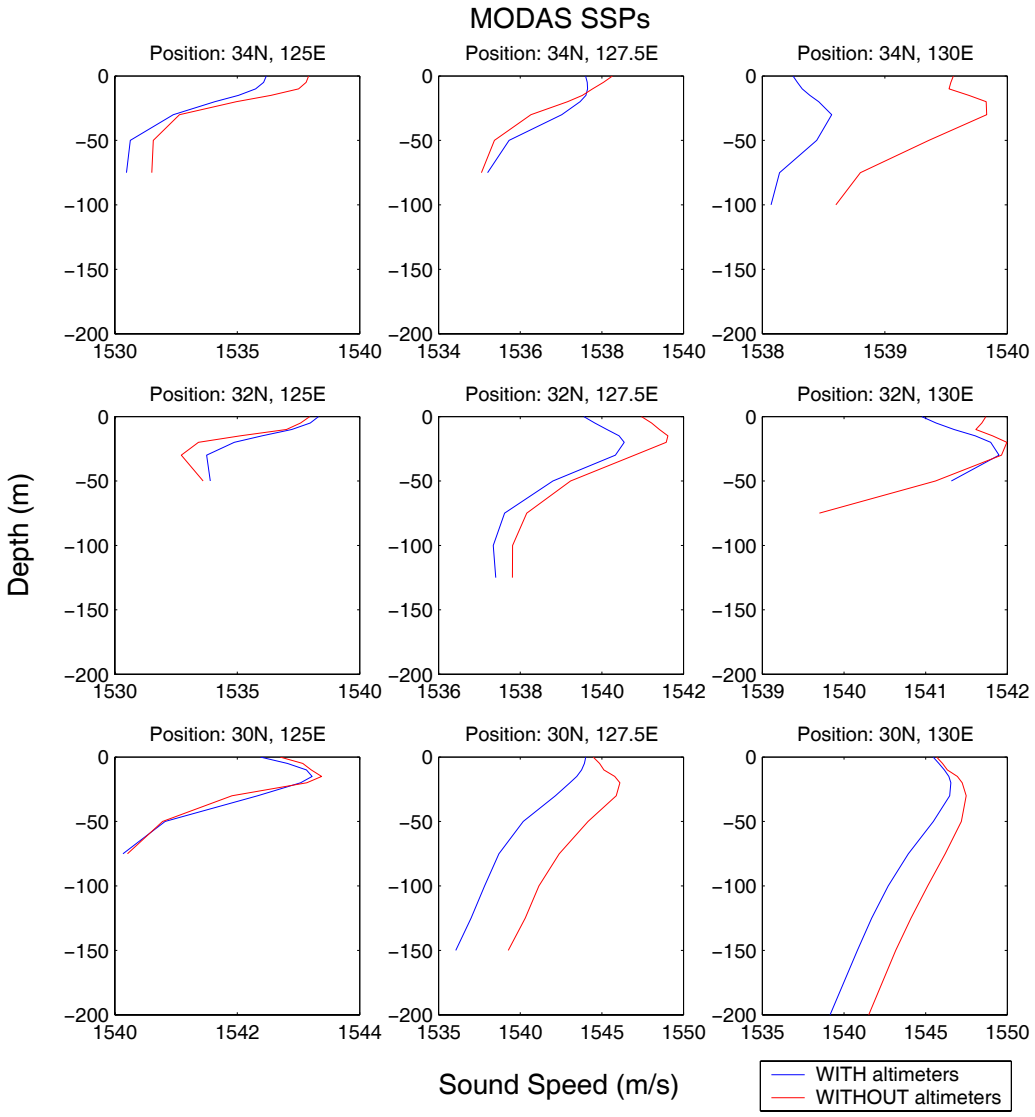

Figure 48. ECS MODAS SSPs for June 30.

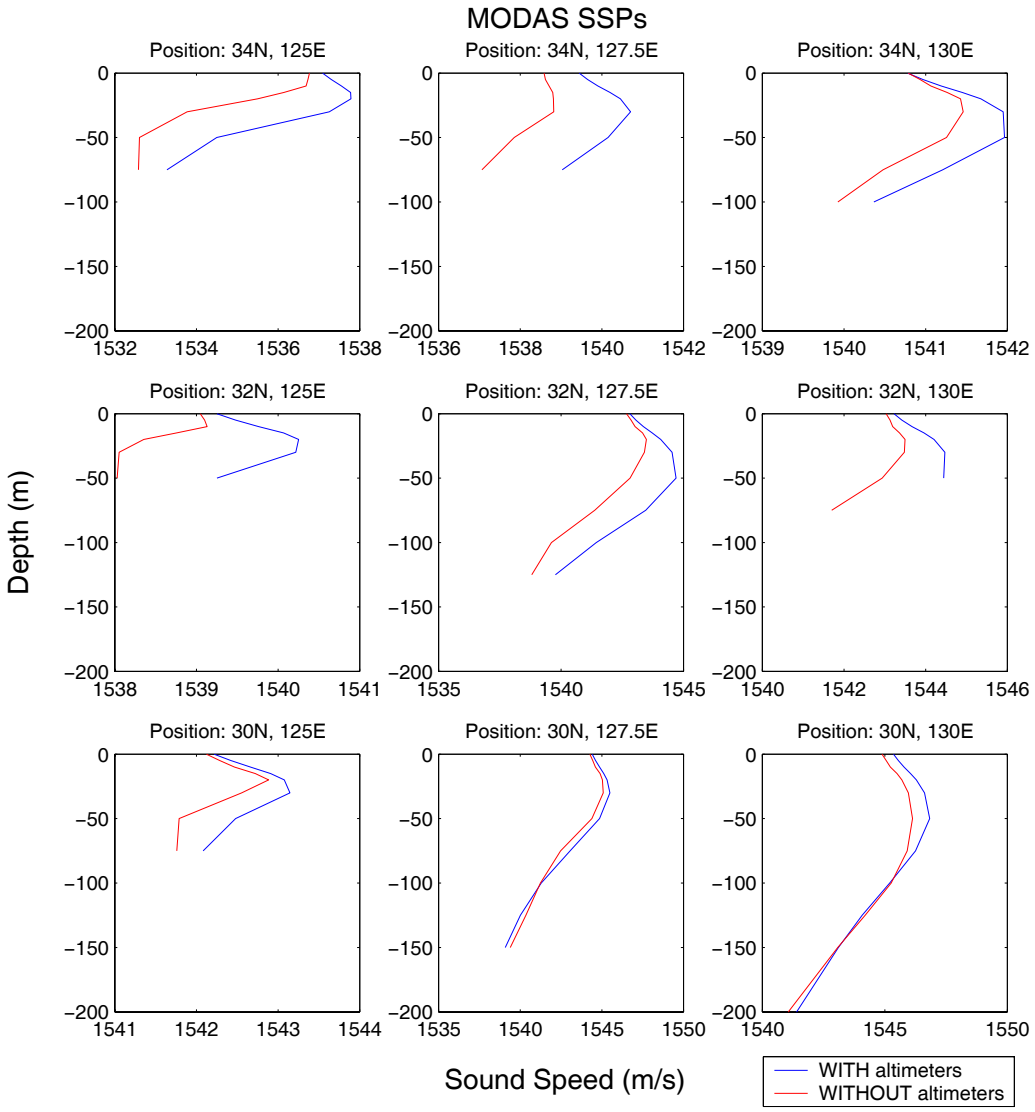

Figure 49. ECS MODAS SSPs for October 10.

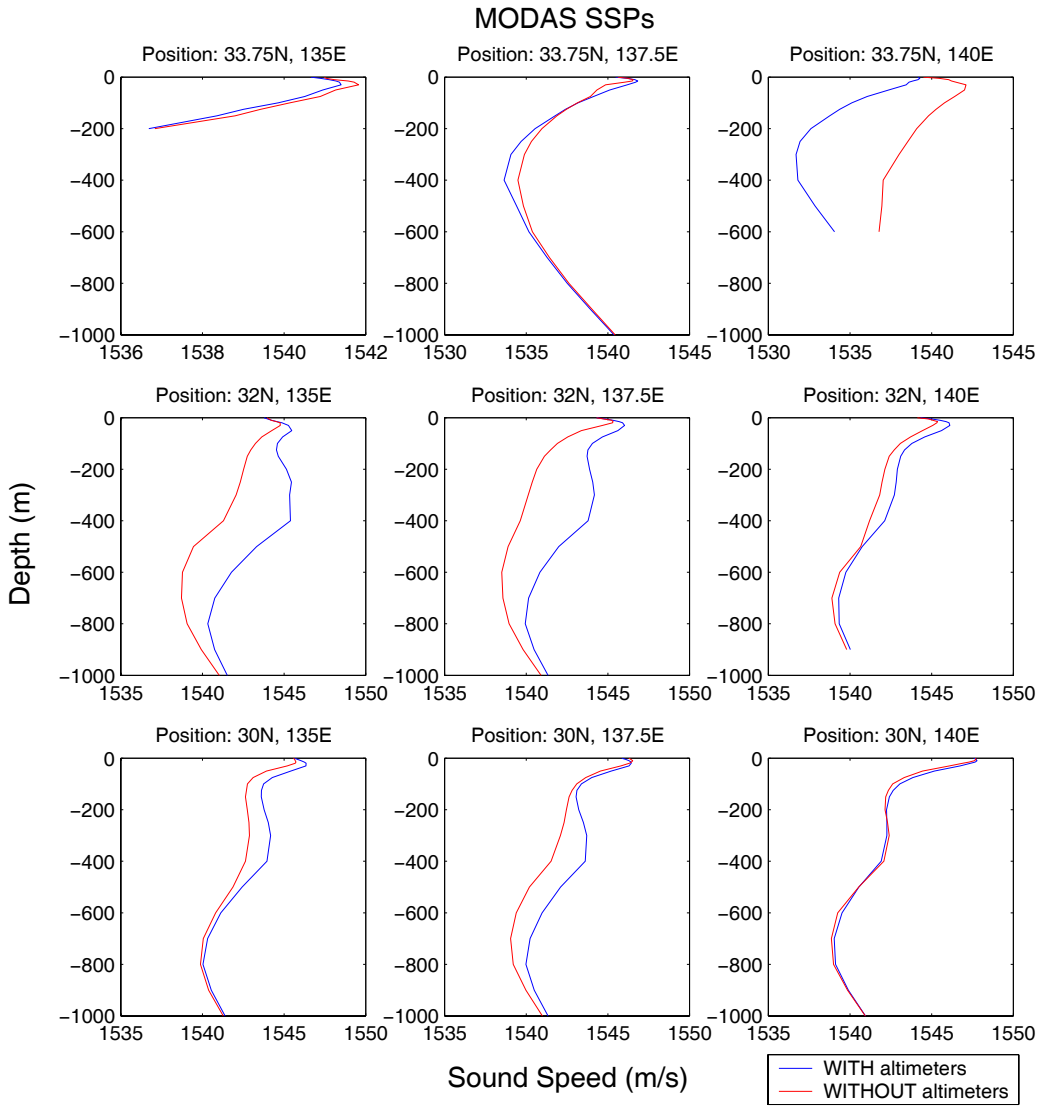

Figure 50. KCA MODAS SSPs for June 30.

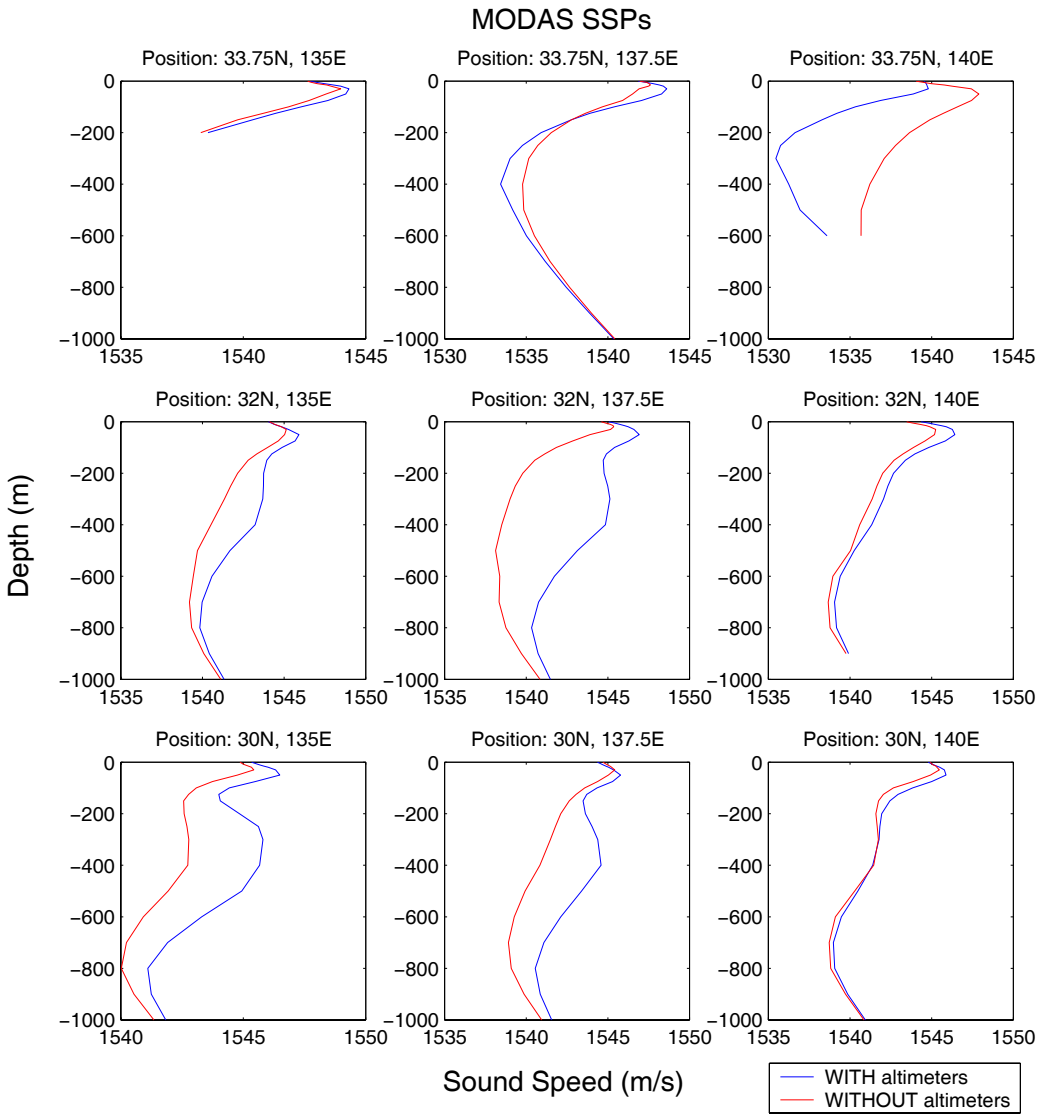

Figure 51. KCA MODAS SSPs for October 10.

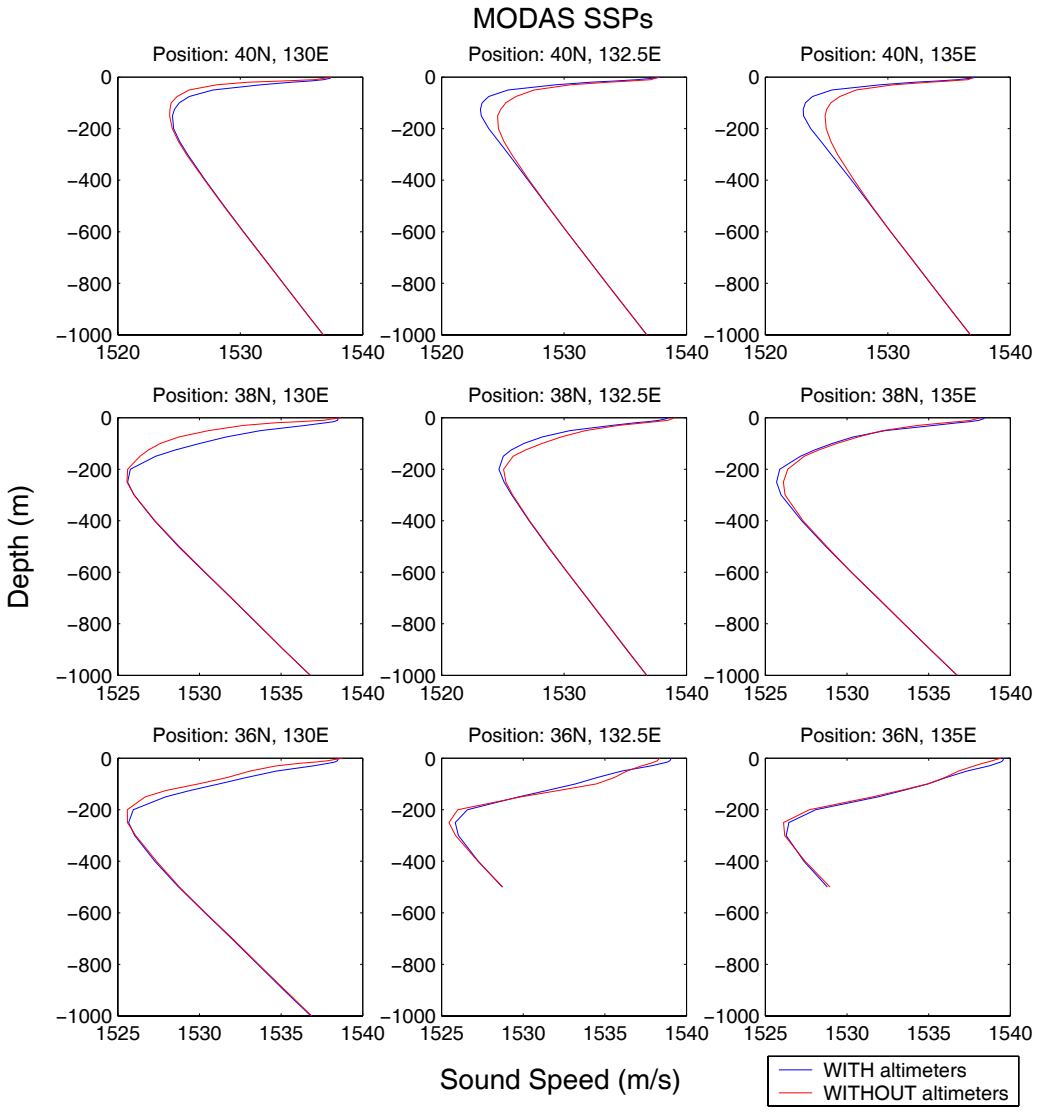

Figure 52. SOJ MODAS SSPs for June 30.

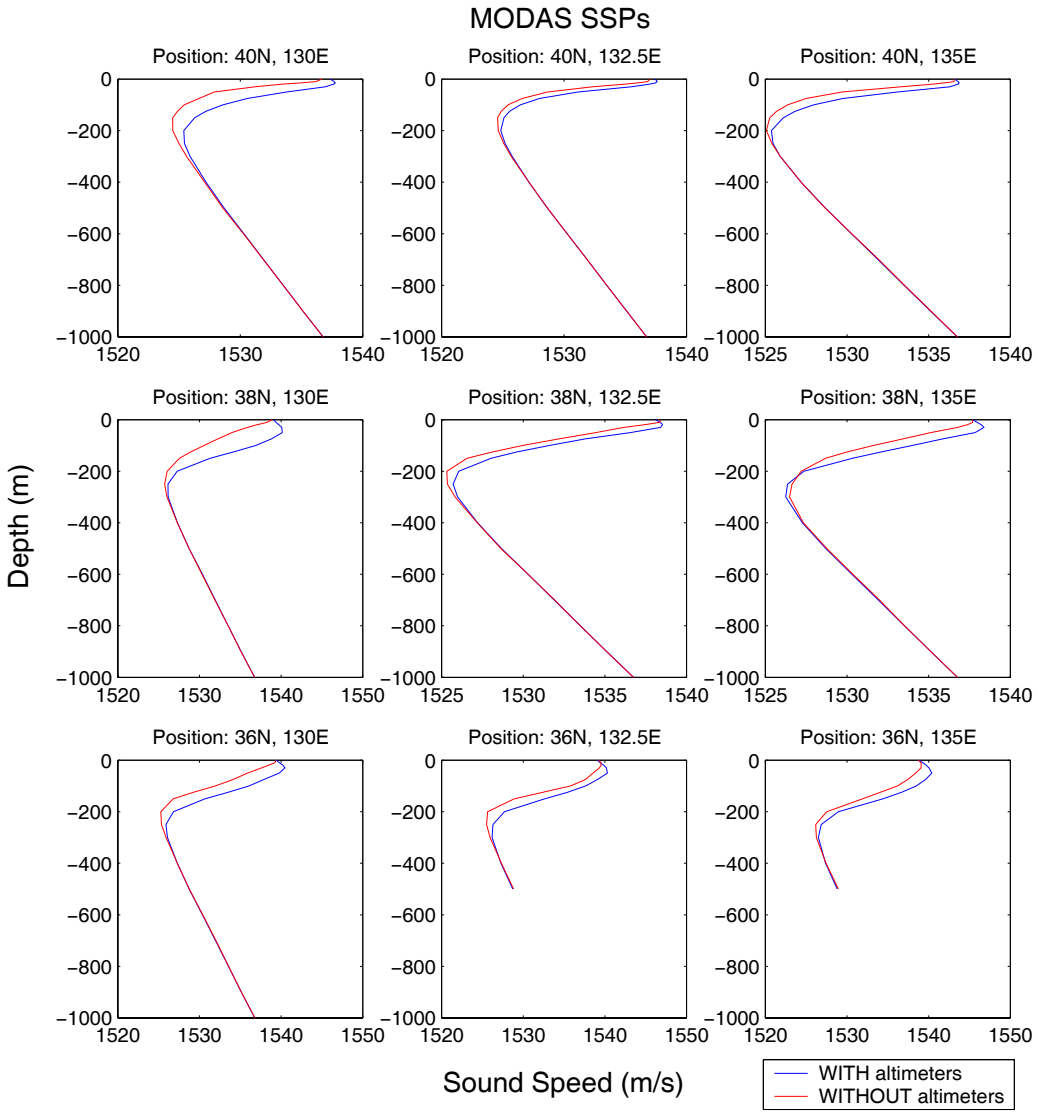

Figure 53. SOJ MODAS SSPs for October 10.

APPENDIX C WAPP OUTPUT HISTOGRAMS

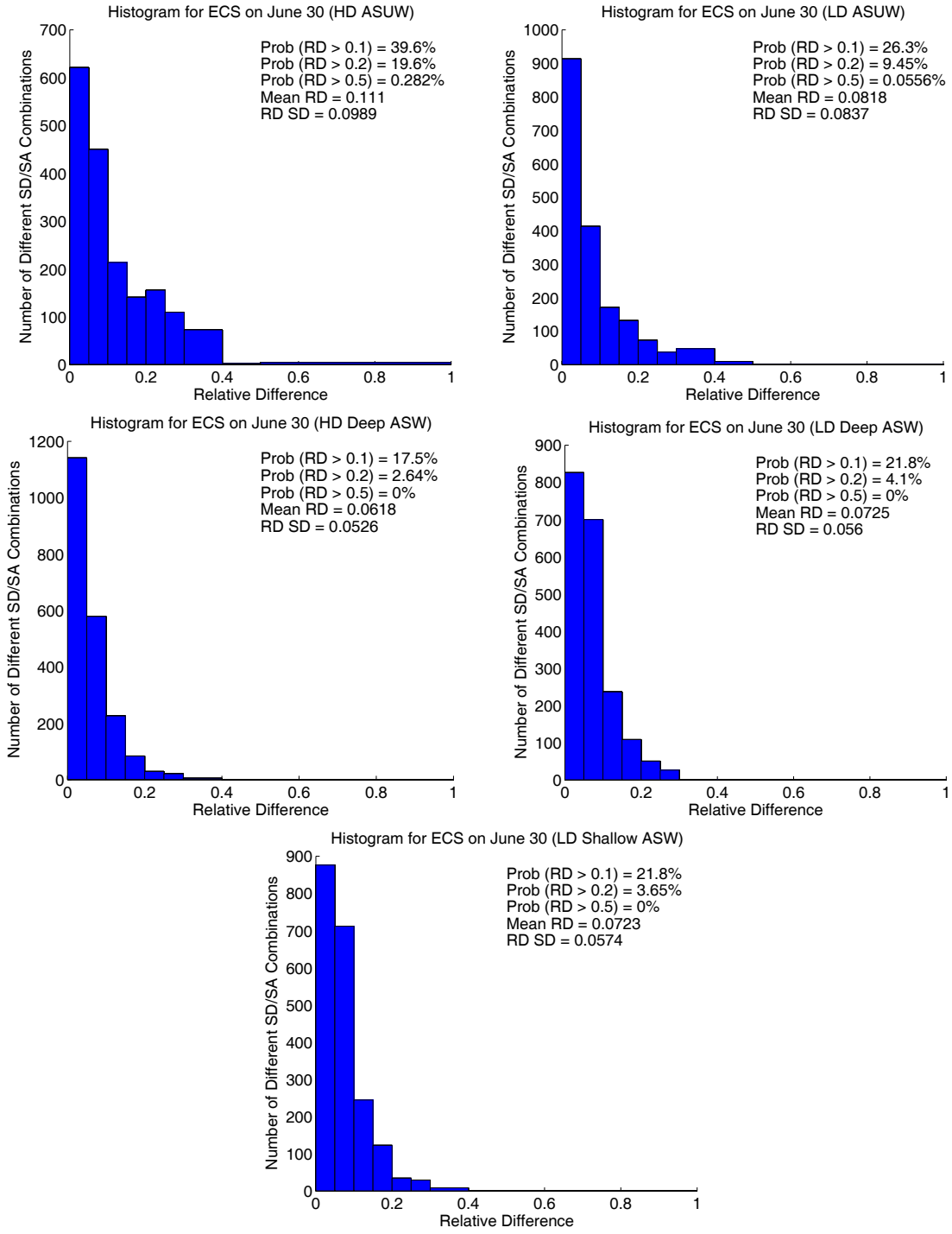

Figure 54. ECS Jun WAPP histograms

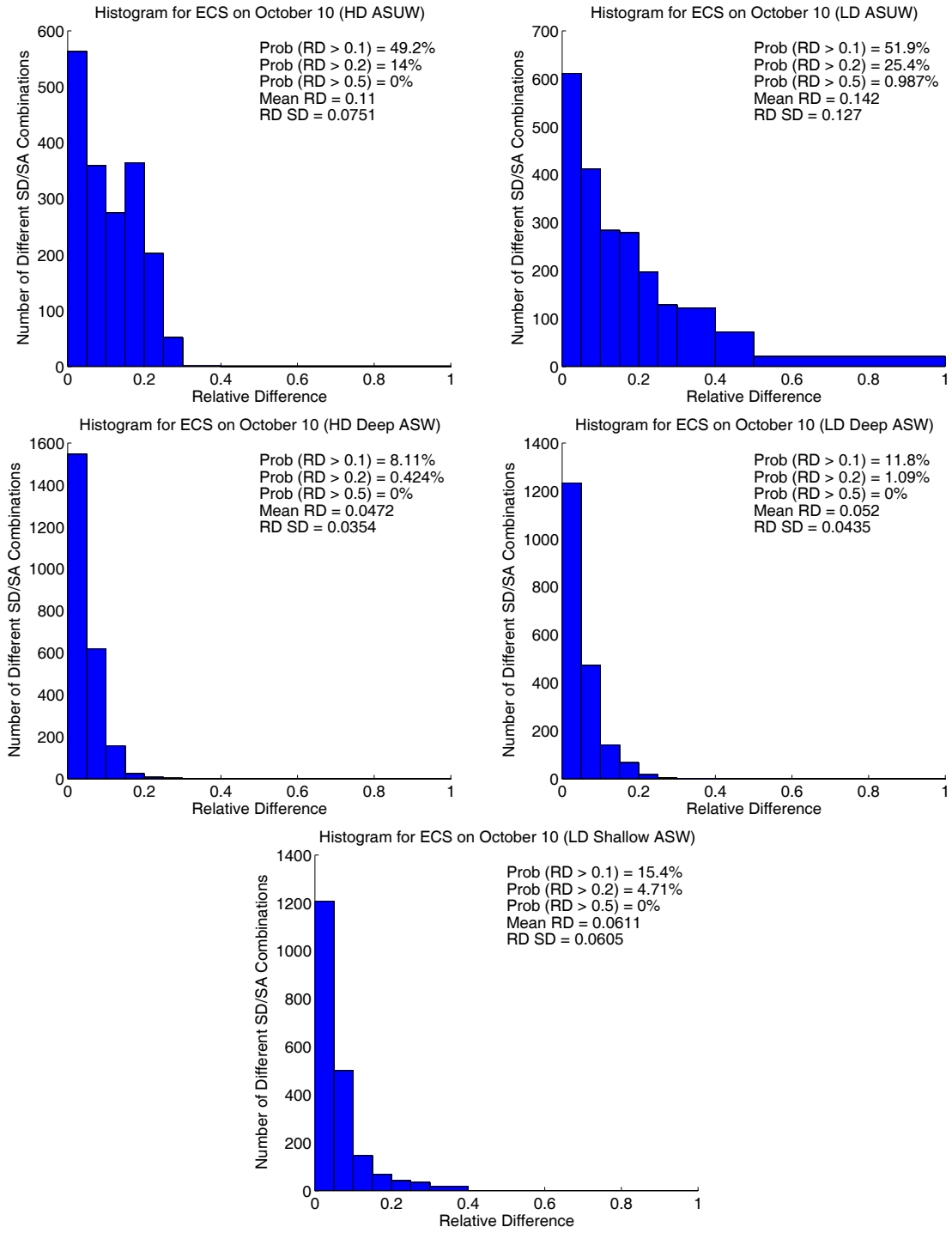

Figure 55. ECS Oct WAPP histograms

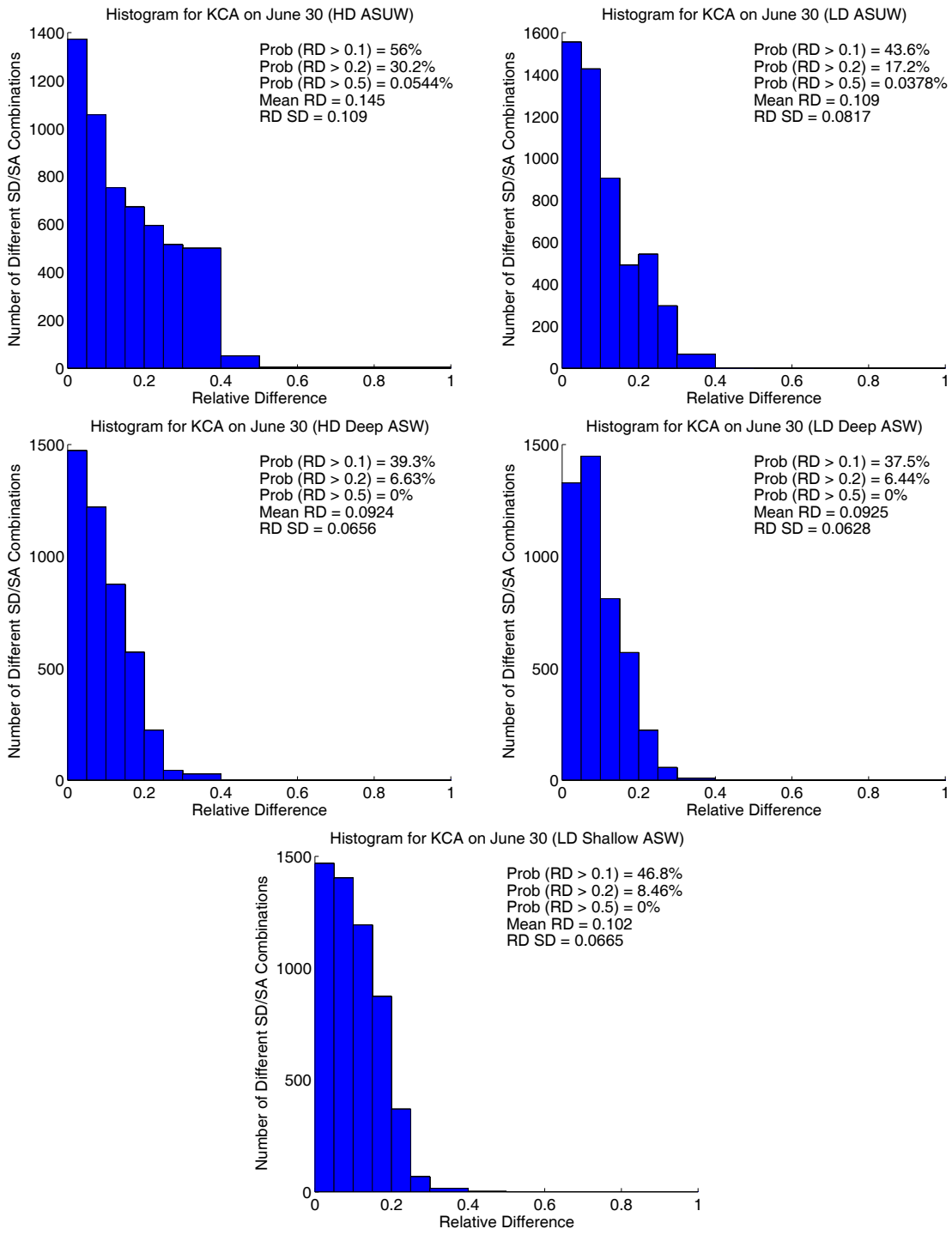

Figure 56. KCA Jun WAPP histograms

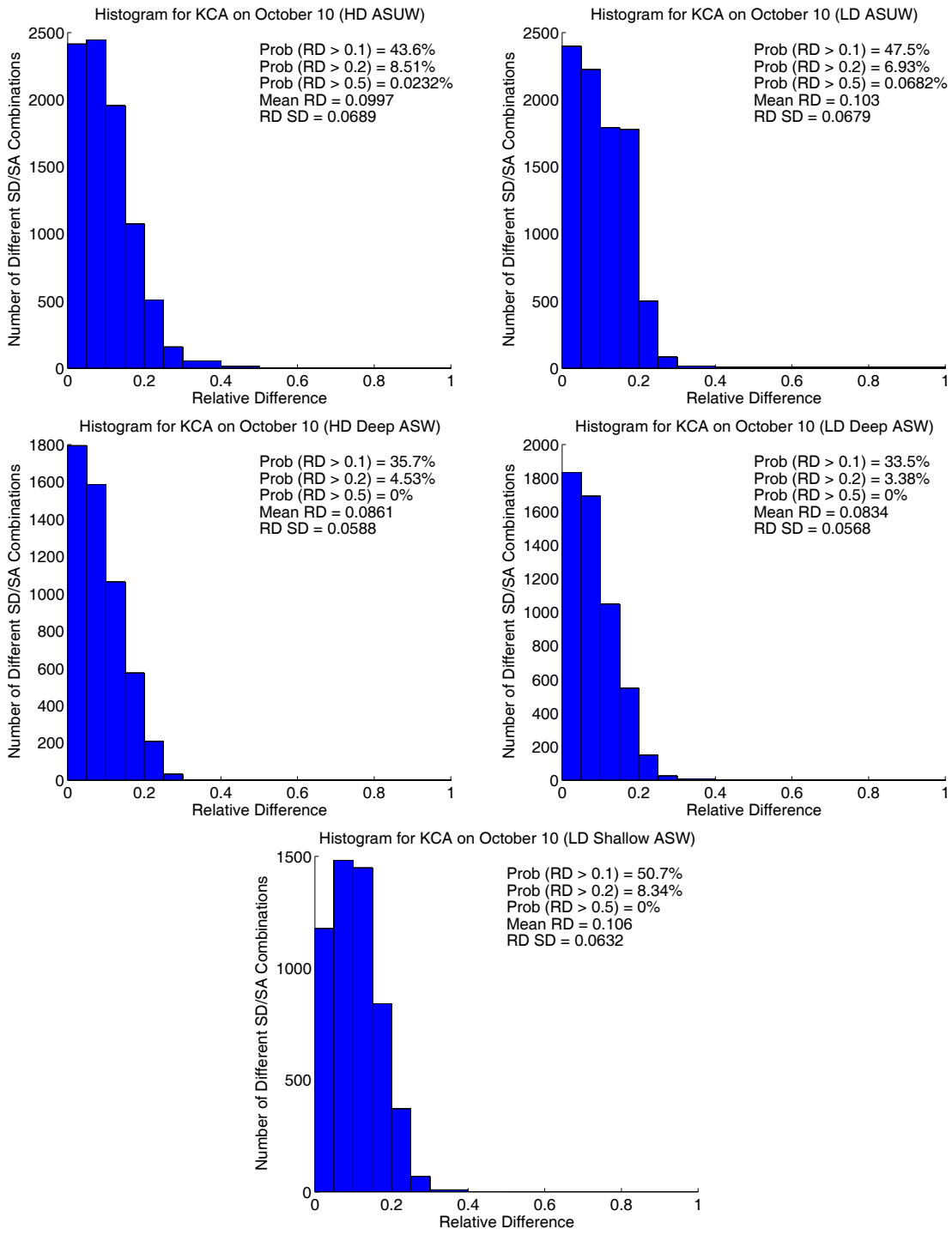

Figure 57. KCA Oct WAPP histograms

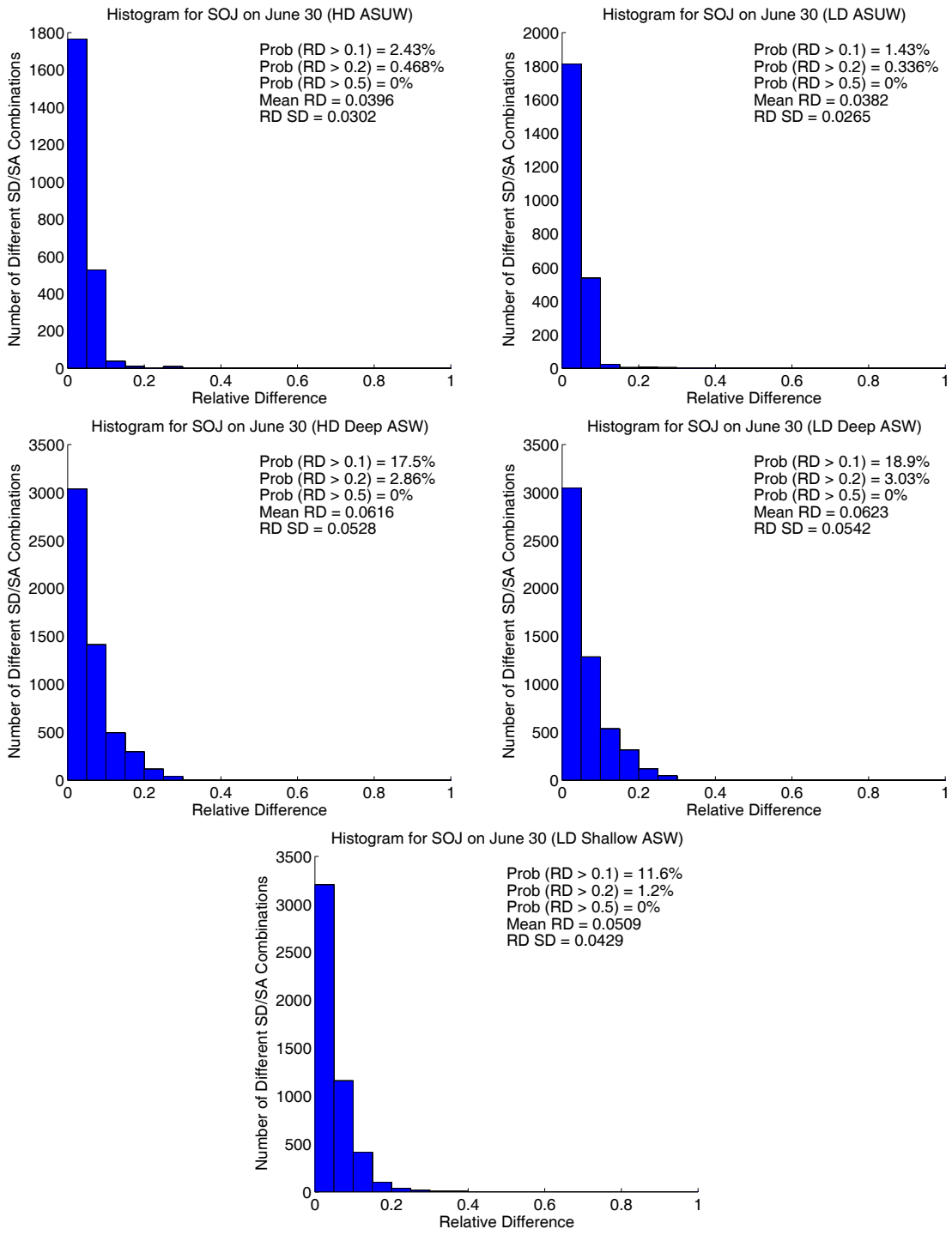

Figure 58. SOJ Jun WAPP histograms

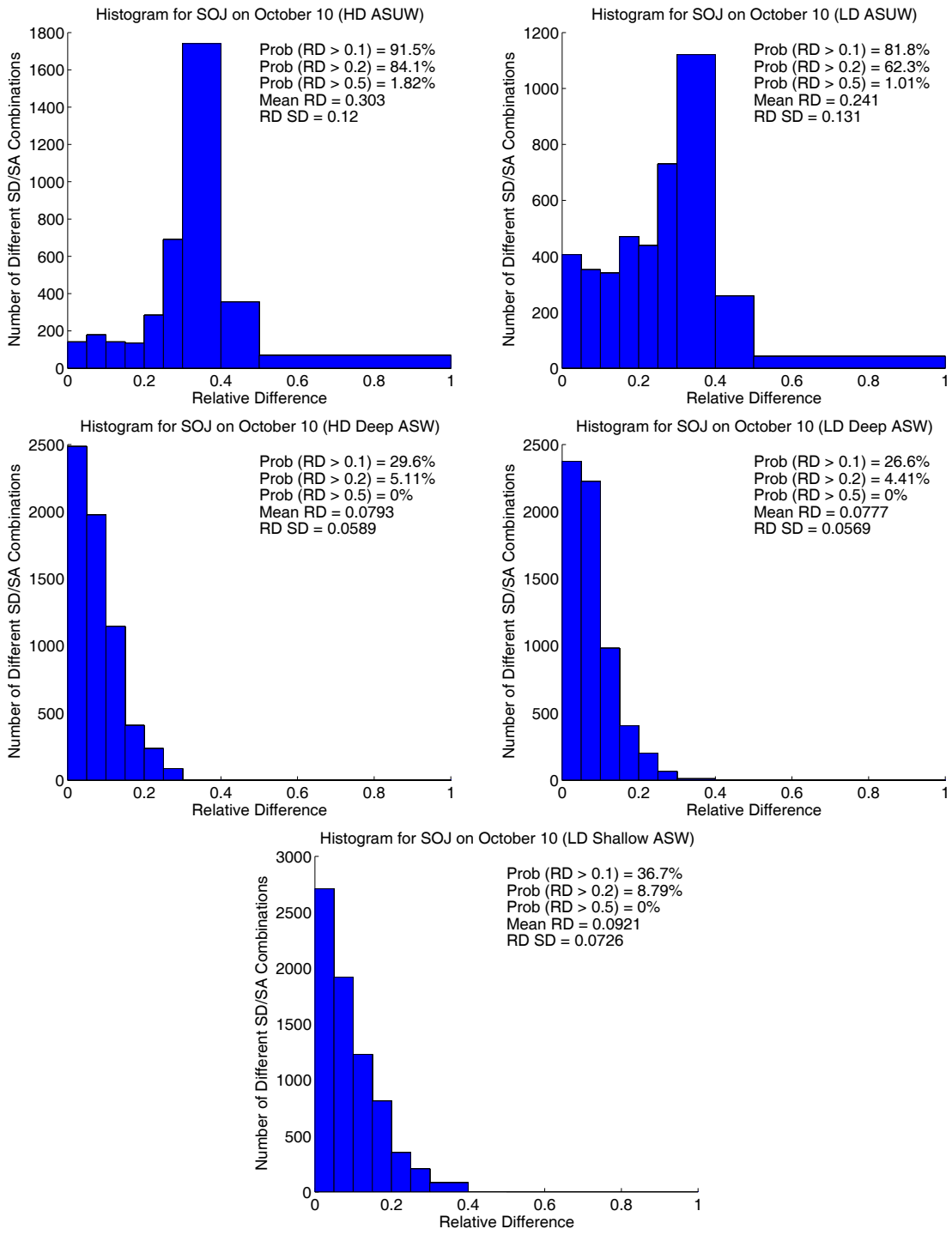

Figure 59. SOJ Oct WAPP histograms

LIST OF REFERENCES

Applied Physics Laboratory University of Washington (APL-UW). *APL-UW High-Frequency Ocean Environmental Acoustic Models Handbook (TR 9407).* Seattle, Washington: APL-UW, 1994.

Chu, P. C., W. Guihua, C. Fan. "Evaluation of the U. S. Navy's Modular Ocean Data Assimilation System (MODAS) Using South China Sea Monsoon Experiment (SCSMEX) Data." *Journal of Oceanography*, in press.

Etter, Paul C. *Underwater Acoustic Modeling: Principles, Techniques and Applications*. Essex, England: Elsevier Science Publishers Ltd, 1991.

Fox, D. N., W. J. Teague, C. N. Barron, M. R. Carnes, and C. M. Lee. "The Modular Ocean Data Assimilation System (MODAS)." *Journal of Atmospheric and Oceanic Technology* 19 (February 2002): 240-252.

Fox, D. N., C. N. Barron, M. R. Carnes, M. Booda, G. Peggion, and J. Gurley. "The Modular Ocean Data Assimilation System." *Oceanography* 15 (No. 1 2002a): 22-28.

Fox, Dan N. MODAS Homepage: http://www7320.nrlssc.navy.mil/modas/ Accessed 25 August, 2004.

Naval Oceanographic Office (NAVO). *Oceanographic and Atmospheric Master Library Summary, April 2004*. Bay St. Louis, Mississippi: Systems Integration Division, Stennis Space Center, 2004.

Naval Undersea Warfare Center (NUWC). USN Torpedoes/Mines, Power Point view graphs, 2004.

THIS PAGE INTENTIONALLY LEFT BLANK

INITIAL DISTRIBUTION LIST

1. Defense Technical Information Center
   Ft. Belvoir, Virginia

2. Dudley Knox Library
   Naval Postgraduate School
   Monterey, California

3. Dr. Brian Almquist
   Office of Naval Research
   Arlington, VA

4. Dr. Charlie Barron
   Naval Research Laboratory
   Stennis Space Center, MS

5. CDR Eric Gottshall
   National Oceanic and Atmospheric Administration
   Silver Spring, MD

6. Dr. Daniel Fox
   Naval Research Laboratory
   Stennis Space Center, MS

7. PMW 180
   SPAWAR
   San Diego, CA

8. Mr. Steve Haeger
   Naval Oceanographic Office
   Stennis Space Center, MS

9. CDR Roy Ledesma
   Naval Oceanographic Office
   Stennis Space Center, MS

10. RDML Timothy McGee
    Commander, Naval Meteorology and Oceanography Command
    Stennis Space Center, MS

11. Mr. Bruce Northridge
    Commander, Naval Meteorology and Oceanography Command
    Stennis Space Center, MS

12. RADM John Pearson
Naval Postgraduate School
Monterey, CA

13. VADM Roger Bacon
Naval Postgraduate School
Monterey, CA

14. Dr. Mary L. Batteen
Naval Postgraduate School
Monterey, CA

15. Mr. David Cwalina
Naval Undersea Warfare Center
Newport, RI

16. Mr. Roberts Rhodes
Naval Research Laboratory
Stennis Space Center, MS

17. Dr. Greg Jacobs
Naval Research Laboratory
Stennis Space Center, MS

18. CAPT Mendal Livezey
Commander, U.S. Fleet Forces Command
Norfolk, VA

19. METOC
Fleet Anti-Submarine Warfare Command
San Diego, CA

20. Oceanographer of the Navy
CNO-N61
Washington D.C.

21. LCDR Patrick Cross
Commander, Submarine Force U.S. Pacific Fleet
Pearl Harbor, HI

22. LCDR David Hone
Commander, Submarine Force U.S. Atlantic Fleet
Norfolk, VA

23. CDR Kenneth Minogue
Commander, Submarine Group Seven
Yokosuka, Japan

24. Dr. Peter Chu
Naval Postgraduate School
Monterey, CA

25. CDR Rebecca Stone
Naval Postgraduate School
Monterey, CA

26. LCDR Ben Reeder
Naval Postgraduate School
Monterey, CA

27. CDR John Joseph
Naval Postgraduate School
Monterey, CA

28. LCDR Steven Mancini
Naval Postgraduate School
Monterey, CA